# Electromagnetic Modeling Using the Partial Element Equivalent Circuit Method

**Jonas Ekman**

EISLAB
Dept. of Computer Science and Electrical Engineering
Luleå University of Technology
Luleå, Sweden

**Supervisor:**

Prof. Jerker Delsing

*To my parents*
*Kjell and Gunilla Ekman*

# Abstract

This thesis presents contributions within the field of numerical simulations of electromagnetic properties using the Partial Element Equivalent Circuit (PEEC) method.

Numerical simulations of electromagnetic properties are of high industrial interest. The two major fields of use are to ensure compliance with electromagnetic compatibility (EMC) regulations and to verify functionality in electronic designs. International EMC regulations bounds companies that develop or assemble electric products to market products that are electromagnetic compatible with other products in their environment. Failure to comply with regulations can result in products withdrawal and fines. To avoid incompatibility, numerical simulations can be used to improve EMC characteristics in the development and assembly stage in a cost efficient way. Functionality of today's compact high-performance electronic systems can be affected by unwanted internal electromagnetic effects. The result can be degradation of performance, malfunction, and product damage. Numerical simulations are used to predict electromagnetic effects at the design phase, thus minimizing the need for post-production actions delaying product releases and increasing product cost.

At the Embedded Internet System Laboratory (EISLAB), Luleå University of Technology, a project concerning numerical simulations of electromagnetic properties in electric systems using the PEEC method is in progress. This thesis focuses on the development of the PEEC method for practical use, thus demanding optimal performance of the basic sections within a PEEC based electromagnetic solver in terms of speed and accuracy. In the PEEC method, the two most demanding sections are the partial element calculations and the solution of the final equation system. The latter problem is a pure mathematical problem with continuous progress while the partial coefficient calculations require further research.

This thesis proposes several techniques for efficient partial element calculations. First, a discretization strategy is used for one-layer structures to enable the use of fast analytic formulas and the resulting simplified PEEC models are solved using a freeware version of SPICE, exemplifying the accessibility of the PEEC method. Second, a fast multi-function method is proposed in which different order of numerical integration is used, in the calculation of the partial elements, depending on a predefined coupling factor. Third, the fast multi-function method is further developed and compared to a fast multipole method applied to partial element calculations. Fourth, the calculation of the three-dimensional node coefficients of potential is addressed and three novel approaches are presented and evaluated in terms of speed and accuracy.

The thesis includes a paper dealing with nonorthogonal PEEC models. This model extension allows the use of nonorthogonal volume and surface cells in the discretization of

objects. This facilitates the modeling of realistic complex structures, improves accuracy by reducing the use of staircase-approximations, and reduces the number of cells in the PEEC model discretizations. The nonorthogonal formulation excludes the use of analytical formulas thus make topical the use of fast multi-function- and multipole-methods.

The fundamentals of the PEEC method makes free-space radiation analysis computationally efficient. Radiated field characterization is important in EMC processes and therefore of great interest. One paper in this thesis explore different possibilities to use PEEC model simulations to determine the electric field emissions from objects.

# Contents

Chapter 1 - Thesis Introduction 1
1.1 Background . . . . . . . . . . 2
1.2 Motivation . . . . . . . . . . 5
1.3 Thesis Outline . . . . . . . . . . 6

Chapter 2 - Introduction to EM Simulation Techniques 7
2.1 Introduction . . . . . . . . . . 8
2.2 Finite Difference Method, FDM . . . . . . . . . . 12
2.3 Finite Element Method, FEM . . . . . . . . . . 14
2.4 Method of Moments, MoM . . . . . . . . . . 16
2.5 Partial Element Equivalent Circuit Method, PEEC . . . . . . . . . . 18

Chapter 3 - The Partial Element Equivalent Circuit (PEEC) Method 21
3.1 Background . . . . . . . . . . 22
3.2 Basic PEEC Theory . . . . . . . . . . 22
3.3 Practical EM Modeling Using the PEEC Method . . . . . . . . . . 36

Chapter 4 - Thesis Summary 63
4.1 Summary of Contributions . . . . . . . . . . 63
4.2 Conclusions . . . . . . . . . . 66
4.3 Future Development of the PEEC Method . . . . . . . . . . 66

Paper A **79**
1 Introduction . . . . . . . . . . 81
2 Derivation of the PEEC Model . . . . . . . . . . 82
3 Simplified PEEC Models . . . . . . . . . . 84
4 Equations for Partial Element Calculations . . . . . . . . . . 85
5 Experiments . . . . . . . . . . 88
6 Conclusions . . . . . . . . . . 91

Paper B **95**
1 Introduction . . . . . . . . . . 97
2 Derivation of the PEEC Model . . . . . . . . . . 98
3 Time Retardation . . . . . . . . . . 100
4 Post-processing Equations . . . . . . . . . . 100
5 Electric Field Sensor . . . . . . . . . . 101
6 Experimental Setup . . . . . . . . . . 102
7 Results . . . . . . . . . . 102
8 Conclusions . . . . . . . . . . 103

Paper C **107**
1 Introduction . . . . . 109
2 The PEEC Method . . . . . 110
3 Integration Order Selection . . . . . 113
4 Validation and Refinements . . . . . 117
5 Conclusions . . . . . 119

Paper D **123**
1 Introduction . . . . . 125
2 Nonorthogonal PEEC Model . . . . . 127
3 Evaluation of Circuit Elements . . . . . 134
4 General Circuit Solver Aspects . . . . . 135
5 Numerical Experiments . . . . . 137
6 Conclusions . . . . . 141

Paper E **149**
1 Introduction . . . . . 151
2 FMM Basic Theory . . . . . 152
3 2-level FMM-based Computation of PEEC Parameters . . . . . 153
4 Multi-Function based Computation of PEEC Parameters . . . . . 156
5 PEEC Parameters Approximation Results . . . . . 157
6 Conclusions . . . . . 160

Paper F **163**
1 Introduction . . . . . 165
2 The PEEC Method . . . . . 166
3 Reduction from Surface to PEEC Node Coefficients of Potential . . . . . 167
4 Circuit Equations for PEEC Problems . . . . . 170
5 Numerical Experiments . . . . . 171
6 Conclusions . . . . . 175

# Preface

This thesis summarizes my research and contributions within numerical simulations of electromagnetic properties using the PEEC method. The contributions focuses on the development of the PEEC method for practical use within research and development. The work has been performed at EISLAB, Luleå University of Technology, Sweden, between 1999 and 2003 under the supervision of Prof. Jerker Delsing.

Funding was provided by the European Union's action in support of regional development, Luleå University of Technology faculty funds and personal grants from Ericsson's Research council.

# Acknowledgements

I would like to thank my supervisor Prof. Jerker Delsing for realizing the importance of this topic within electrical engineering and guiding me towards my Ph.D. It has been an interesting and rewarding journey.

I spent most of the second part of my Ph.D. at the University of L'Aquila EMC Laboratory, Italy, and a short period at IBM T.J. Watson Research Center, N.Y. I would like to thank all people working there for taking me in and sharing their knowledge, especially Dr. Giulio Antonini, Prof. Antonio Orlandi and Dr. Albert E. Ruehli. Further I would like to thank Alessandra for her help and support, Antonio for his hospitality and Joris for helping me out at Yorktown.

Among all the people that have helped me with my work I would like to give special thanks to Åke, Urban, and Jonny at LTU.

Jonas Ekman, March 2003.

# Part I

# Chapter 1

# Thesis Introduction

*This chapter presents a fundamental problem description of the field of numerical simulation of electromagnetic properties followed by the thesis motivation.*

## 1.1 Background

This thesis deals with the numerical modeling of electromagnetic (EM) properties using the *Partial Element Equivalent Circuit* (PEEC) method. Numerical modeling is widely used in, for example, product research and development, design of mechanical parts, and in the prediction of the weather forecast. The main reason for performing numerical simulation and modeling within research and industries is the possibility to test parts or products before production. For instance, mechanical parts can be tested for durability, water flow in piping systems can be verified, and ventilation in office spaces can be tuned. Numerical modeling of electromagnetic properties are used by, for example, the electronics industry to :

1. *Ensure functionality of electric systems.* The basic functions of large and complex electric systems must be verified using numerical simulations, i.e. circuit simulation software. For instance, the functionality of an amplifier in terms of amplification and bandwidth is traditionally verified using circuit simulation tools like SPICE. However, the fast development within the electronic industry and the trends in the society have emphasized the threat of electromagnetic interference (EMI) which is not accounted for in the traditional SPICE-like solvers. EMI is caused by unwanted EM energy penetrating and effecting electric components and/or systems. EMI may cause malfunction of electric systems, loss of data, and permanent damage in sensible equipment. It is possible to identify sources contributing to the increased EMI threat. They are:

    - *Increased performance.* Increased performance (clock frequencies) of electric systems is often generated by faster current- and voltage fluctuations within an electric system. This fast current- and voltage fluctuations can generate, in combination with the system geometry, radiated EM fields making the system a source of EM energy.
    - *Miniaturization.* Miniaturization of electric components and systems reduces separating distances and thereby increases internal capacitive and inductive couplings (parasitics).
    - *Plastic enclosures.* The increased use of plastic, compared to metallic, enclosures for electric systems reduces shielding effects and increases the risks of EMI.
    - *Wireless communication.* The increased use of wireless communication creates more sources and victims to EM energy. The replacement of cables with wireless communication increases the electromagnetic pollution and consequently the risk for EMI.
    - *E-community.* The increased usage and availability of electronic systems in houses, offices, and cars etc. introduces more sources and thereby more victims of EMI.

    Since the effects of EMI can be severe, the traditional circuit analysis needs to be completed with an EM analysis, for instance, using the PEEC method. *The* *consequence of not adopting the aspect of EMI in a product development process can result in large economical costs from post-production product fixing.* This can result in *delayed product releases* which is reported to be the main concern for electronic companies [1].

2. *Ensure compliance with electromagnetic compatibility (EMC) regulations and directives.* Legislation concerning electromagnetic compatibility was introduced within the European Union[1] on the 1st of January 1992 by the European Commission of the EMC Directive, 89/336/EEC [2]. The 1992 EMC Directive was the first attempt to:

   - Unify the legislation within the EU to facilitate the free movement of goods between the European states.
   - Prevent the public from serious EMI incidents and effects. Where examples on serious incidents regarding electromagnetic incompatibility are [3] :
     - Malfunction of electronic medical devices caused by radio frequency (RF) radiation.
     - Effects on vehicle braking and motors systems caused by high power broadcast transmitters.
     - Airplane navigation system malfunction during high frequency communication.

   The term EMC is defined [4] as:

   *The ability of a device, unit of equipment or system to function satisfactorily in its electromagnetic environment without introducing intolerable electromagnetic disturbances to anything in that environment.*

   The EMC regulations set the essential requirements which must be satisfied before products are placed on or taken into use on the internal EU market. The requirements are collected in standards drawn up by International and European standard bodies, where the European bodies are:

   **CEN** (The European Committee for Standardization)
   Publishes harmonized standards for non electrotechnical equipment.

   **CENELEC** (The European Committee for Electrotechnical Standardization)
   Mandated by the Commission of the EC to produce EMC standards for use with the European EMC Directive.

   **ETSI** (The European Telecommunications Standards Institute)
   Mandated by the Commission of the EC to produce EMC standards for telecommunications equipment for use with the European EMC Directive.

[1] Countries outside EU have similar legislation concerning EMC. For example, U.S. Federal Communications Commission (FCC) regulations in USA.

*Figure 1.1: The CE mark indicates conformity with essential health and safety requirements set out in European Directives.*

Products that comply with EMC regulations must be attested with two things:

- *A declaration of conformity* has to be available to the enforcement authority for up to ten years after product release.
- A *CE mark* (Conformitè Europèenne, French for European conformity), Fig. 1.1. to indicate conformity with the essential health and safety requirements, not only EMC, set out in European Directives.

National and international EMC regulations are often completed by company specific internal EMC directives. The internal EMC directives are used to ensure higher quality products and can also form the basis for future revised EMC regulations.

*The consequence of not adopting the aspect of EMC in a product development process can result in large economical damage*, for example :

- Product withdrawal from large markets with long- or short-term damage to product and company profile.
- Re-designs causing increasing costs and most importantly delayed product releases.
- Post-production actions resulting in increased cost per produced item, estimated by local companies[5] in the order of 10%, and delayed product releases. *This is especially noticeable for the electronic industries that profit from short time - large quantity sales.*

Even though the EMC problem is not a new issue for companies developing electric products or systems, the problem has increased due to the reasons presented above. Traditionally the problem was kept at a minimum by good design principles, rules of thumb, and experienced personnel. This is no longer possible with the increased complexity in many modern electric systems. Instead numerical methods are efficient tools when designing electronics and systems to improve their EMC characteristics.

The wide variety of problems within the area of numerical modeling of EM properties, presented in Chapter 2.1, require the continuous development and advancements of new and existing numerical techniques, like the PEEC method described in this thesis. This facilitates the development of new innovative products complying with EMC regulations, pre-production, in the industry. And potentially dangerous products and economical consequences could be minimized by using computer based simulations of EM properties.

## 1.2 Motivation

At EISLAB[2] the use of SPICE based simulation tools in both education and research is extensive. SPICE offers an easy-to-use tool to design and realize schematics for students and teachers. While for researchers SPICE offers a multi faceted environment in which electrical equivalents of mechanical systems and electronic components can be treated together.

Until the beginning of this thesis in August 1999, a large part of the research at EISLAB involved SPICE modeling of acoustic and electronic systems. With the EMC Center as a resource at the department my thesis was initiated by Prof. Jerker Delsing who wished to be able to incorporate the electromagnetic behavior of electronic systems in the existing SPICE platform. With a numerous of electromagnetic modeling techniques, see further Chapter 2, the *Partial Element Equivalent Circuit* (PEEC) method was identified as an important technique for future electronic systems within research and industrial development requiring full-wave[3] and full-spectrum[4] solution possibilities. In the PEEC method an equivalent circuit is created of a heterogeneous, mixed circuit and electromagnetic field problem which can be analyzed using circuit theory and/or SPICE-like solvers. The advantages of the PEEC method compared to other EM simulation techniques are :

1. The circuit based formulation allowing the simple inclusion of additional circuit elements when using the PEEC method with commercial circuit simulation software.

2. The same PEEC model can be used for both time- and frequency- domain analysis.

3. The cell flexibility (mixed orthogonal and nonorthogonal) in the volume- and surface-cell discretization offers very good modeling possibilities.

A more thorough comparison to other electromagnetic modeling methods is given in Chapter 2. The limitations with the method, at that time, were identified to be the lack of material (text books and articles), the efficient calculation of the partial elements, the solution of the large linear system describing the circuit equations, and the dielectric cell representation which drastically increases the problem size. Further, an important motivation for this thesis was to perform research to support the usage of the PEEC method in engineering work (ingenjörsmässig, Swedish translation).

[2]Embedded Internet Systems Laboratory, at the Department of Computer Science and Electrical Engineering, Luleå University of Technology, Sweden.

[3]Full-wave refers to the fact that up to a certain upper frequency limit all modes of propagation are calculated.

[4]Full-spectrum techniques delivers the result for the complete frequency spectrum, DC to HF.

## 1.3 Thesis Outline

This thesis is divided in two parts. In part I, the thesis motivation and background is given followed by an introduction to EM simulations and EM simulation techniques with emphasis on the PEEC method. Conclusions and future development of the PEEC method is given in Chapter 4 in part I. Part II includes the six papers this thesis is based on.

# Chapter 2

# Introduction to EM Simulation Techniques

*This chapter introduces the area of numerical simulation of electromagnetic properties. A short survey of four important numerical simulation methods used within the research today is also presented.*

## 2.1 Introduction

Functionality in electric systems can be ensured using basic circuit theory and/or computer based simulations in SPICE-like environments. This type of analysis is *suitable when the electric system geometry is small compared to the wavelength* of the frequencies involved in the analysis. Under this condition, the radiated electromagnetic effects in the system is negligible and lumped circuit analysis can be used. When electric system geometries starts to be comparable to the wavelength of the corresponding frequencies, the conductors, cables, connectors, pins, and vias in a system can start to act like antennas radiating or receiving electromagnetic energy. This type of systems require a combined circuit and electromagnetic analysis.

To include radiation effects, electric and magnetic field couplings, in the analysis of electric systems Maxwell's equations, (2.1) - (2.4), have to be solved. Maxwell's equations are a set of coupled partial differential equations relating the EM fields ($\vec{E}$, $\vec{H}$) to the current- and charge distributions ($\vec{J}$, $\rho$) and the material characteristics ($\varepsilon$, $\mu$) in a system.

*Maxwell's equations*

| *Differential form* | *Integral form* | |
|---|---|---|
| $\nabla \times \vec{H} = \vec{J} + \frac{\partial \vec{D}}{\partial t}$ | $\oint_L \vec{H} \cdot d\vec{l} = \int_S (\vec{J} + \frac{\partial \vec{D}}{\partial t}) \cdot d\vec{S}$ | (2.1) |
| $\nabla \times \vec{E} = -\frac{\partial \vec{B}}{\partial t}$ | $\oint_L \vec{E} \cdot d\vec{l} = -\int_S \frac{\partial \vec{B}}{\partial t} \cdot d\vec{S}$ | (2.2) |
| $\nabla \cdot \vec{D} = \rho_v$ | $\oint_S \vec{D} \cdot d\vec{S} = \int_v \rho_v \, dv$ | (2.3) |
| $\nabla \cdot \vec{B} = 0$ | $\oint_S \vec{B} \cdot d\vec{S} = 0$ | (2.4) |

$\vec{E}$ – Electric field intensity, $[\frac{V}{m}]$ | $\vec{H}$ – Magnetic field intensity, $[\frac{A}{m}]$
$\vec{D}$ – Electric flux density, $[\frac{C}{m^2}]$ | $\vec{B}$ – Magnetic flux density, $[\frac{W}{m^2}]$
$\rho_v$ – Volume charge density, $[\frac{C}{m^3}]$ | $\vec{J}$ – Electric current density, $[\frac{A}{m^2}]$
$\varepsilon$ – Capacitivity of the medium, $[\frac{F}{m}]$ | $\mu$ – Inductivity of the medium, $[\frac{H}{m}]$

In addition, there are three medium-dependent equations

$$\vec{D} = \epsilon \vec{E} \tag{2.5}$$

$$\vec{B} = \mu \vec{H} \tag{2.6}$$

$$\vec{J} = \sigma \vec{E} \tag{2.7}$$

These are the constitutive relations for the medium in which the fields exist.

The techniques for solving field problems, Maxwell's equations, can be classified as experimental, analytical (exact), or numerical (approximate). The experimental techniques are expensive and time consuming but are still widely used. The analytical solution [6] of Maxwell's equations involve, among others, Separation of variables and Series expansions, but are not applicable in a general case. The numerical solution of field problems became possible with the availability of high performance computers. The most popular numerical techniques are :

- Finite difference methods (FDM), Section 2.2.
- Finite element methods (FEM), Section 2.3.
- The method of moments (MoM), Section 2.4.
- The partial element equivalent circuit (PEEC) method, Section 2.5 and Chapter 3.

The differences in the numerical techniques have its origin in the basic mathematical approach and therefore make one technique more suitable for a specific *class of problem* compared to the others. Typical classes of problems, with the suitable modeling techniques indicated in parenthesis, in the area of EM modeling are :

- Electrical interconnect packaging (EIP) analysis (PEEC, MoM).
- Printed circuit board (PCB) simulations (mixed circuit and EM problem) (PEEC).
- Coupling mechanism characterization (MoM, PEEC).
- Electromagnetic field strength and pattern characterization (MoM).
- Antenna design (MoM).
- Scattering problems (FEM, FDM).

Further, the problems presented above require different kinds of analysis in terms of :

- Requested solution domain (time and/or frequency).
- Requested solution variables :
  - Circuit variables (currents and/or voltages).
  - Field variables (electric and/or magnetic fields).

This categorization of EM problems into classes and requested solutions in combination with the complexity of Maxwell's equations emphasizes the importance of using the right numerical technique for the right problem to enable a solution in terms of accuracy and computational effort.

The numerical techniques used for EM simulations, such as FDM, FEM, MoM, and PEEC, can be classified depending on which formulation of Maxwell's equations are solved numerically. The two formulations are displayed in parallel in (2.1) - (2.4) as *Differential form* and *Integral form*. The main differences between the two formulations are :

- *The discretization of the structure.* For the differential formulation the complete structure, including the air needs to be discretized. For the integral formulation only the materials needs to be discretized. This implies a larger number of cells for the differential based techniques and that the computational domain need to be terminated using mathematical 'tricks' to avoid reflection of outgoing EM waves.

- *The solution variables.* The differential based techniques where the discretization of the complete computational domain is performed, delivers predominantly the solution in field variables, i.e. $\vec{E}$ and $\vec{H}$. This is suitable for scattering problems, antenna near field radiation patterns, and EM field excited structures. Post-processing of the field variables are needed to obtain the currents and voltages in a structure. For the integral based techniques the solution is expressed in circuit variables, i.e. currents and voltages. This is suitable for EIP-, EMI-, and PCB-analysis. To convert the system current and voltages to EM field components, post-processing is needed.

Table 1 further displays the differences among the available computational techniques. The differences have triggered the use of hybrid techniques, where advantages of two or more techniques are combined in a hybrid method to solve a specific class of problems [7, 8].

In the following sections, four different types of EM computational techniques are briefly presented. The first three, FDM, FEM, and MoM, are the most common techniques used today for simulating EM problems. The fourth technique, the PEEC method, widely used within signal integrity (SI) as indicated above, is presented briefly in Section 2.5 and more careful in Chapter 3 and the references cited.

*Table 1: Main features of the most common EM simulation techniques.*

| Method | FDM | FEM | MoM | PEEC |
|---|---|---|---|---|
| Formulation | Differential | Differential | Integral | Integral |
| Solution variables | Field | Field | Circuit | Circuit |
| Solution domain | TD or FD | TD or FD | TD or FD | TD and FD |
| Cell geometries | Orthogonal | Nonorthogonal | Nonorthogonal | Nonorthogonal |
| Advantages | Easy to use<br>Robust<br>Complex materials | Cell flexibility<br>Complex materials | Cell flexibility | Same TD/FD model<br>Comb. circuit & EM<br>Cell flexibility |
| Drawbacks | Cell nonflexibility<br>Storage requirements | Solve large lin.syst. | Green's fun. knowledge<br>Computationally heavy | Green's fun. knowledge<br>Computationally heavy |

## 2.2 Finite Difference Method, FDM

In this section a *finite difference time domain method*, (FDTD), is briefly explained. The method is widely used within EM modeling mainly due to its *simplicity*. The FDTD method can be used to model arbitrary heterogeneous structures, for instance, PCBs and the human body, as shown in Fig. 2.1 [9].

*Figure 2.1: Model for a human body used in EM simulations.*

In the FDTD method finite difference equations are used to solve Maxwell's equations for a restricted computational domain. The method require the whole computational domain to be divided, or discretized, into volume elements (cells) for which Maxwell's equations have to be solved. The volume element sizes are determined by considering two main factors [10] :

1. *Frequency*. The cell size should not exceed $\frac{\lambda}{10}$, where $\lambda$ is the wavelength corresponding to the highest frequency in the excitation.

2. *Structure*. The cell sizes must allow the discretization of thin structures.

The volume elements are not restricted to cubical cells, parallelepiped cells can also be used with a side to side ratio not exceeding 1:3 [10], mainly to avoid numerical problems. After discretizing the structure, the electromagnetic field components, $E_X$, $E_Y$, $E_Z$, $H_X$, $H_Y$, and $H_Z$, are defined for the cells, for example as shown in Fig. 2.2.

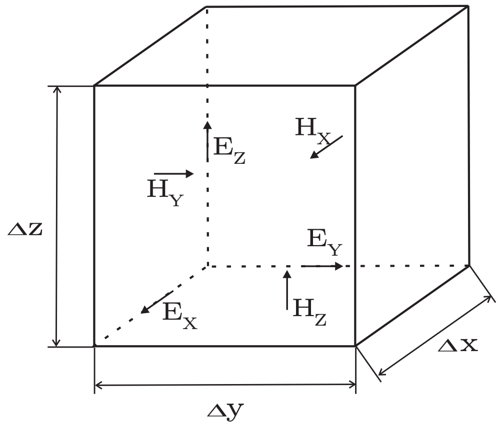


*Figure 2.2: FDTD cell with indicated field components.*

If the field components are defined as in Fig. 2.2 the resulting FDTD method is based according to the well known Yee formulation [11]. There are other FDTD methods that are not based on the Yee cell and thus have another definition of the field components. To be able to apply Maxwell's equations in differential form to the Yee cell the time and spatial derivatives are written as partial derivatives. For a rectangular coordinate system this results in (2.8) for original equation (2.1) and (2.9) for original equation (2.2).

$$\begin{bmatrix} \frac{\partial H_Z}{\partial y} - \frac{\partial H_Y}{\partial z} \\ \frac{\partial H_X}{\partial z} - \frac{\partial H_Z}{\partial x} \\ \frac{\partial H_Y}{\partial x} - \frac{\partial H_X}{\partial y} \end{bmatrix} = \begin{bmatrix} \varepsilon \frac{\partial E_X}{\partial t} \\ \varepsilon \frac{\partial E_Y}{\partial t} \\ \varepsilon \frac{\partial E_Z}{\partial t} \end{bmatrix} + \begin{bmatrix} J_X \\ J_Y \\ J_Z \end{bmatrix} \tag{2.8}$$

$$\begin{bmatrix} \frac{\partial E_Z}{\partial y} - \frac{\partial E_Y}{\partial z} \\ \frac{\partial E_X}{\partial z} - \frac{\partial E_Z}{\partial x} \\ \frac{\partial E_Y}{\partial x} - \frac{\partial E_X}{\partial y} \end{bmatrix} = \begin{bmatrix} -\mu \frac{\partial H_X}{\partial t} \\ -\mu \frac{\partial H_Y}{\partial t} \\ -\mu \frac{\partial H_Z}{\partial t} \end{bmatrix} \tag{2.9}$$

Finally, by substituting time and spatial partial derivatives using finite difference expressions, results in the FDTD equations [12].

To be able to solve the discretized Maxwell's equations in the FDTD method the following must be specified [10] :

1. *Initial conditions and excitation.* The initial electromagnetic field components for each discrete point in the discretized structure must be specified. The excitation of the structure is also specified at this point.

2. *Boundary conditions.* Many problems in EMI/EMC simulations involve open region problems that are impossible to discretizise in the FDTD method. This problem can be solved using mathematical formulations, absorbing boundary conditions (ABC), or absorbing material at the computational boundary.

3. *Time step,* $\Delta t$. To ensure that the electromagnetic wave propagation between the nodes does not exceed the speed of light a time step condition, Courant condition [18], has to be fulfilled. The Courant condition for three dimensional models is given by

$$\Delta t \leq \frac{1}{\sqrt{\frac{1}{\Delta x^2} + \frac{1}{\Delta y^2} + \frac{1}{\Delta z^2}}\; c} \tag{2.10}$$

   where $\Delta x$, $\Delta y$, and $\Delta z$ are the spatial step sizes and $c$ the propagation speed between the nodes.

The equations are then solved by :

1. Calculating the electric field components for the complete structure.
2. Advance time by $\frac{\Delta t}{2}$.
3. Calculate the magnetic field components for the complete structure based on the electric field components calculated in 1.
4. Advance time by $\frac{\Delta t}{2}$ and continue to 1.

The FDTD method delivers the result in field variables, $\vec{E}$ and $\vec{H}$, at all locations in the discretized domain and at every time point. To obtain structure currents and voltages post-processing is needed for the conversion.

## 2.3 Finite Element Method, FEM

The finite element method [13] is a powerful numerical technique for handling problems involving complex geometries and heterogeneous media. The method is more complicated than the previously mentioned FDTD method but also applicable to a wider range of problems. FEM is based on the differential formulation of Maxwell's equations in which the complete field space is discretized. The method is applicable in both the time and frequency domain. In the method, partial differential equations (PDEs) are solved by a transformation to matrix equations [14]. This is done by minimizing the energy for a PDE using the mathematical concept functional, $F$ [15], where the energy can be obtained by integrating the (unknown) fields over the structure volume. The procedure [10, 16] is commonly explained by considering a PDE described by the function $u$ with corresponding driving, excitation, function $f$ as:

$$L\,u = f \tag{2.11}$$

where $L$ is a PDE operator. For example, Laplace's equation is given by $L = \nabla^2$, $u = V$, and $f = 0$. The next step is to discretizise the solution region into finite elements, examples given in Fig. 2.3, for which the functional can be written. The functional for each FEM element, $F_e$, is then calculated by expanding the unknown fields as a sum of

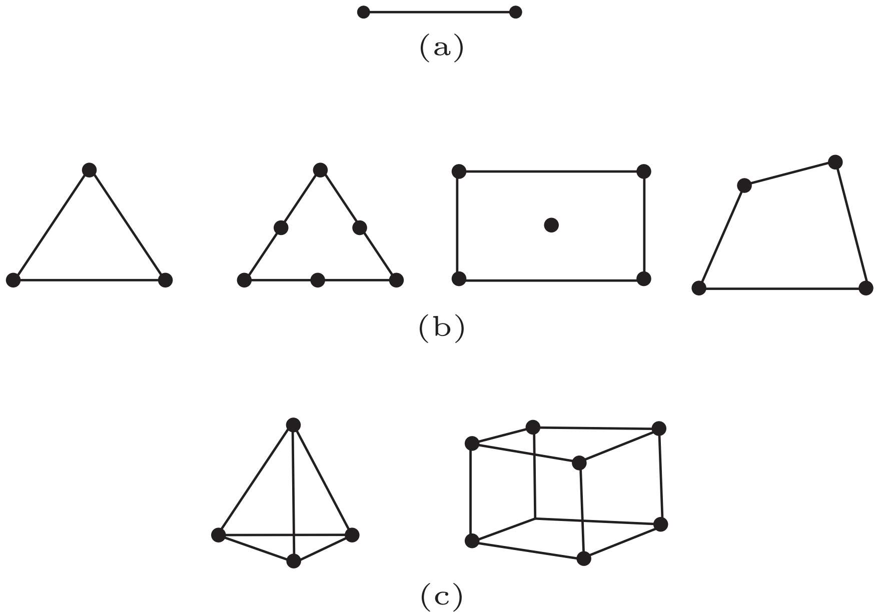


*Figure 2.3: Typical finite elements used in the discretization: (a) One-dimensional, (b) two-dimensional, and (c) three-dimensional. Figure from [6].*

known basis functions, $u_{e_i}$, with unknown coefficients, $\alpha_i$, see further Section 2.4. The total functional is solely dependant on the unknown coefficients $\alpha_i$ and can be written as

$$F = \sum_{\forall e} F_e \tag{2.12}$$

where $e$ is the number of finite elements in the discretized structure and

$$F_e = \sum_{\forall i} \alpha_i \, u_{e_i} \tag{2.13}$$

where $i$ depend on what kind of finite elements are used in the discretization. For instance, for the one-dimensional element shown in Fig. 2.3, $i = 2$ while the elements used for the dipole discretization in Fig. 2.4 utilizes three-node triangles and $i = 3$. The last step is to minimize the functional for the entire region and solve for the unknown coefficients $\alpha_i$. This require the partial derivatives of $F$ with respect to each unknown node coefficient, $\alpha$, to be zero, i.e.

$$\frac{\partial F}{\partial \alpha_i} = 0, \qquad \forall i \tag{2.14}$$

Since the FEM is a volume based technique, like the FDTD method, the computational domain has to be terminated using different techniques to avoid reflection at the computational domain. This can be done using [10, 16] :

1. *Infinite elements.* In this technique, the outer most finite elements are extended to infinity, satisfying the boundary conditions. Unfortunately, the integrals associated with these elements can diverge depending on the finite elements used.

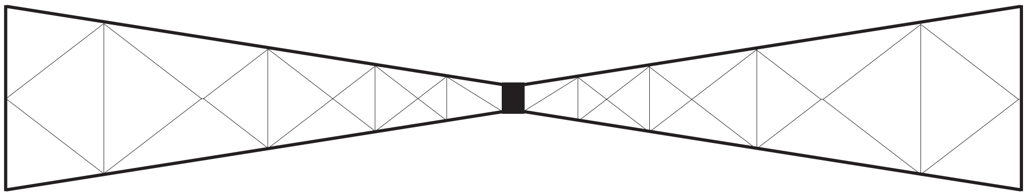

*Figure 2.4: Example of 2D FEM discretization of a broad-band dipole antenna.*

2. *Absorbing boundary conditions (ABC).* Different technique where specific properties are enforced on the boundary of the computational domain to minimize reflection of field components.

The method offers great flexibility to model complicated geometries with the use of nonuniform elements as illustrated in Fig. 2.4.

As for the FDTD method the FEM delivers the result in field variables, $\vec{E}$ and $\vec{H}$, for general EM problems at all locations in the discretized domain and at every time or frequency point. To obtain structure currents and voltages post-processing is needed for the conversion.

## 2.4 Method of Moments, MoM

Method of moments (MoM) [17] is based on the integral formulation of Maxwell's equations, (2.1) - (2.4) right column. This basic feature makes it possible to exclude the air around the objects in the discretization. The method is usually employed in the frequency domain but can also be applied to time domain problems.

In the MoM, integral based equations, describing as an example the current distribution on a wire or a surface, are transformed into matrix equations easily solved using matrix inversion. When using the MoM for surfaces a wire-grid approximation of the surface can be utilizes as described in [10]. The wire formulation of the problem simplifies the calculations and are often used for far field calculations.

The starting point for the theoretical derivation [10, 17], is a linear (integral) operator, $L$, involving the appropriate Green's function $G(\vec{r}, \vec{r}\prime)$ applied to an unknown function, $I$, where $f$ is the known excitation function for the system as

$$L\,I = f \tag{2.15}$$

For example, (2.15) can be the Pocklington Integral Equation, describing the current distribution $I(z\prime)$ on a cylindrical antenna, written as

$$\int_{-\frac{l}{2}}^{\frac{l}{2}} I(z\prime)\left(\frac{\partial^2}{\partial z^2} + k^2\right) G(z, z\prime) \;=\; j\omega\epsilon E_z \tag{2.16}$$

Then the wanted function, $I$, can be expanded into as a series of known functions, $u_i$,

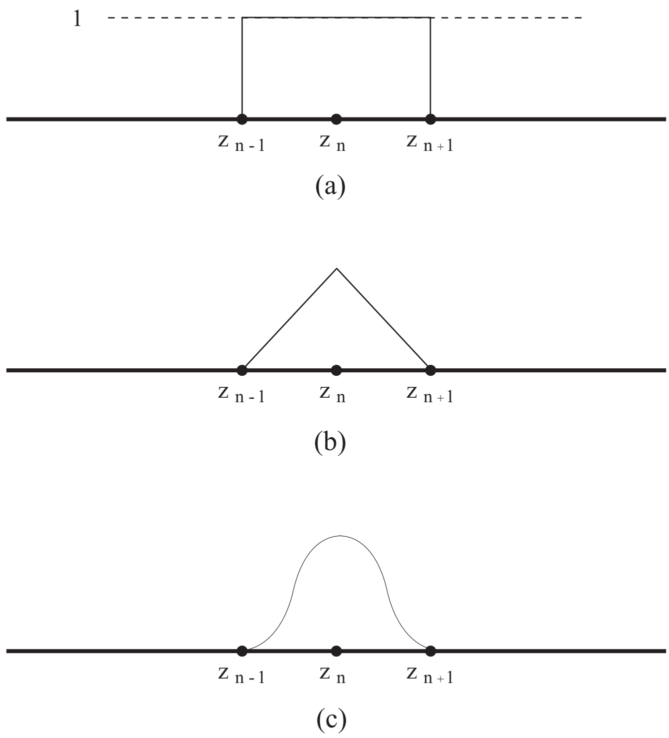


*Figure 2.5: MoM typical basis functions. (a) Piecewise pulse function, (b) piecewise triangular function, (c) piecewise sinusoidal function. Figure from [6].*

with unknown amplitudes, $I_i$, resulting in

$$I = \sum_{i=1}^{n} I_i \, u_i \tag{2.17}$$

where $u_i$ are called basis (or expansion) functions. Fig. 2.5 shows typical examples on basis functions used in the MoM. To solve for the unknown amplitudes, $n$ equations are derived from the combination of (2.15) and (2.17) by the multiplication of $n$ weighting (or testing) functions, integrating over the wire length, and the formulation of a suitable inner product [6]. This results in the transformation of the problem into a set of linear equations which can be written in matrix form as

$$[Z][I] = [V] \tag{2.18}$$

where the matrices $[Z]$, $[I]$, and $[V]$ are referred to as generalized impedance, current, and voltage matrices and the desired solution for the current I is obtained by matrix inversion. See Fig. 2.6 for MoM example results.

The Method of Moments describes the basis of all the electromagnetic analysis techniques in this chapter. The unknown solution is expressed as a sum of known basis functions where the weighting coefficients corresponding to the basis functions are determined for best fit. The same process applied to differential equations is known as a

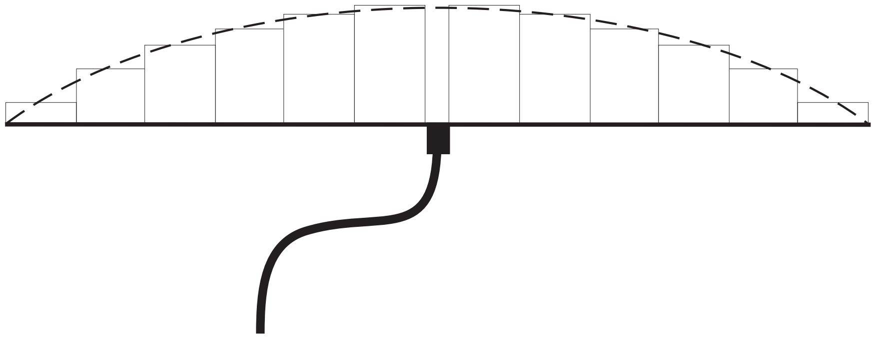

*Figure 2.6: Staircase-approximation of current distribution at resonance frequency for a half-wavelength dipole (dashed line indicate theoretical current distribution) for MoM using pulse basis functions.*

"weighted-residual" method [18] or the finite element method, Section 2.3. The MoM delivers the result in system current densities $\vec{J}$ and/or voltages at all locations in the discretized structure and at every frequency point (depending on the integral equation in (2.15)). To obtain the results in terms of field variables post-processing is needed for the conversion.

The well-known computer program Numerical Electromagnetics Code, often refereed to as NEC [19, 20, 21], utilizes the MoM for the calculation of the electromagnetic response for antennas and other metal structures.

## 2.5 Partial Element Equivalent Circuit Method, PEEC

This section gives a short introduction to the PEEC method [22, 23, 24] as for the previous three EM simulation techniques. A more complete derivation is given in Chapter 3 and in the included papers in Part II.

The PEEC method, developed by Dr. Albert E. Ruehli, is like the MoM based on the integral formulation of Maxwell's equations making the technique well suited for free space simulations. The main feature with the PEEC method is the *combined circuit and EM solution* that is performed with the same equivalent circuit in both the *time- and frequency domain.*

The starting point for the theoretical derivation [25] is the total electric field, at observation point $\vec{r}$, expressed in terms of the vector magnetic potential, $\vec{A}$, and the scalar electric potential, $\Phi$, as

$$\vec{E}(\vec{r},\omega) = -j\omega\vec{A}(\vec{r},\omega) - \nabla\Phi(\vec{r},\omega) \tag{2.19}$$

The vector potential [26] term is given by

$$\vec{A}(\vec{r},\omega) = \mu \int_{v\prime} G(\vec{r},\vec{r}\prime)\ \vec{J}(\vec{r}\prime,\omega) dv\prime \tag{2.20}$$

where $\vec{J}$ is the volume current density at a source point $\vec{r\prime}$ and $G$ is the free-space Green's function

$$G(\vec{r}, \vec{r\prime}) = \frac{e^{-j\beta R}}{4\pi R} \tag{2.21}$$

where $R$ is given by $R = |\vec{r} - \vec{r\prime}|$. The scalar potential [26] term is given by

$$\Phi(\vec{r}, \omega) = \frac{1}{\varepsilon} \int_{v\prime} G(\vec{r}, \vec{r\prime})\; q(\vec{r\prime}, \omega) dv\prime \tag{2.22}$$

where $v\prime$ is the volume of the conductor and $q$ is the charge density at the conductor. If (2.20) and (2.22) is substituted into (2.19) an electric field integral equation (EFIE) in the unknown variables $\vec{J}$ and $q$ is obtained as

$$\vec{E}(\vec{r}, \omega) = -j\omega\mu \int_{v\prime} G(\vec{r}, \vec{r\prime})\; \vec{J}(\vec{r\prime}, \omega) dv\prime - \frac{\nabla}{\varepsilon} \int_{v\prime} G(\vec{r}, \vec{r\prime})\; q(\vec{r\prime}, \omega) dv\prime \tag{2.23}$$

Equation (2.23) is then solved by expanding each unknown, $\vec{J}$ and $q$, into a series of pulse basis functions with unknown amplitude [25]. Pulse functions are also selected for the weighting functions resulting in a Galerkin method [6]. This corresponds to a special discretization strategy in the practical modeling of structures into one inductive and one capacitive discretization (partition). Then, each part of (2.23) can be interpreted as circuit elements [25, 27] since :

- The term on the left hand side can be shown to equal the voltage drop over a conductive volume cell.
- The first term on the right hand side can be show to equal the inductive voltage drop over the volume cell and can be interpreted as the summation of the voltage drops over the partial inductance between the nodes (self partial inductance) and the mutual partial inductance between the volume cells (representing the magnetic field coupling).
- The second term on the right hand side is the difference in the potentials of the two nodes of the current volume cell. This term can be rewritten using the partial capacitance to each node (self partial capacitance) and the mutual partial capacitance between the surface cells (representing the electric field coupling).

The inductive and capacitive discretizations are used for the calculation of the partial elements (discrete components) shown in Fig. 2.7 for a quasi-static PEEC model. In the figure three nodes have been used in the discretization resulting in two volume cells from which the partial inductances, $Lp$, (self and partial) are calculated. To each node one self capacitance, $C_{nn}$, is associated and all the nodes are connected through mutual capacitances, $C_{nm}$, which are calculated from the surface cell discretization. The figure is not showing the volume cell resistances and the mutual inductive couplings.

The PEEC model is then 'solved' by using a circuit solver program as SPICE [28] or by setting up and solving the corresponding circuit equations. This makes the excitation, by using current- and voltage sources, and the inclusion of additional discrete components easy.

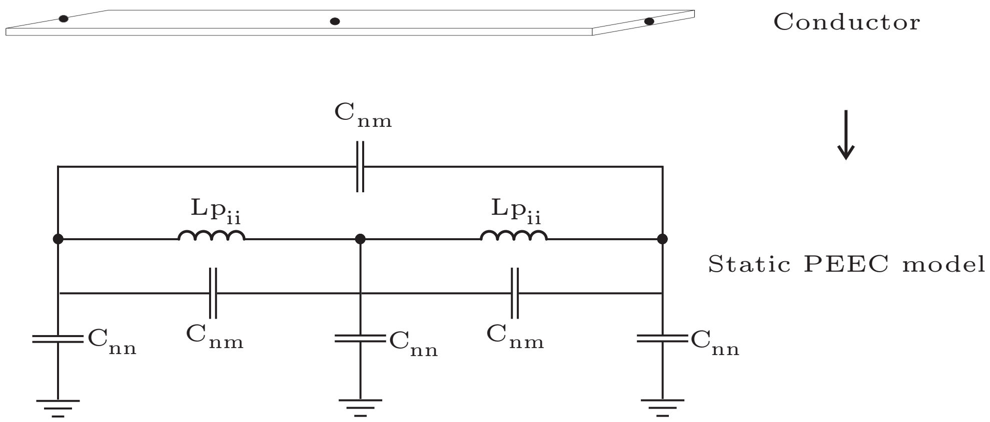


*Figure 2.7: Quasi-static PEEC model for simple conductor geometry.*

The inclusion of the retarded [29] electric and magnetic field couplings can be handled in modified SPICE-solvers [30] or by the use of (1) complex partial elements in the frequency domain and (2) neutral delay differential equations (NDDEs) in the time domain. The PEEC method has recently been extended to use nonorthogonal volume- and surface cells, included Paper D, *Nonorthogonal PEEC Formulation for Time- and Frequency-Domain EM and Circuit Modeling*, which substantially improves the modeling capabilities but also requires the use of efficient partial element calculation algorithms.

Results from the PEEC method are in circuit variables $I$ and $\phi$. To calculate EM field components post-processing equations have to be used as described in included Paper B, *Experimental Verification of PEEC Based Electric Field Simulations*.

# Chapter 3

# The Partial Element Equivalent Circuit (PEEC) Method

*This chapter introduces the numerical method entitled the Partial Element Equivalent Circuit (PEEC) method that is used in the included papers in this thesis.*

## 3.1 Background

The basis of the PEEC method originates from VLSI inductance calculations [22] performed by Dr. Albert E. Ruehli at IBM T.J. Watson Research Center, during the first part of 1970. Dr. Ruehli was working with electrical interconnect problems and understood the benefits of breaking a complicated problem into basic partitions, for which inductances could be calculated, to model the inductive behavior of the complete structure [22, 31]. By doing so, return current paths need not to be known *a priori* as required for regular (loop) inductance calculations.

The concept of partial inductance was first introduced by Rosa [32] in 1908, further developed by Grover [33] in 1946 and Hoer & Love [34] in 1965. However, Dr. Ruehli included the theory of partial coefficients of potential and introduced the partial element equivalent circuit (PEEC) theory in 1972 [35]. Significant contributions in the development of the PEEC method includes :

- The inclusion of dielectrics [36].
- The equivalent circuit representation with coefficients of potential [37].
- The retarded partial element equivalent circuit representation [38, 39].
- PEEC models to include incident fields, scattering formulation [40].
- Nonorthogonal PEECs [41, 42].

The interest and research effort for the PEEC method [43, 44] have increased during the last five year period. The reasons can be an increased need for combined circuit and EM simulations, due to reasons discussed in Chapter 1.1, and the increased performance of personal computers enabling large EM system simulations. This development reflects on the areas of current PEEC research, for instance, model order reduction (MOR), model complexity reduction, and general speed up [45, 46].

## 3.2 Basic PEEC Theory

This section describe the time domain PEEC formulation for orthogonal structures discretized using orthogonal cells. The usage of triangular cells is detailed in [47] and the extension to nonorthogonal structures for orthogonal cells is presented in the included paper D, *Nonorthogonal PEEC Formulation for Time- and Frequency-Domain EM and Circuit Modeling.*

### 3.2.1 Derivation of the electric field integral equation (EFIE)

The theoretical derivation starts from the expression of the total electric field in free space, $\vec{E}^T(\vec{r},t)$, by using the magnetic vector and electric scalar potentials, $\vec{A}$ and $\phi$ respectively [18].

$$\vec{E}^T(\vec{r},t) = \vec{E}^i(\vec{r},t) - \frac{\partial \vec{A}(\vec{r},t)}{\partial t} - \nabla\phi(\vec{r},t) \tag{3.1}$$

where $\vec{E}^i$ is a potential applied external electric field. If the observation point, $\vec{r}$, is on the surface of a conductor, the total electric field can be written as

$$\vec{E}^T(\vec{r},t) = \frac{\vec{J}(\vec{r},t)}{\sigma} \tag{3.2}$$

in which $\vec{J}(\vec{r},t)$ is the current density in a conductor and $\sigma$ is the conductivity of the conductor. Combining (3.1) and (3.2) results in

$$\vec{E}^i = \frac{\vec{J}(\vec{r},t)}{\sigma} + \frac{\partial \vec{A}(\vec{r},t)}{\partial t} + \nabla\phi(\vec{r},t) \tag{3.3}$$

To transform (3.3) into the electric field integral equation (EFIE) the definitions of the electromagnetic potentials, $\vec{A}$ and $\phi$ are used. The magnetic vector potential, $\vec{A}$, at the observation point $\vec{r}$ is given by [18]

$$\vec{A}(\vec{r},t) = \sum_{k=1}^{K} \mu \int_{v_k} G(\vec{r},\vec{r}\prime)\vec{J}(\vec{r}\prime,t_d)dv_k \tag{3.4}$$

in which the summation is over $K$ conductors and $\mu$ is the permeability of the medium. Since no magnetic material medium are considered in this thesis $\mu = \mu_0$. In (3.4) the free space Green's function is used and is defined as [18]

$$G(\vec{r},\vec{r}\prime) = \frac{1}{4\pi}\frac{1}{|\vec{r}-\vec{r}\prime|} \tag{3.5}$$

In (3.4) $\vec{J}$ is the current density at a source point $\vec{r}\prime$ and $t_d$ is the retardation time between the observation point, $\vec{r}$, and the source point given by

$$t_d = t - \frac{|\,\vec{r}-\vec{r}\prime\,|}{c} \tag{3.6}$$

where $c = 3\cdot 10^8 m/s$. The electric scalar potential, $\phi$, at the observation point $\vec{r}$ is given by [18]

$$\phi(\vec{r},t) = \sum_{k=1}^{K} \frac{1}{\epsilon_0} \int_{v_k} G(\vec{r},\vec{r}\prime)q(\vec{r}\prime,t_d)dv_k \tag{3.7}$$

in which $\epsilon_0$ is the permittivity of free space and $q$ is the charge density at the source point. Combining (3.3), (3.4) and (3.7) results in the well known *electric field integral equation* (EFIE) or *mixed potential integral equation* (MPIE) that is to be solved according to

$$\begin{aligned}
\hat{n}\times\vec{E}^i(\vec{r},t) &= \hat{n}\times\left[\frac{\vec{J}(\vec{r},t)}{\sigma}\right] \\
&+ \hat{n}\times\left[\sum_{k=1}^{K}\mu\int_{v_k} G(\vec{r},\vec{r}\prime)\frac{\partial\vec{J}(\vec{r}\prime,t_d)}{\partial t}\,dv_k\right] \\
&+ \hat{n}\times\left[\sum_{k=1}^{K}\frac{\nabla}{\epsilon_0}\int_{v_k} G(\vec{r},\vec{r}\prime)q(\vec{r}\prime,t_d)\,dv_k\right]
\end{aligned} \tag{3.8}$$

where $\hat{n}$ is the surface normal to the body surfaces. In the PEEC method the EFIE, (3.8), is discretized using a method of moments process, interpreted as an equivalent circuit and solved using circuit theory. The solution from PEEC model simulations are in general :

- Current, $I$, in the materials, where $I = \vec{J}a$ and $a$ is the cross sectional area normal to the current flow.
- Node potentials, $\phi$, in the materials.

The results, $I$ and $\phi$, gives together with the PEEC model a complete characterization of the EM behavior of the modelled structure from which all quantities in Maxwell's equations, (2.1) - (2.4), can be calculated.

### 3.2.2 General EFIE for PEEC formulation

The transformation of the EFIE in (3.8) into the PEEC formulation starts by expanding the current- and charge-densities according to this section. This results in a general form of the EFIE for the PEEC formulation, (3.15), from which the equivalent circuit can be derived, Section 3.2.3.

#### PEEC current density expansion

The total current density, $\vec{J}$, in (3.8) is expanded in the PEEC formulation to include the conduction current density, $\vec{J}^C$, due to the losses in the material and a polarization current density, $\vec{J}^P$, due to the dielectric material properties resulting in [25]

$$\vec{J} = \vec{J}^C + \vec{J}^P \tag{3.9}$$

where

$$\vec{J}^C = \sigma \vec{E} \tag{3.10}$$

$$\vec{J}^P = \epsilon_0(\epsilon_r - 1)\frac{\partial \vec{E}}{\partial t} \tag{3.11}$$

For perfect conductors, the total current density $\vec{J}$ reduces to $\vec{J}^C$. While for perfect dielectrics the total current density reduces to $\vec{J}^P$. The polarization current density is added in the differential form of the generalized Ampere's circuital law according to

$$\nabla \times \vec{H} = \vec{J}^C + \epsilon_0(\epsilon_r - 1)\frac{\partial \vec{E}}{\partial t} + \epsilon_0\frac{\partial \vec{E}}{\partial t} \tag{3.12}$$

which is reduced to the original form

$$\nabla \times \vec{H} = \vec{J}^C + \epsilon_0\frac{\partial \vec{E}}{\partial t} \tag{3.13}$$

for $\epsilon_r = 1$. In this way the displacement current due to the bound charges for the dielectrics with $\epsilon_r > 1$ are treated separately from the conduction currents due to the free charges [36].

### PEEC charge density expansion

In (3.15) the charge density is denoted $q^T$ to indicate the combination of the free, $q^F$, and bound, $q^B$, charge density.

$$q^T = q^F + q^B \tag{3.14}$$

This allows the modeling of the displacement current due to the bound charges for dielectrics with $\epsilon_r > 1$ separately from the conducting currents due to the free charges [36]. For perfect conductors, the total charge density $q^T$ reduces to $q^F$. While for perfect dielectrics the total charge density reduces to $q^B$

The resulting EFIE for the PEEC formulation can then be written as

$$\begin{aligned}
\hat{n} \times \vec{E}^i(\vec{r}, t) &= \hat{n} \times \left[ \frac{\vec{J}^C(\vec{r}, t)}{\sigma} \right] \\
&+ \hat{n} \times \left[ \sum_{k=1}^{K} \mu \int_{v_k} G(\vec{r}, \vec{r}\prime) \frac{\partial \vec{J}^C(\vec{r}\prime, t_d)}{\partial t} \, dv_k \right] \\
&+ \hat{n} \times \left[ \sum_{k=1}^{K} \epsilon_0 (\epsilon_r - 1) \mu \int_{v_k} G(\vec{r}, \vec{r}\prime) \frac{\partial^2 \vec{E}(\vec{r}\prime, t_d)}{\partial t^2} \, dv_k \right] \\
&+ \hat{n} \times \left[ \sum_{k=1}^{K} \frac{\nabla}{\epsilon_0} \int_{v_k} G(\vec{r}, \vec{r}\prime) q^T(\vec{r}\prime, t_d) \, dv_k \right]
\end{aligned} \tag{3.15}$$

## 3.2.3 Interpretation as equivalent circuit

The conversion from integral equation to equivalent circuit for the complete EFIE in (3.15) is for practical reasons broken down in the three following sections. First, the fundamental partial element equivalent circuit is given for a strict conductor environment. The following section details the extension to include lossy dielectric objects. Then the inclusion of an externally applied electric fields is discussed.

### Partial Element Equivalent Circuit for Conductors

In this section the PEEC method for conductors, perfect or lossy, is detailed. The exclusion of dielectric bodies and external fields reduces (3.15) to

$$\begin{aligned}
0 &= \hat{n} \times \left[ \frac{\vec{J}^C(\vec{r}, t)}{\sigma} \right] \\
&+ \hat{n} \times \left[ \sum_{k=1}^{K} \mu \int_{v_k} G(\vec{r}, \vec{r}\prime) \frac{\partial \vec{J}^C(\vec{r}\prime, t_d)}{\partial t} \, dv_k \right] \\
&+ \hat{n} \times \left[ \sum_{k=1}^{K} \frac{\nabla}{\epsilon_0} \int_{v_k} G(\vec{r}, \vec{r}\prime) q^F(\vec{r}\prime, t_d) \, dv_k \right]
\end{aligned} \tag{3.16}$$

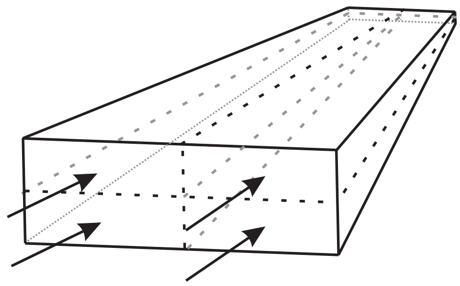

*Figure 3.1: Four volume cells, separated by dashed lines, accounting for the current flowing in the direction of the arrows. The currents in the volume cells are constant and determined by the final PEEC model solution.*

Note that the system of equations in (3.16) have two unknowns, the conduction current density, $\vec{J}^C$, and the charge density, $q^F$. To solve the system of equations the following procedure is employed :

1. *The current densities* are discretized into volume cells that gives a 3D representation of the current flow. This is done by defining rectangular pulse functions

$$P_{\gamma nk} = \begin{cases} 1, & \text{inside the } nk\text{:th volume cell} \\ 0, & \text{elsewhere} \end{cases} \tag{3.17}$$

where $\gamma = x, y, z$ indicates the current component of the $n$:th volume cell in the $k$:th conductor.

2. *The charge densities* are discretized into surface cells that gives a 2D representation of the charge over the corresponding volume cell. This is done by defining the rectangular pulse functions

$$p_{mk} = \begin{cases} 1, & \text{inside the } mk\text{:th surface cell} \\ 0, & \text{elsewhere} \end{cases} \tag{3.18}$$

for the charge density on the $m$:th volume cell of the $k$:th conductor.

Using the definitions in (3.17) and (3.18) the current and charge densities can be written as

$$\vec{J}^C_{\gamma k}(\vec{r}\prime, t_d) = \sum_{n=1}^{N_{\gamma k}} P_{\gamma nk}\ J_{\gamma nk}(\vec{r}_{\gamma nk}\prime, t_{\gamma nk}) \tag{3.19}$$

$$q^T_k(\vec{r}\prime, t_d) = \sum_{m=1}^{M_k} p_{mk}\ q_{mk}(\vec{r}_{mk}\prime, t_{mk}) \tag{3.20}$$

where

$$t_{\gamma nk} = t - \frac{|\vec{r} - \vec{r}_{\gamma nk}\prime|}{v} \tag{3.21}$$

$$t_{mk} = t - \frac{|\vec{r} - \vec{r}_{mk}\prime|}{v}$$

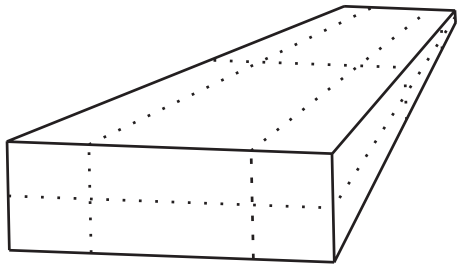

*Figure 3.2: Surface cells, separated by dotted lines, accounting for the charge distribution on the conductors. The charge distributions at the surface cells are constant are determined by the final PEEC model solution.*

The vector $\vec{r}_{\gamma nk}\prime$ is the source position vector indicating the center of the $n$:th volume cell of the $k$:th conductor in the $\gamma$ discretization and $\vec{r}_{mk}\prime$ is the source position vector indicating the center of the $m$:th surface cell of the $k$:th conductor. In (3.19), the summation is over all the volume cells in conductor $k$ with $\gamma$ directed current while in (3.20) the summation is over all the surface cells in conductor $k$.

Pulse functions are also used for the testing functions resulting in a Galerkin solution [6]. The inner product is defined as a weighted volume integral over a cell as

$$< f, g >= \frac{1}{a} \int_v f(\vec{r})g(\vec{r})\, dv \tag{3.22}$$

Combining (3.16), (3.19) and (3.20) while using the inner product defined in (3.22) results in a systems of equations given by

$$\begin{aligned} 0 &= \hat{n} \times \left[ \frac{\vec{J}^C(\vec{r}, t)}{\sigma} \right] \\ &+ \hat{n} \times \left[ \sum_{k=1}^{K} \sum_{n=1}^{N\gamma k} \mu \int_{v\prime} \int_{v_{\gamma nk}} G(\vec{r}, \vec{r}_{\gamma nk}\prime) \frac{\partial P_{\gamma nk} J_{\gamma nk}(\vec{r}_{\gamma nk}\prime, t_{\gamma nk})}{\partial t}\, dv_{\gamma nk} dv\prime \right] \\ &+ \hat{n} \times \left[ \sum_{k=1}^{K} \sum_{m=1}^{Mk} \frac{\nabla}{\epsilon_0} \int_{v_{mk}} G(\vec{r}, \vec{r}_{mk}\prime) p_{mk} q_{mk}(\vec{r}_{mk}\prime, t_{mk})\, dv_{mk} \right] \end{aligned} \tag{3.23}$$

(3.23) is the basic discretized version of the electric field integral equation for the PEEC method from which the partial elements can be identified as will be shown in the following paragraphs.

**Partial Inductances** The basic expression for partial inductances can be derived from the second term in (3.23) by using :

- The free space Green's function, (3.5).
- The expression $I_{\gamma m} = J_{\gamma m} a_m$ for the total current, $I_{\gamma m}$, through a cross sectional area, $a_m$.

This results in

$$\sum_{k=1}^{K}\sum_{n=1}^{N\gamma k}\frac{\mu}{4\pi}\frac{1}{a_{v\prime}\,a_{v_{\gamma nk}}}\int_{v\prime}\int_{v_{\gamma nk}}\frac{\frac{\partial}{\partial t}I_{\gamma nk}(\vec{r}_{\gamma nk}\prime, t_{\gamma nk})}{|\vec{r}-\vec{r}\prime|}\,dv_{\gamma nk}dv\prime \tag{3.24}$$

and can be interpreted as the inductive voltage drop, $v_L$, over the corresponding volume cell. By defining the partial inductance [48] as

$$Lp_{\alpha\beta} = \frac{\mu}{4\pi}\frac{1}{a_\alpha a_\beta}\int_{v_\alpha}\int_{v_\beta}\frac{1}{|\vec{r_\alpha}-\vec{r_\beta}|}dv_\alpha dv_\beta \tag{3.25}$$

(3.24) can be rewritten as

$$v_L = \sum_{k=1}^{K}\sum_{n=1}^{N\gamma k} Lp_{v\prime\,\gamma nk}\frac{\partial}{\partial t}I_{\gamma nk}(t-\tau_{v\prime\,v_{\gamma nk}}) \tag{3.26}$$

where $\tau_{v\prime\,v_{\gamma nk}}$ is the center to center delay between the volume cells $v\prime$ and $v_{\gamma nk}$.

(3.25) is the basic definition for the partial self and mutual inductance using the volume formulation. It is from this definition that simplified and analytical formulas for the partial inductances for special geometries have been developed. This will be further discussed in Section 3.3.4.

The interpretation of the second term in (3.23) as the inductive voltage drop (using the partial inductance concept) results in :

- The connection of nearby nodes using the partial self inductance ($Lp_{\alpha\alpha}$) of the corresponding volume cell ($\alpha$).
- The mutual inductive coupling of all volume cells using the concept of partial mutual inductance.

This is illustrated in Fig. 3.3 where a voltage source, $V_m^L$, has been used to sum all the inductive (magnetic field) couplings from all other volume cells, corresponding to the summation in (3.26).

The voltage source is defined as [36]

$$V_m^L(t) = \sum_{\forall n, n\neq m} L_{p_{mn}}\frac{\partial i_n(t-\tau_{mn})}{\partial t} \tag{3.27}$$

Where $i_n(t-\tau_{mn})$ is the current through volume cell $n$ at an earlier instance in time, $(t-\tau_{mn})$. (3.27) can be rewritten [49] using the voltage $v_n$ (node potential difference) over the volume cell $n$ as

$$V_m^L(t) = \sum_{\forall n, n\neq m}\frac{L_{p_{mn}}}{L_{p_{nn}}}v_n(t-\tau_{mn}) \tag{3.28}$$

A PEEC model only consisting of partial inductances is entitled a $(L_p)$PEEC model, Fig. 3.3.

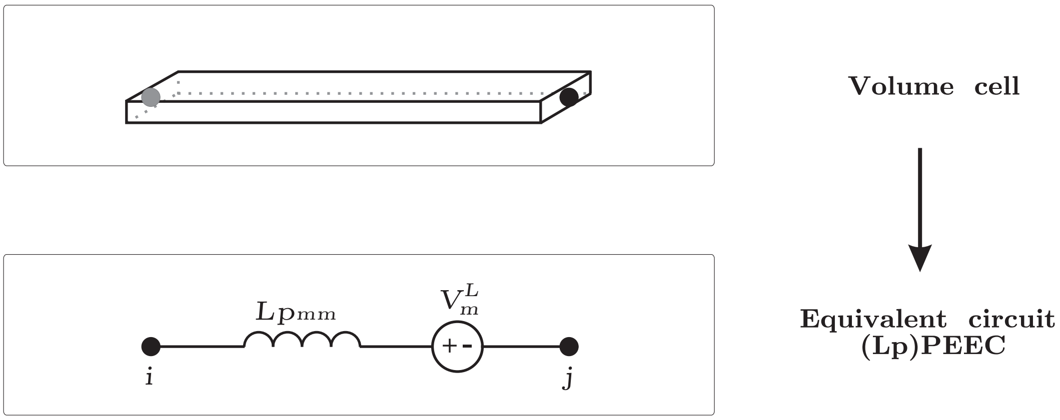


*Figure 3.3: ($L_p$)PEEC model for volume cell $m$ connecting node $i$ and $j$ where $L_{p_{mm}}$ is the partial self inductance for the volume cell and $V_m^L$ accounts for the mutual inductance (magnetic field) coupling from other volume cells, Eq (3.27).*

**Coefficients of Potential** The basic definition for partial coefficients of potential can be derived from the third term in (3.23) by using the following approximations :

- The charges only resides on the surface of the volumes, i.e. converting the volume integral to a surface integral.
- The integral in the $\gamma$ coordinate can be calculated using a finite difference (FD) approximation according to

$$\int_v \frac{\partial}{\partial\gamma} F(\gamma) dv \approx a \left[ F\left(\gamma + \frac{l_m}{2}\right) - F\left(\gamma - \frac{l_m}{2}\right)\right] \tag{3.29}$$

This results in

$$\sum_{k=1}^{K}\sum_{m=1}^{M_k}\left[ q_{mk}(t_{mk}) \frac{1}{4\pi\epsilon_0}\int_{S_{mk}} \frac{1}{|\vec{r}^{+} - \vec{r}\prime|} ds\prime - q_{mk}(t_{mk})\frac{1}{4\pi\epsilon_0}\int_{S_{mk}} \frac{1}{|\vec{r}^{-} - \vec{r}\prime|} ds\prime \right] \tag{3.30}$$

which can be interpreted as the capacitive voltage drop, $v_C$, over the actual cell and the vectors $\vec{r}^{+}$ and $\vec{r}^{-}$ are associated with the positive and negative end of the cell respectively [24]. By defining the partial coefficient of potential as

$$p_{ij} = \frac{1}{S_i S_j}\frac{1}{4\pi\epsilon_0}\int_{S_i}\int_{S_j} \frac{1}{|\vec{r_i} - \vec{r_j}|}\, dS_j\, dS_i \tag{3.31}$$

the capacitive voltage drop can be written as

$$v_C = \sum_{k=1}^{K}\sum_{m=1}^{M_k} Q_{mk}(t - t_{mk})[pp^{+}_{i(mk)} - pp^{-}_{i(mk)}] \tag{3.32}$$

using the total charge, $Q_{mk}$, of the $mk$:th cell.

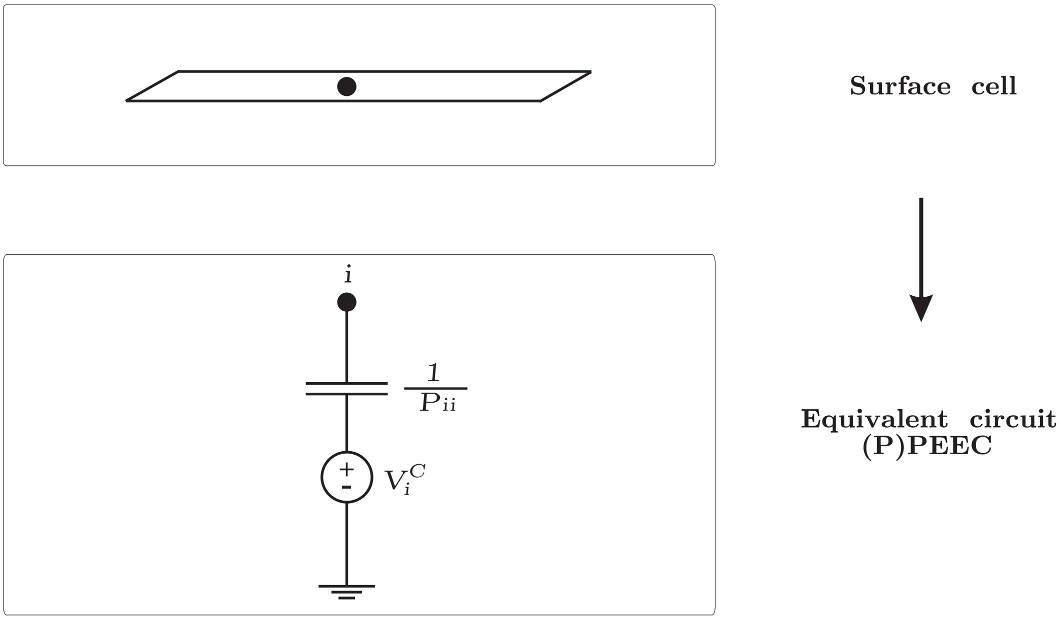


*Figure 3.4: (P)PEEC model for one surface cell/node i where $P_{ii}$ is the partial self coefficient of potential for the surface cell and $V_i^C$ accounts for the mutual capacitive (electric field) coupling from other surface cells, Eq (3.33).*

From the basic definition in (3.31) a number of simplified and analytical formulas for partial coefficients of potential can be derived for special geometries configurations, see further Section 3.3.4.

The interpretation of the third term in (3.23) as self and mutual (partial) coefficient of potential (capacitive) coupling results in :

- The connection of each surface cell (node) to infinity through self partial (*pseudo-*) capacitances.
- Mutual capacitive couplings of all surface cells (nodes).

This is illustrated in Fig. 3.4 where a voltage source, $V_i^C$ has been used to sum all the capacitive (electric field) couplings from all other surface cells.

The voltage source is defined as [49]

$$V_i^C(t) = \sum_{\forall j, j \neq i} \frac{P_{ij}}{P_{jj}} V_{C_j}(t - \tau_{ij}) \tag{3.33}$$

where $V_{C_j}(t - \tau_{ij})$ is the voltage over the pseudo-capacitance, $\frac{1}{P_{jj}}$ , of the $j$:th node, at an earlier instance in time, $(t - \tau_{ij})$.

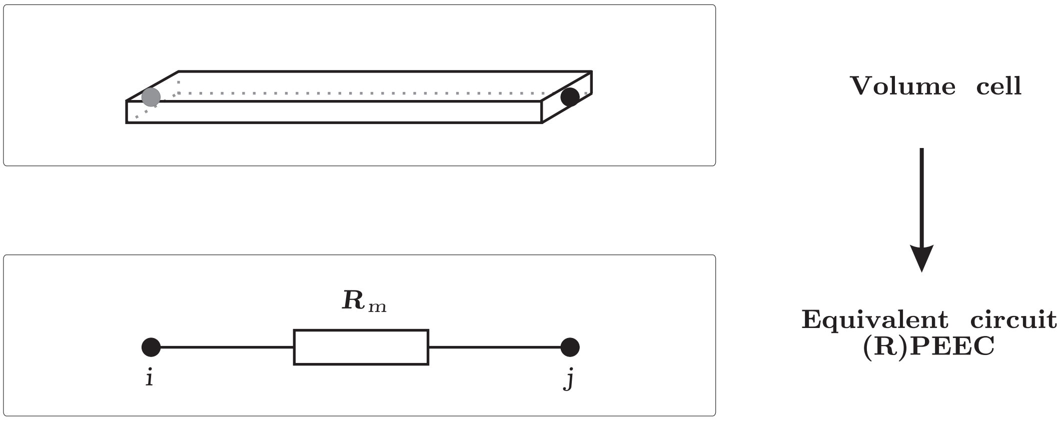


*Figure 3.5: (R)PEEC model for volume cell $m$ connecting node $i$ and $j$.*

A PEEC model only consisting of partial coefficients of potential is entitled a $(P)$PEEC model.

**Resistances** The first term in (3.23) can be shown to equal the resistive voltage drop over the volume cell. By assuming a constant current density over the volume cell the term is rewritten as

$$\frac{\vec{J}_{\gamma}^{C}}{\sigma_{\gamma}} = \frac{I_{\gamma}}{a_{\gamma}\sigma_{\gamma}} \tag{3.34}$$

where $a_{\gamma}$ is the cross section of the volume cell normal to the $\gamma$ direction. The resistance is then calculated as

$$R_{\gamma} = \frac{l_{\gamma}}{a_{\gamma}\sigma_{\gamma}} \tag{3.35}$$

where $l_{\gamma}$ is the volume cell length in the $\gamma$ direction.

The interpretation of the first term in (3.23) as the voltage drop in a conductor results in a lumped resistance connection between the nodes in the PEEC model. A PEEC model only consisting of volume cell resistances is entitled a $(R)$PEEC model, Fig. 3.5.

**Combined $(L_p)$PEEC, $(P)$PEEC, and $(R)$PEEC Models.** When partial inductances are used in the $(R)$PEEC model a series connection of the resistance and partial inductance is made. This results in a $(L_p, R)$PEEC model, Fig. 3.6.

The inclusion of partial coefficients of potential results in a $(L_p, R, P)$PEEC model, Fig. 3.7. In the figure one surface cell at each node is used to account for the capacitive coupling to corresponding node.

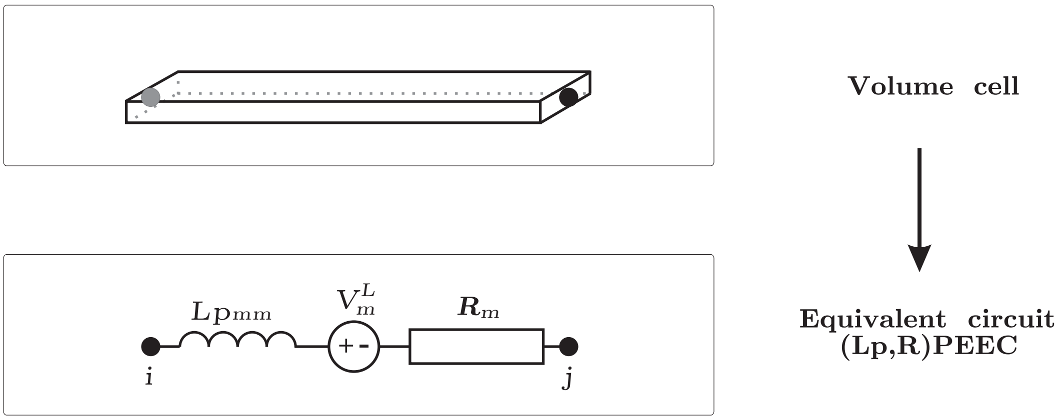


*Figure 3.6: ($L_p, R$)PEEC model for volume cell $m$ connecting node $i$ and $j$.*

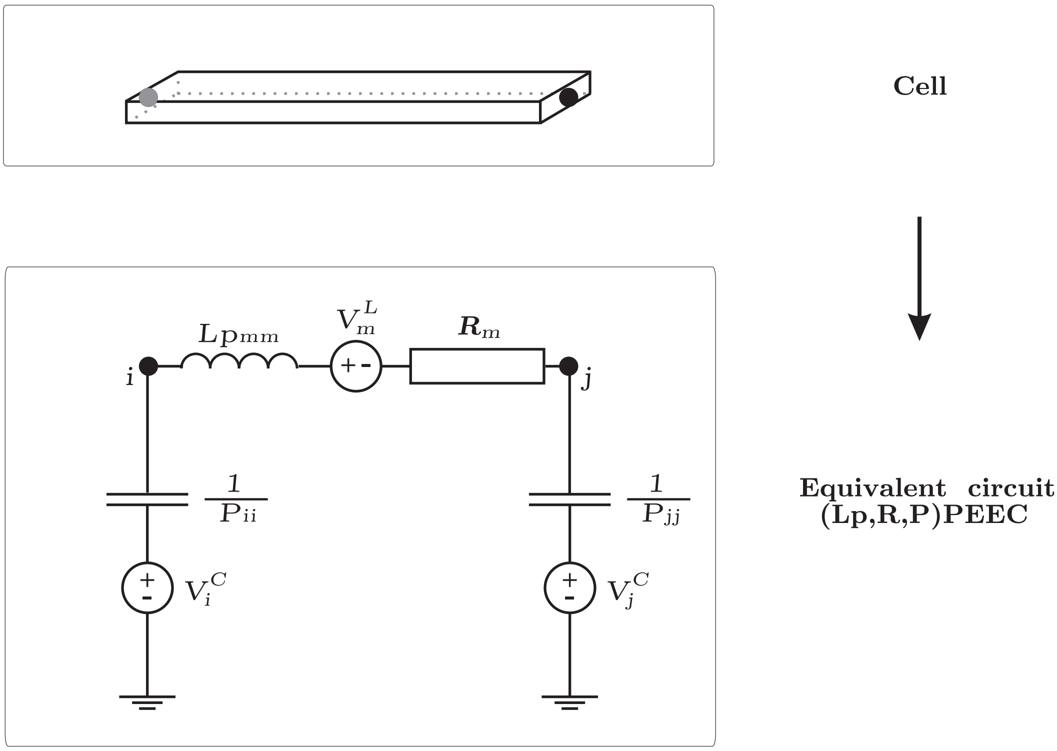


*Figure 3.7: ($L_p, R, P$)PEEC model for volume cell $m$ connecting node $i$ and $j$.*

### Partial Element Equivalent Circuit for Dielectric Materials

The inclusion of dielectric materials as dielectric cells is detailed in [25, 36] and concludes that :

1. The conductor PEEC model detailed above is unchanged.

2. The discretization into dielectric cells are performed as for the conductor cells.

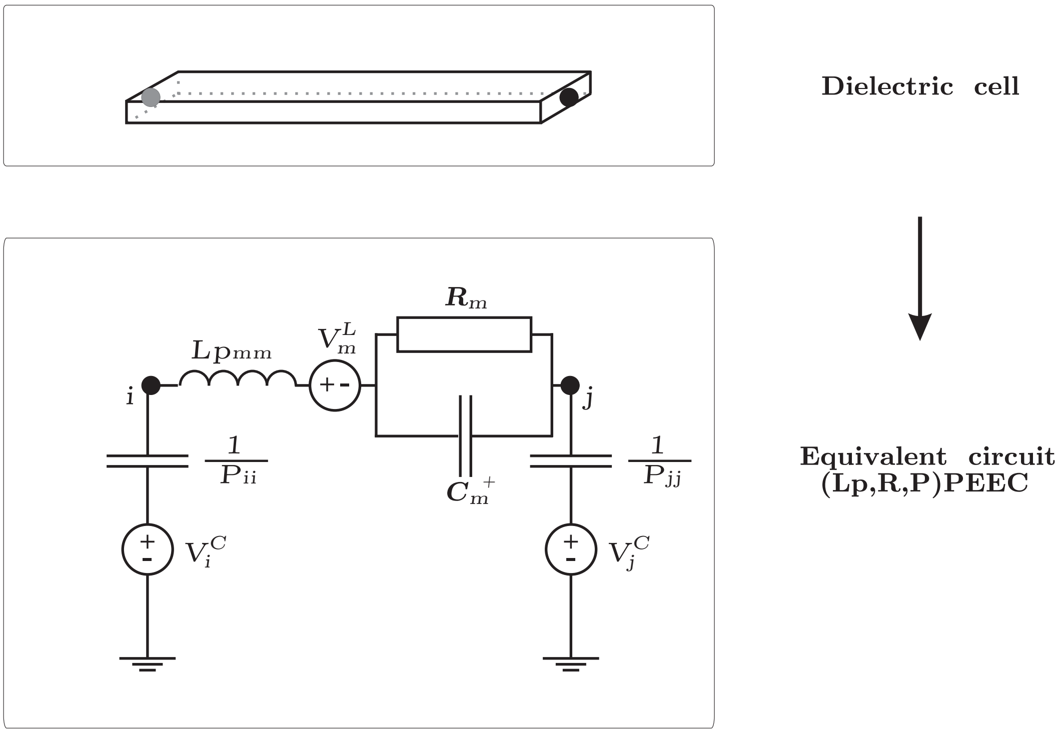


*Figure 3.8: $(L_p, R, P)$PEEC model for dielectric volume cell $m$ connecting node $i$ and $j$.*

3. That lossy dielectric cells can be modelled as a series connection of the volume cell partial inductance and a parallel combination of the volume cell resistance and a capacitor entitled the *excess capacitance*, (3.36), of the dielectric cell, Fig. 3.8.

The *excess capacitance* is calculated using the geometrical data of volume cell $m$ as

$$C_m^+ = \frac{\epsilon_0(\epsilon_m - 1)a_m}{l_m} \tag{3.36}$$

where $\epsilon_m$ is the relative permittivity, $l_m$ is the length (in the current direction), and $a_m$ is the cross sectional area of the dielectric cell (normal to the current direction).

The dielectric losses for PEECs are further discussed in [50].

### Partial Element Equivalent Circuit to Include External Applied Fields

To excite a PEEC model, current and/or voltage-sources can be used. But in some situations an object is excited by an external electric field and the scattering version of PEEC (sPEEC) has to be used. The inclusion of incident fields in the PEEC method is detailed in [40] where a source equivalence, $V_p$, is derived from the left hand side in (3.15). The equivalent voltage source, $V_p$, is placed in series with each inductive volume cell equivalent circuit and calculated for a volume cell $m$ using

$$V_{P_m}(t_m) = \frac{1}{a_m} \int_{a_m} \int_{l_m} \vec{E}^i(\vec{r}, t_m) da\, dl \tag{3.37}$$

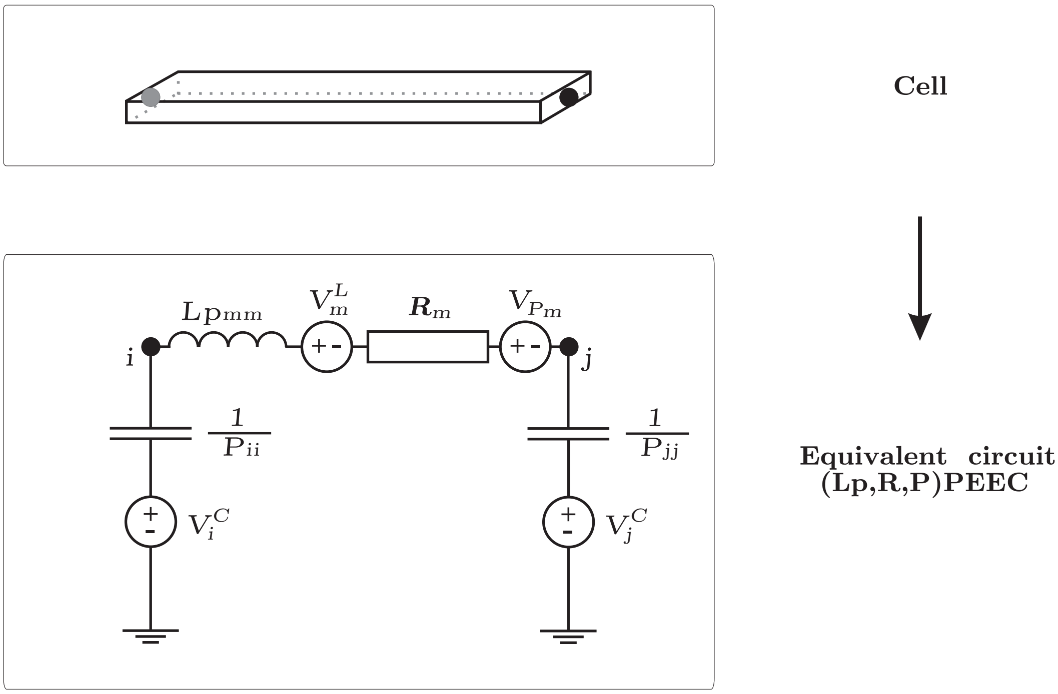


*Figure 3.9: $(L_p, R, P)$sPEEC model for volume cell $m$ connecting node $i$ and $j$.*

where

$$\vec{E}^i(\vec{r},t) = \vec{E}^i_x(\vec{r},t)\hat{x} + \vec{E}^i_y(\vec{r},t)\hat{y} + \vec{E}^i_z(\vec{r},t)\hat{z} \tag{3.38}$$

Fig. 3.9 displays the schematics of the basic sPEEC cell.

### PEEC Frequency Domain Formulation

The thesis presents the theoretical development of the time domain PEEC formulation. The frequency domain PEEC formulation is obtained by converting the appropriate integral equations by using the Fourier transform and the frequency domain Green's function

$$G(\vec{r},\vec{r}\prime) = \frac{e^{-j\omega\tau}}{4\pi|\vec{r}-\vec{r}\prime|} \tag{3.39}$$

where the exponential term models the finite time delays for the retarded electric and magnetic couplings as a phase shift. This result in complex mutual partial elements for $(\tau)$PEEC models as is apparent from the Fourier transform pair

$$\begin{array}{cc} Function & Fourier\ transform \\ \\ f(t-\tau) & F(\omega)\ e^{-j\omega\tau} \end{array} \tag{3.40}$$

The corresponding FD-EFIE for the PEEC formulation is then expressed as

$$
\begin{aligned}
\hat{n} \times \vec{E}^i(\vec{r},\omega) &= \hat{n} \times \left[ \frac{\vec{J}^C(\vec{r},\omega)}{\sigma} \right] \\
&+ \hat{n} \times \left[ \sum_{k=1}^{K} j\omega \frac{\mu e^{-j\omega\tau}}{4\pi} \int_{v_k} \frac{\vec{J}^C(\vec{r\prime},\omega)}{|\vec{r}-\vec{r\prime}|}\, dv_k \right] \\
&- \hat{n} \times \left[ \sum_{k=1}^{K} \omega^2 \frac{\epsilon_0(\epsilon_r - 1)\mu}{4\pi} \int_{v_k} \frac{\vec{E}(\vec{r\prime},\omega)}{|\vec{r}-\vec{r\prime}|}\, dv_k \right] \\
&+ \hat{n} \times \left[ \sum_{k=1}^{K} \frac{\nabla}{\epsilon_0} \int_{v_k} G(\vec{r},\vec{r\prime}) q^T(\vec{r\prime},\omega)\, dv_k \right]
\end{aligned}
\tag{3.41}
$$

**Concluding remarks**

The practical implication of the theoretical development in the previous sections can be summarized as :

- The structure to be analyzed must be partitioned into cells (the discretization stage) for which the currents and charges are to be considered constant. This is performed by placing nodes in a structure to create volume cells to account for the current distribution and surface cells to account for the charge distribution. The surface cells are shifted half a cell length with respect to the volume cells.

- The geometric shape, decided by the discretization, of the volume cells are used to calculate the partial inductances. All nodes in a discretized structure are connected by partial self inductances. The partial mutual inductances account for the retarded magnetic field coupling. A SPICE like representation using the inductive coupling factor K is valid for quasi-static PEEC models. For full-wave PEEC models, ($\tau$)PEEC, the representation using delayed coupled voltage or current sources is necessary to account for the delayed magnetic field couplings.

- The geometric shape, decided by the discretization, of the surface cells are used to calculate the partial coefficients of potential (capacitive couplings). All nodes, connected to a surface, in a discretized structure are connected to a zero/infinite node by partial self capacitances or *pseudo-capacitances*, $\frac{1}{P_{\alpha\alpha}}$. The partial mutual coefficients of potential account for the retarded electric field coupling. The capacitive representation, using lumped capacitances, is valid for quasi-static models. For full-wave PEEC models, delayed voltage or current sources and a coefficients of potential representation is necessary to account for the delayed electric field couplings.

- The losses in the conductors are included by calculating the resistive drop in the current direction of the volume cells and creating a series connection with the corresponding partial self inductance.

- The inclusion of dielectric materials are performed using the theory for *excess capacitance* of a dielectric cell.

## 3.3 Practical EM Modeling Using the PEEC Method

The theory presented in the previous sections form the theoretical basis for the PEEC method. As stated, the PEEC method is known for its suitability for combined circuit- and EM-analysis, as described in [51]. However, the method has been successfully applied to numerous areas within EM modeling including :

- EM radiation from printed circuit boards [52]
- Transmission line modeling [53].
- Noise effect modeling [54].
- Inductance calculations [55].
- Scattering problems [40].
- Power electronic systems [56, 57].
- Antenna analysis, included paper C.
- Lightning-induced effects [58].
- Lightning protection systems [59].
- Inductance effects in chip design [60].

Possible applications for the PEEC method is increasing with the continuous development of the method. The following section describes the basic steps involved in creating PEEC models by considering each part in a PEEC based EM simulation tool.

### 3.3.1 Introduction

It is possible to identify six core components in a PEEC based EM simulation tool. This is illustrated in Fig. 3.10 where a flowchart describes a general PEEC EM solver. The shaded rectangles represents the six core components while the diamond-shaped involve the stability of the PEEC model, see further Section 3.3.8, and finally the three white rectangles are actions to improve stability and PEEC model accuracy.

The following sections explains each component in Fig. 3.10 and gives examples on 1D, 2D, and 3D PEEC models.

### 3.3.2 Graphical tool / Front end

A *Front End* is needed :

1. To create, edit, and visualize the *geometrical shape* of the structure that will be simulated.
2. To add *simulation options and PEEC model parameters* to the actual simulation.

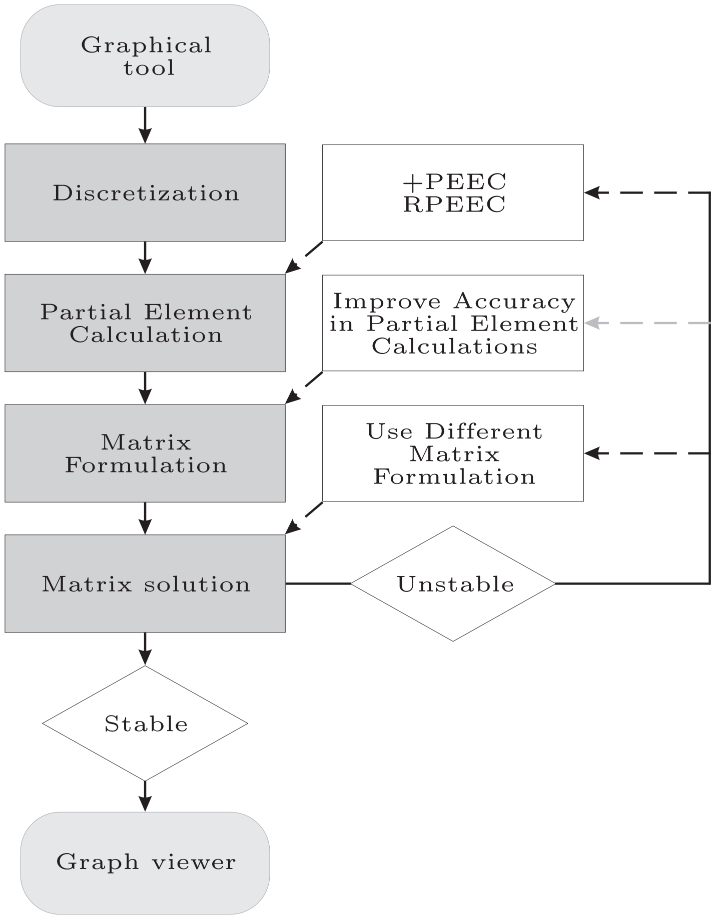


*Figure 3.10: Flowchart for PEEC based EM simulation tool.*

3. To export the structure and simulation options according to a specified syntax for use with the following stages, i.e. *Discretization, Partial Element Calculation, Matrix Formulation*, and *Matrix Solution* in Fig. 3.10.

A graphical user interface (GUI) for the PEEC method [61] allows the creation of orthogonal and nonorthogonal building blocks for which material properties and discretization level can be given, see example screenshot in Fig. 3.11.

The GUI is *not necessary* since the function can be realized *by hand*, for simple structures, using a text editor in which the structure and simulation options are set using a specified syntax. However, advanced GUIs are required for today's complex structures. Even for moderate problems the graphical version is faster, suitable for engineering work, and reliable since man made errors are minimized by the instant visualization of the structure.

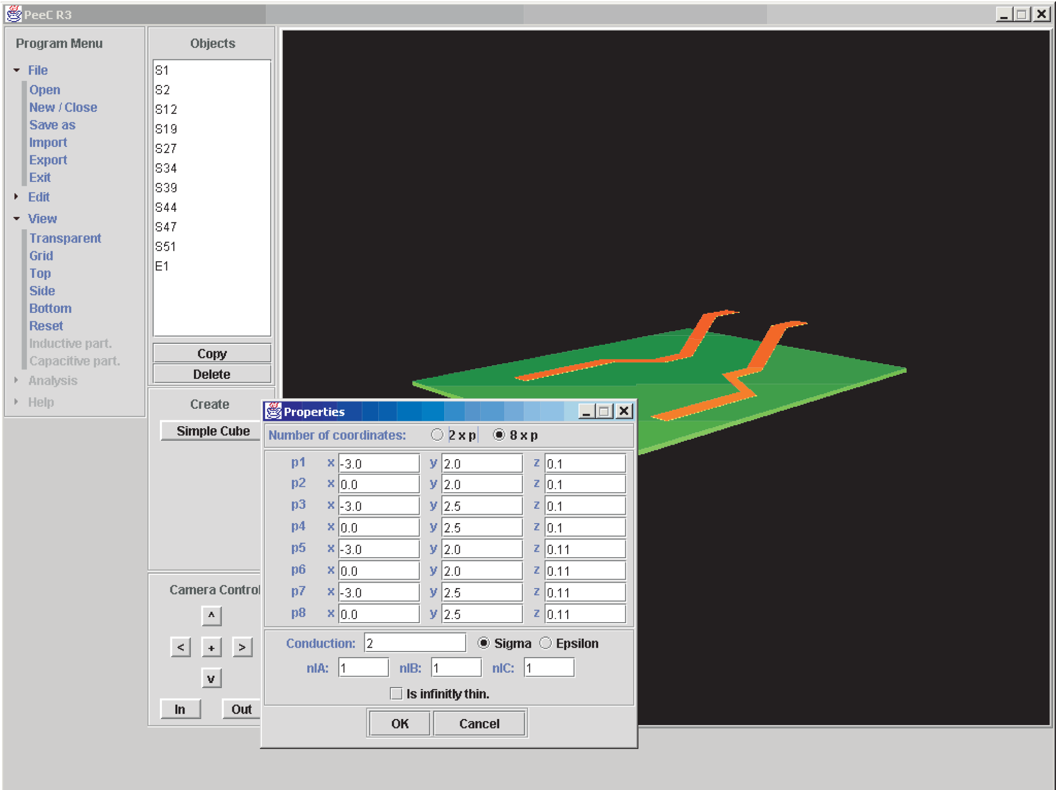


*Figure 3.11: Graphical tool for use with the PEEC method. Screenshot for a nonorthogonal conductor geometry located on a dielectric material.*

### 3.3.3 Discretization

At the discretization stage the user or an algorithm decides how fine the discretization of the original structure should be and how the partitions are created. In the Cartesian coordinate system this results in three different volume cell discretizations (x, y and z-direction) over which the current in each volume cell is considered to be constant. One additional discretization is required to account for the surface charges.

The discretization performed at this stage forms the basic volume and surface cells from which the partial elements are calculated, described in Section 3.3.4.

The level of the discretization, i.e. the sizes of the volume and surface cells, are determined by :

1. *The highest frequency the PEEC model is intended for.* A rule of thumb for EMI/EIP modeling is that the size of the volume and surface cells must never exceed one twentieth of the shortest wavelength to ensure a correct representation of the actual waveforms.

2. *The shape of the conductors.* Length to width to thickness ratios must be considered to ensure good accuracy in the calculated partial element values [62]. Too large ratios in the cell dimensions can cause numerical problems in the partial element calculation routines when using numerical integration and closed form equations.

3. *The proximity to other conductors.* For closely spaced, overlapping, parallel, or perpendicular conductors the discretization in some cases has to be commensurate, see subsection below.

4. *Time and memory limitations.* The number of partial elements used in a PEEC model is directly proportional to the discretization. Thus, the calculation time of the partial elements and the solution time of the final system increases drastically for over-discretized problems.

The discretization starts with the placement of nodes in the structure. The current is flowing between the nodes, in the volume cells, while each node charge is approximated with one surface cell. This is illustrated in the following subsections describing a discretization strategy for general 1D, 2D, and 3D PEEC models.

### 1D Discretization

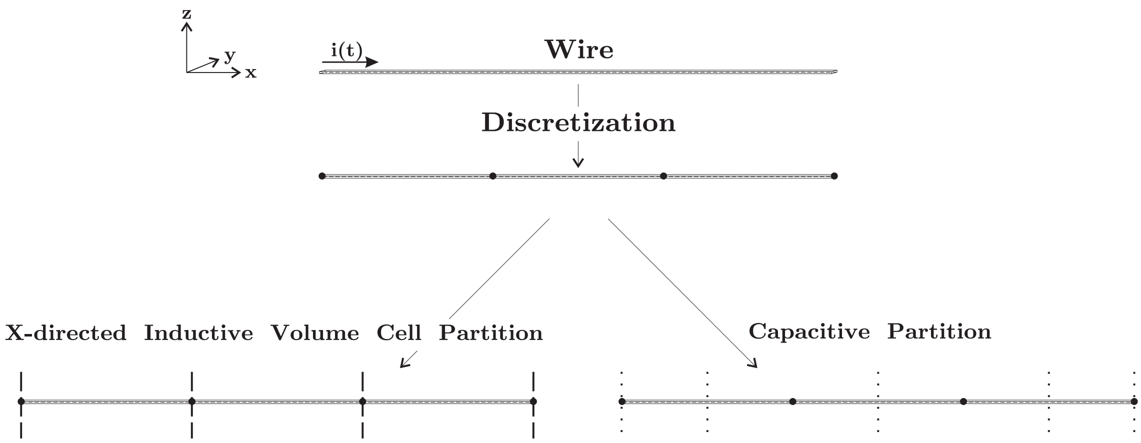


*Figure 3.12: 1D discretization of current carrying wire. Dark circles indicates nodes, dashed lines separate volume cells, and dotted lines separate surface cells.*

In Fig. 3.12 a 1D discretization is performed of a thin wire carrying the current, $i(t)$. In this discretization the user has decided to account only for currents along the wire (x-direction) and to neglect the cross sectional currents. The wire is located along the x-axis and the resulting inductive partition is entitled *X-directed Inductive Volume Cell Partition*. The surface charge distribution is entitled *Capacitive Partition* in the figure. As can be seen from the figure, a discretization using three volume cells of equal size is used. However, there are no restrictions on homogeneous volume cell sizes. In fact, the discretization should be performed with respect to the physics in the actual problem. Thus, an asymmetric discretization with smaller volume and surface cells near sharp edges and terminations can improve simulation results due to the high charge densities at these location. The surface cell discretization is performed with regards to the volume cell discretization. The finite difference approximation in (3.29) used in the derivation of

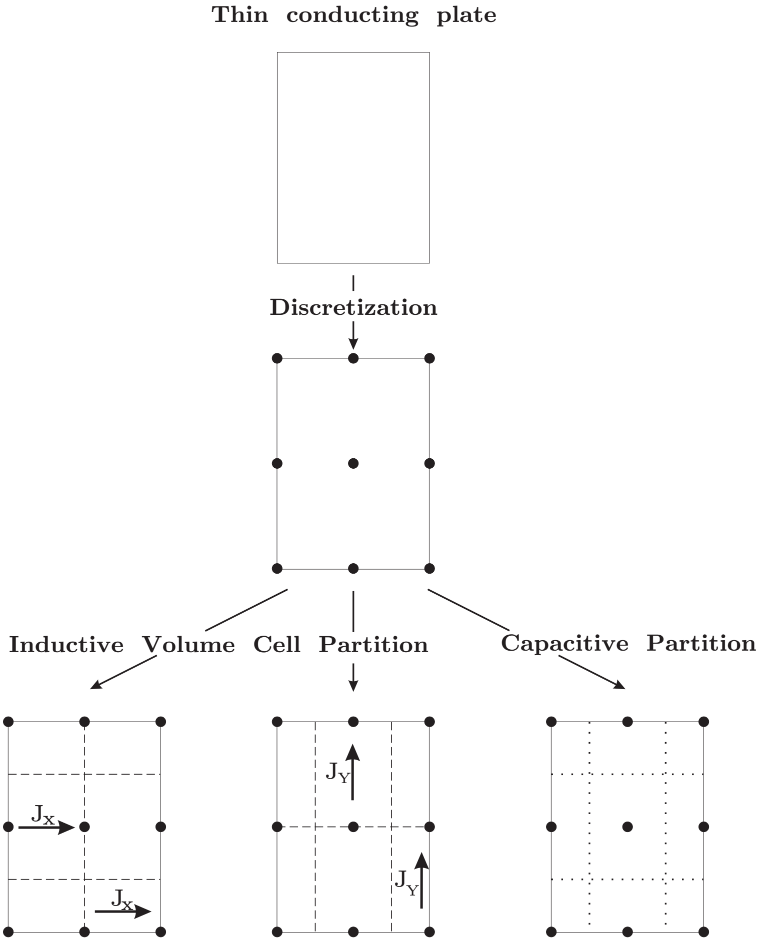


*Figure 3.13: 2D discretization of thin conductive plate. Dark circles indicates nodes, dashed lines separate volume cells, and dotted lines separate surface cells.*

the coefficients of potential, results in a half cell shift of the surface cells with respect to the volume cells. This results in the surface cell discretization, Fig. 3.12, into two full surface cells and two half surface cells.

### 2D Discretization

A two dimensional discretization is used to approximate current and charge distributions in :

- Objects where currents can be approximated to flow in one plane.
- Three dimensional systems modelled using 2D objects, for instance, a metallic chassis or the planar inverted F antenna (PIFA) from included *Paper C*.

The use of 2D PEEC discretization is cost effective, in terms of problem size, and flexible in the modeling possibilities since the approach in not only restricted to coplanar

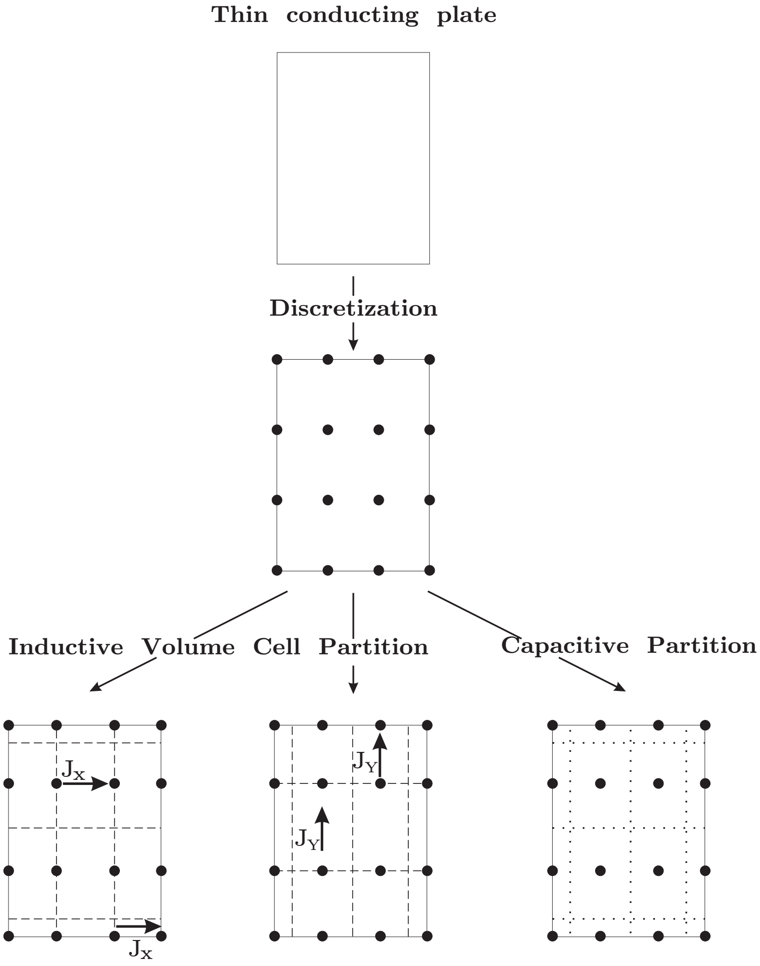


*Figure 3.14: Asymmetric discretization of a 2D structure.*

structures. A 2D PEEC discretization of a thin conducting plate is shown in Fig. 3.13 where the currents, $J_X$ and $J_Y$, are considered to be dominant and the third current components, $J_Z$, can be neglected.

The figure 3.13 shows :

- The original structure at the top (thin conducting plate).
- The placement of the nodes decided by the user considering the conditions detailed above.
- The volume and surface cell discretization based on the node placement. The 2D discretization of the structure results in two different current discretizations, $J_x$ and $J_y$, to account for a general current, $\vec{J} = J_x\hat{x} + J_y\hat{y}$, in the original structure.

The node placement in Fig. 3.13 is symmetric and can approximate the current and charges in the structure in a good way for certain problems. But if edge effects are considered to be important an asymmetric discretization can be used, as shown in Fig. 3.14, to improve the model. In this discretization seven additional nodes were introduced and the partitions formed in an asymmetric manner.

### 3D Discretization

The third dimension in the discretization is introduced in PEEC models when significant currents can appear in all directions, i.e. $x, y, z$-directions, in the analyzed objects. The volume cell discretization is performed in the same routine as for 1D and 2D discretization with the addition of the third dimension according to Fig. 3.15.

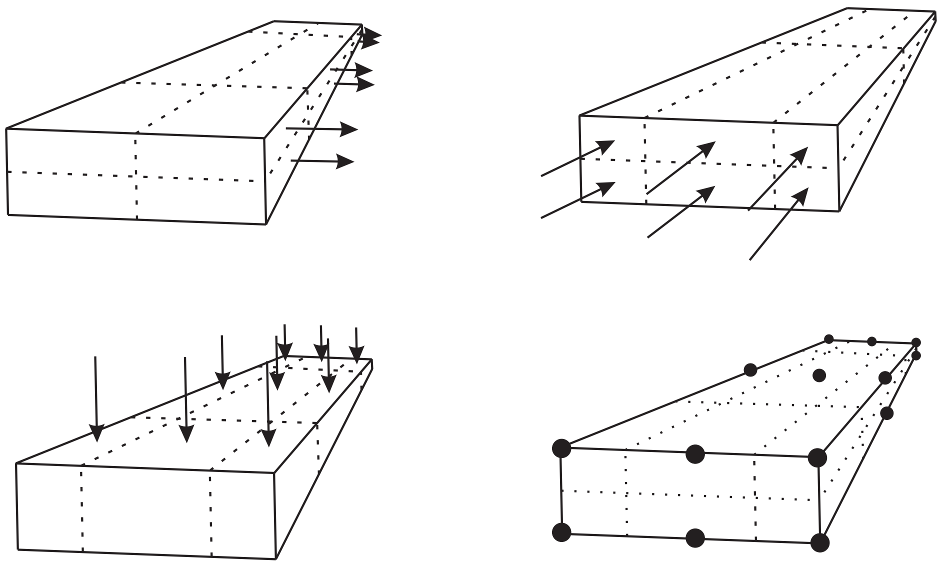

*Figure 3.15: 3D discretization of conductor with indicated current directions (arrows) in the inductive partitions. Dark circles indicates nodes, dashed lines separate volume cells, and dotted lines separate surface cells.*

To be noted is the difference in the surface cell discretization where multiple surfaces can be associated to one PEEC node. This require the 'summation' of the coefficient of potential contributions from the surfaces. This is detailed in included Paper F, *3D PEEC Capacitance Calculation*.

### Commensurate Discretization/Projection Gridding

One important discretization issue is the use of projection gridding for coplanar, closely spaced, and overlapping structures. It was shown in [63] that capacitive couplings could be erroneous if projection gridding was not used for the structures detailed above due to the sudden change in charge. Projection gridding for PEEC models results in matched surface cells for over- and underlying structures, as shown in Fig. 3.16. Projection gridding is also used in method of moment types of codes for improving simulation results [64].

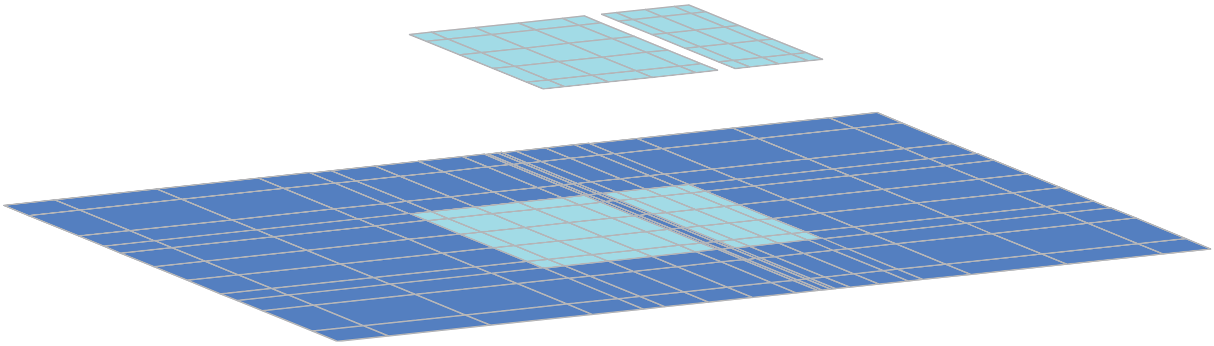

*Figure 3.16: Commensurate surface cell discretization for a planar inverted F antenna (PIFA) PEEC model. The surface cell discretization of the two antenna elements are mirrored in the ground plane.*

### 3.3.4 Partial element calculation

The calculation of the partial elements is the next step in the flowchart in Fig. 3.10 describing a general PEEC EM simulation tool. The partial element calculations are based on the mathematical formulas in Section 3.2.3 and the discretization detailed in the previous section. In this step the following calculations are performed :

- Partial inductances.
- Partial coefficients of potential.
- Volume cell resistances.
- Surface- and volume cell delays.
- Excess capacitance of dielectric cells.

The expressions for the partial inductances and coefficients of potentials, (3.25) and (3.31) respectively, must for general geometries be solved using numerical integration techniques. A simple and well known numerical integration technique is the Gauss-Legendre quadrature integration technique [14]. The included paper C, *Integral Order Selection Rules for a full wave PEEC Solver*, gives an introduction to the use of the Gauss-Legendre technique for partial elements evaluation. The disadvantages with the use of numerical integration techniques are the :

- Introduced errors in the partial element values.
- Time consuming calculation routines.

To avoid these problems exact analytical expressions have been developed to calculate the partial elements for a number of basic geometries [22, 23, 62]. The basic geometries for the different partial elements are presented in the corresponding subsections below.

### Partial Inductances

The basic formula for calculating the partial inductances, (3.25), is repeated here for clarity.

$$Lp_{\alpha\beta} = \frac{\mu}{4\pi} \frac{1}{a_\alpha a_\beta} \int_{v_\alpha} \int_{v_\beta} \frac{1}{R} dv_\alpha dv_\beta \tag{3.42}$$

in which $\alpha$ and $\beta$ are two volume cells created in the discretization detailed in the previous section. If $\beta = \alpha$ the result is entitled the *partial self inductance* of volume cell $\alpha$. Further, $a_\alpha$ and $a_\beta$ is the cross section of cell $\alpha$ and $\beta$ normal to the current direction and $v_\alpha$ and $v_\beta$ is the volume of the corresponding cell. The nominator $R$ is the center to center distance between cell $\alpha$ and $\beta$ expressed as $R = |\vec{r}_\alpha - \vec{r}_\beta|$.

The evaluation of (3.42) can be done using a proper numerical integration method. To avoid the problems detailed above, basic geometries have been defined for which analytical expressions for the partial element values exists. The basic geometries differs for the evaluation of the self and mutual terms and is therefore presented separately.

**Partial Self Inductances** To obtain good accuracy and fast evaluation of the partial inductances basic geometries, building blocks, have been defined. To each basic geometry a formulation for the evaluation of the partial inductance is given. The most important basic geometry is the *rectangular conductor* (ReC) depicted in Fig. 3.17 where the length direction is in the direction of the current flow.

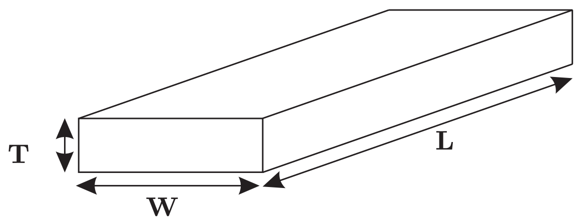


*Figure 3.17: Rectangular conductor geometry for the evaluation of the partial self inductance. Current is flowing in length (L) direction and is assumed to be constant in the volume cell.*

The formula for the evaluation of the partial self inductance for the general rectangular conductor is given by (15) in [22]. To retain good accuracy in the evaluation of the partial self inductance two extreme geometries have been developed from the rectangular conductor in Fig. 3.17. This refinement results in one partial inductance formula for the *long conductor* (LoC), given by (8) in [62], and one partial inductance formula for the *thin conductor* (ThC), given by (16) in [22]. The formulas are invoked according to a scheme [62] based on the rectangular conductor length, width, and thickness ratios according to Table 1.

**Partial Mutual Inductances** Effective calculation routines for partial mutual inductances are even more important than for partial self inductances due to the *mutual*

*Table 1: Decision scheme for the calculation of the partial self inductances. The abbreviations are indicated in Fig. 3.17.*

| | | | | |
|---|---|---|---|---|
| If | $T > W$ | | | use $T = \frac{1}{T}$ |
| If | $L > 0.1W$ | and | $W > 3333T$ | use ThC-routine |
| If | $L > 80W$ | and | $W < 3333T$ | use LoC-routine |
| If | $L < 0.1W$ | and | $50000T > W > 3333T$ | use ReC-routine |
| If | $L < 80W$ | and | $W < 3333T$ | use ReC-routine |

*inductive/magnetic field* coupling of all volume cells in the discretization. For the partial mutual inductance calculations two basic geometries have been defined to speed up and retain good accuracy in the partial element calculations. The most important basic geometry is the mutual inductive coupling between two rectangular conductors, Fig. 3.18.

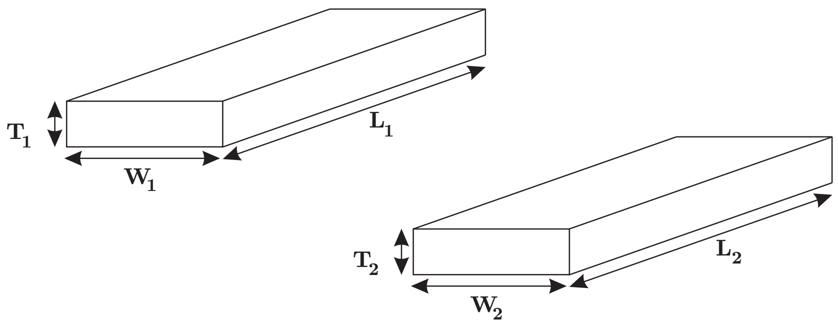


*Figure 3.18: Rectangular conductors geometries for the evaluation of the partial mutual inductance. Currents are flowing in the length (L) directions and are assumed to be constant in the volume cells.*

The formula for the evaluation of the partial mutual inductance for the general conductor configuration in Fig. 3.18 is given by (19) and (20) in [22]. This evaluation of the partial mutual inductance uses the filament approximation resulting in a (VFI)PEEC model [55]. The filament approximation for partial mutual inductances partitions the cross sections of the conductors into filaments for which the partial mutual inductances are calculated and a geometrical mean is finally calculated. For problems in which Skin effects are of importance the (VFI)PEEC model and a surface impedance model [65] is widely used. It has been shown that the (VFI)PEEC model is not suitable for thin, wide, and partially overlapping conductor configurations [62]. For this case a *thin tape-tape (TT)* algorithm has been developed, (9) in [62]. A decision algorithm to select between the VFI or TT evaluation of the partial mutual inductance is based on the thickness to width ratios according to Table 2.

In the evaluation of the partial mutual inductances the direction of the volume cells are of great importance. The basic equation in (3.42) can be rewritten as (3.43) to

*Table 2: Decision scheme for the calculation of the partial mutual inductances. The abbreviations are indicated in Fig. 3.18.*

| | | | | |
|---|---|---|---|---|
| If | $W_1 > 3333T_1$ | and | $W_2 > 3333T_2$ | use TT |
| else | | | | use VFI |

illustrate the sign convention used for partial mutual inductances.

$$Lp_{\alpha\beta} = \frac{\mu}{4\pi}\frac{1}{a_\alpha a_\beta}\int_{a_\alpha}\int_{a_\beta}\int_{l_\alpha}\int_{l_\beta}\frac{|d\vec{l}_\alpha \cdot d\vec{l}_\beta|}{R}da_\alpha da_\beta \tag{3.43}$$

where $d\vec{l}$ is an element of a conductor with direction decided by the volume cell discretization (current direction), performed in the previous step. As noted from (3.43), there exists no (partial) mutual inductance between perpendicular discretized volume cells.

**Alternative Calculation Formulas for the Partial Inductances** The calculation of partial elements in the PEEC method can be performed using a number of different formulations applicable to specific cases. If the conductors have negligible thickness and are rectangular the basic formulation, (3.25), can be converted to a double surface integral over the two conductors [66] resulting in

$$Lp_{mn} = \frac{\mu}{4\pi}\frac{1}{w_m w_n}\iint_{s_m}\iint_{s_n}\frac{1}{R}\,ds_n\,ds_m \tag{3.44}$$

in which $w_{m,n}$ are the widths of the surface cells $s_m$ and $s_n$. Further, for two 'zero-thickness' cells, orthogonal and/or nonorthogonal, located in the same plane the original double volume integral can be converted to a double contour integral as described in [67] resulting in

$$Lp_{mn} = -\frac{\mu}{4\pi}\frac{1}{s_m s_n}\cdot\sum_{m=1}^{4}\sum_{n=1}^{4}\int_{l_m}\int_{l_n}R\,(\vec{u_n}\cdot\vec{u_m})\,dl_n\,dl_m \tag{3.45}$$

in which $\vec{u}_{m,n}$ are the outward normal vectors to surface cells $s_m$ and $s_n$. The main reason for performing the conversions is the reduced computational effort when using numerical integration routines, as detailed in the included Paper C, *Integration Order Selection Rules for a Full Wave PEEC Solver.*

**Coefficients of Potential**

The basic formula for calculating the *partial coefficients of potential*, (3.31), is repeated here for clarity.

$$p_{ij} = \frac{1}{S_i S_j}\frac{1}{4\pi\epsilon_0}\int_{S_i}\int_{S_j}\frac{1}{R}\,dS_j\,dS_i \tag{3.46}$$

In (3.46) $i$ and $j$ are two surface cells created in the discretization detailed in the previous section. If $j = i$ the result is entitled the *partial self coefficient of potential* of surface cell

$i$ while the general form of (3.46) gives the *partial mutual coefficients of potential* between two surfaces. Further, $S_i$ and $S_j$ are the surface areas of cell $i$ and $j$ respectively. The nominator $R$ is the center to center distance between cell $i$ and $j$ expressed as $R = |\vec{r}_i - \vec{r}_j|$.

The coefficients of potential representation is used for full wave PEEC models (models including time retardation) where the capacitive couplings are modelled using *pseudo-capacitances* [37] and delayed current- and/or voltage- sources. A simplification from the coefficient of potential representation to a lumped capacitive representation can be performed for quasi-static PEEC models since the lumped capacitive coupling is instant. The capacitive representation in the PEEC method is further discussed in [23, 68, 69].

The evaluation of (3.46) can be done using a proper numerical integration method. To avoid the problems detailed above, basic geometries have been defined for which analytical expressions for the partial element values exists. The basic geometries differs for the evaluation of the self and mutual terms and is therefore presented separately.

**Partial Self Coefficient of Potential** To obtain good accuracy and fast evaluation of the partial coefficients of potential basic geometries, building blocks, have been defined. To each basic geometry a formulation for the evaluation of the partial coefficient of potential is given. The most important basic geometry is the *rectangular surface cell* (ReSc) depicted in Fig. 3.19.

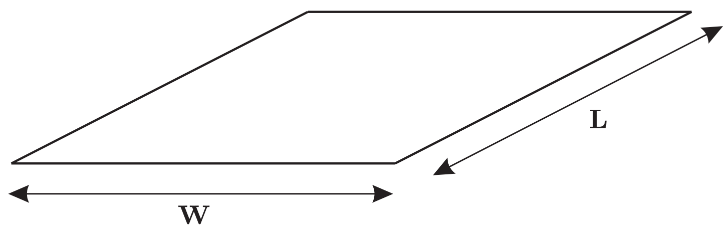


*Figure 3.19: Rectangular conductor geometry for the evaluation of the partial self coefficient of potential.*

The formula for the evaluation of the partial self coefficient of potential for the general rectangular conductor, (3.47), is given by a modified version of (16) in [22] which is used for the evaluation of the partial self inductance for thin conductors, see previous section.

$$\begin{aligned} p_{ii} &= \frac{L}{4\pi\epsilon_0}\frac{2}{3}\Bigg\{ 3\,ln[u + (u^2+1)^{\frac{1}{2}}] + u^2 + \frac{1}{u} \\ &+ 3\,u\,ln\left[\frac{1}{u} + (\frac{1}{u^2}+1)^{\frac{1}{2}}\right] - \left[u^{\frac{4}{3}} + (\frac{1}{u})^{\frac{2}{3}}\right]^{\frac{3}{2}}\Bigg\} \end{aligned} \tag{3.47}$$

where $u = \frac{L}{W}$ using the definitions from Fig. 3.19.

**Partial Mutual Coefficients of Potential** Effective calculation routines for partial mutual coefficients of potential are, as for the partial inductances, more important than for partial self coefficients of potential due to the mutual capacitive/electric field coupling of all surface cells in the discretization. For the partial mutual coefficients of potential calculations two basic geometries have been defined to speed up and retain good accuracy in the partial element calculations. The most important basic geometry is the mutual coupling between two rectangular surface cells, Fig. 3.20.

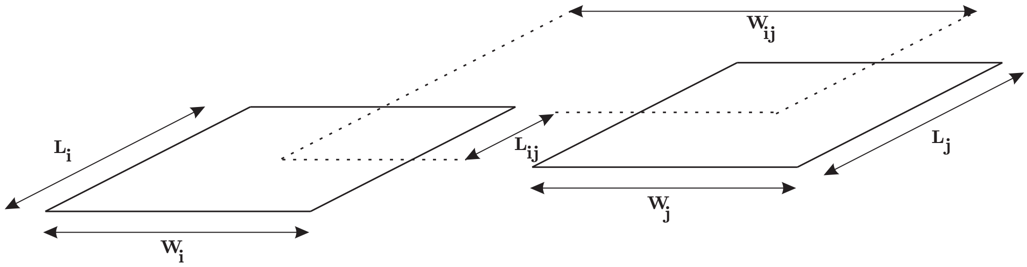


*Figure 3.20: Coplanar rectangular conductor geometry for the evaluation of the partial mutual coefficient of potential.*

The formula for the evaluation of the partial mutual coefficient of potential for the general conductor configuration in Fig. 3.20 is given by a modified version of the *thin tape-tape* (TT) algorithm used for partial mutual inductances for thin and wide conductors. The equation uses the notations in Fig. 3.20 and is given by

$$\begin{aligned} p_{ij} &= \frac{1}{4\pi\epsilon}\frac{1}{W_i L_i W_j L_j}\sum_{k=1}^{4}\sum_{m=1}^{4}(-1)^{m+k}\left[\frac{b_m^2 - C^2}{2}a_k\,\ln(a_k+\rho)\right. \\ &\left. + \frac{a_k^2 - C^2}{2}b_m\,\ln(b_m+\rho) - \frac{1}{6}(b_m^2 - 2C^2 + a_k^2)\rho - b_m\,C\,a_k\tan^{-1}\frac{a_k\,b_m}{\rho\,C}\right] \end{aligned} \tag{3.48}$$

where

$$\rho = (a_k^2 + b_m^2 + C^2)^{\frac{1}{2}}$$

$$a_1 = W_{ij} - \frac{W_i}{2} - \frac{W_j}{2}, \qquad a_2 = W_{ij} + \frac{W_i}{2} - \frac{W_j}{2}$$

$$a_3 = W_{ij} + \frac{W_i}{2} + \frac{W_j}{2}, \qquad a_4 = W_{ij} - \frac{W_i}{2} + \frac{W_j}{2}$$

$$b_1 = L_{ij} - \frac{L_i}{2} - \frac{L_j}{2}, \qquad b_2 = L_{ij} + \frac{L_i}{2} - \frac{L_j}{2}$$

$$b_3 = L_{ij} + \frac{L_i}{2} + \frac{L_j}{2}, \qquad b_4 = L_{ij} - \frac{L_i}{2} + \frac{L_j}{2}$$

and $C$ is the distance between the two planes containing surface cell $i$ and $j$.

The second basic geometry is the coupling between two cells oriented perpendicular to each other as seen in Fig. 3.21. The evaluation of the perpendicular surface cell partial mutual coefficient of potential is given by (16) in [23].

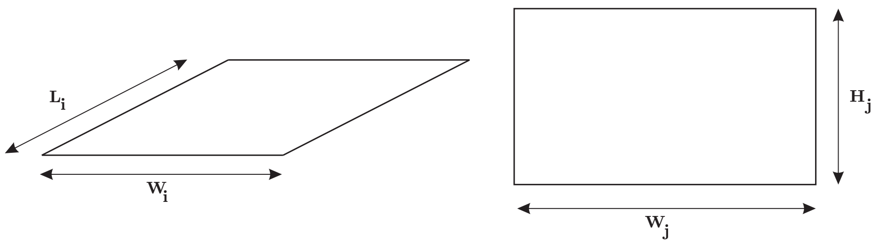


*Figure 3.21: Rectangular surface conductor geometry for the evaluation of the partial mutual coefficient of potential.*

**Alternative Calculation Formulas for the Partial Capacitances** The alternative calculation routine for partial inductances using the conversion to a contour integral, (3.45), is applicable for partial coefficients of potential calculation as well [70].

### Resistances

The partial resistances in a PEEC model is calculated using the volume cell discretization and the resistance formula from (3.35) as

$$R_\gamma = \frac{l_\gamma}{a_\gamma \sigma_\gamma} \tag{3.49}$$

where $l_\gamma$ is the length of the volume cell in the current direction, $a_\gamma$ is the cross section normal to the current direction, and $\sigma_\gamma$ is the conductivity of the volume cell material.

The resistance in the PEEC models accounts for the losses in the conductors and can be omitted for loss-less PEEC models and/or to improve agreement with theoretical results, see further included paper D, *Nonorthogonal PEEC Formulation for Time- and Frequency-Domain EM and Circuit Modeling.*

### Surface- and volume cell delays

For ($\tau$)PEEC models, PEEC models including retardation, the retarded electric and magnetic field couplings are represented by the mutual partial elements and the corresponding free space travel time. The retarded formulation for the mutual partial inductances ensures that a current flowing in one volume cell couples through the mutual inductance to all other volume cells at a delayed time to correctly model the magnetic field coupling. The retarded formulation for the mutual partial capacitances ensures that a charge density on one surface cell couples through the mutual capacitances to all other surface cells at a delayed time to correctly model the electric field coupling.

The retarded time, $\tau$, is calculated as the free space travel time between the center points, $\vec{r_1}$ and $\vec{r_2}$, of the corresponding volume or surface cells as

$$\tau = \frac{|\vec{r_1} - \vec{r_2}|}{c} \tag{3.50}$$

where $c = 3 \cdot 10^8$ m/s.

#### Excess Capacitance

When using dielectric materials in the PEEC method the excess capacitance of a dielectric cell needs to be calculated as defined by (3.36). The calculation is straightforward and requires no further investigation.

### 3.3.5 Matrix formulation

This section describes the collection of the partial elements into a solvable equation system used for the extraction of the currents in the volume cells, the charge densities at the surface cells, and the node potentials. Focus is on the frequency domain solution of PEEC models, however, the time domain solution is briefly discussed.

For the solution of PEECs in the time and frequency domain an *Admittance Method* and a *Modified Nodal Analysis* (MNA) [71, 72] method is presented. The Admittance Method produces a minimal but dense system matrix to obtain the voltages in the structure. The MNA solves for both voltages and currents in a structure and therefore produces a larger, and sparse, system matrix. The MNA method is widely used in modern circuit analysis software due to its full-spectrum properties and flexibility to include additional circuit elements. The choice between the two methods depend on the specific problem at hand and the computational resources available.

The time- and frequency- domain solution of PEECs resorts on a general rule to store partial elements and circuit specific parameters. The approach is detailed in the next section and utilized in the following time- and frequency domain circuit equation formulation.

#### Matrix Storage of Partial Elements

The calculated values of all the partial elements, as detailed in the previous section, are stored in matrices to facilitate the formulation of circuit equations and the following solution. The approach is explained using a simple geometry, Fig. 3.22, representing a three conductor geometry.

The partial elements are stored according to the following scheme:

- *The Partial Inductance Matrix*, **L**
  The partial inductances are calculated using (3.25) and the discretization resulting from the node-placement in Fig. 3.22. For simplicity the volume cells are separated using Greek letters according to Fig. 3.23.

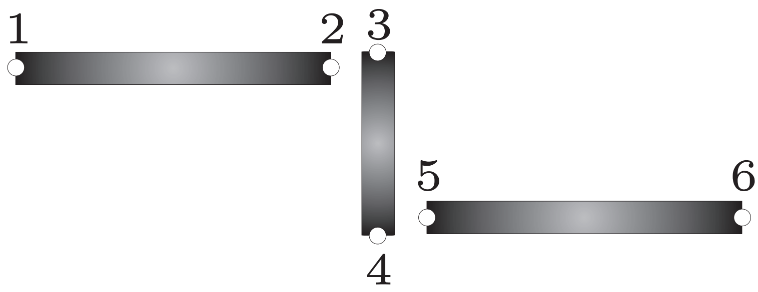


*Figure 3.22: Three conductor geometry with numbered nodes indicated by white circles.*

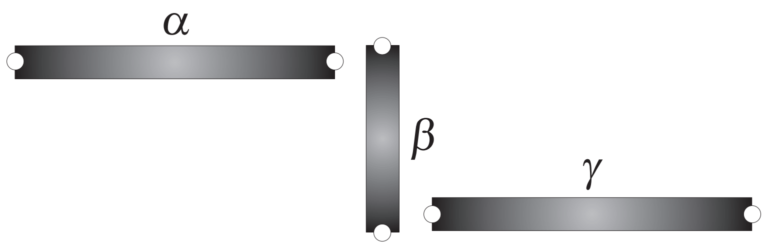


*Figure 3.23: Three conductor geometry with volume cell partitions $\alpha, \beta$, and $\gamma$.*

The corresponding partial inductance matrix is then

$$\mathbf{L} = \begin{bmatrix} L_{\alpha\alpha} & 0 & L_{\alpha\gamma} \\ 0 & L_{\beta\beta} & 0 \\ L_{\gamma\alpha} & 0 & L_{\gamma\gamma} \end{bmatrix} \tag{3.51}$$

where the notation $L_{xx}$ is used for the partial self inductance for volume cell $x$ and $L_{xy}$ for the partial mutual inductance between volume cell $x$ and $y$. Since inductive partition $\beta$ is perpendicular to the other two inductive partitions, $\alpha$ and $\gamma$, the partial mutual inductance is zero. Since the partial inductance matrix is symmetric, $L_{\gamma\alpha} = L_{\alpha\gamma}$, for $N$ inductive partitions, $N$ partial self and $\frac{N^2-N}{2}$ partial mutual inductances have to be calculated. The symmetry can also be used to reduce the storage requirements for the partial inductance matrix and the partial coefficients of potential matrix as described below.

- *The Partial Coefficient of Potential Matrix*, **P**
  The partial coefficients of potential are calculated using (3.31) and the discretization resulting from the node-placement in Fig. 3.22. For simplicity the surface cells are separated using the same numbers as the nodes according to Fig. 3.24.

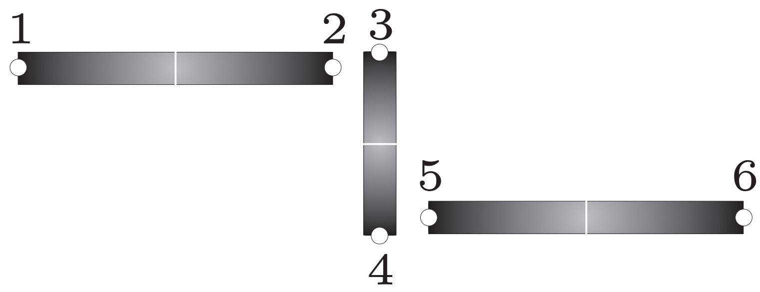


*Figure 3.24: Three conductor geometry with surface cell partitions 1 to 6.*

The corresponding partial coefficient of potential matrix is then

$$\mathbf{P} = \begin{bmatrix} p_{11} & p_{12} & p_{13} & p_{14} & p_{15} & p_{16} \\ p_{21} & p_{22} & p_{23} & p_{24} & p_{25} & p_{26} \\ p_{31} & p_{32} & p_{33} & p_{34} & p_{35} & p_{36} \\ p_{41} & p_{42} & p_{43} & p_{44} & p_{45} & p_{46} \\ p_{51} & p_{52} & p_{53} & p_{54} & p_{55} & p_{56} \\ p_{61} & p_{62} & p_{63} & p_{64} & p_{65} & p_{66} \end{bmatrix} \tag{3.52}$$

where the notation $p_{xx}$ is used for the partial self coefficient of potential for surface cell $x$ and $p_{xy}$ for the partial mutual coefficient of potential between surface cells $x$ and $y$. The **P**-matrix is full in this case since all surfaces are coupled to each other. However, for 3D PEEC models, charge free surfaces can exist and cause zero elements in the **P**-matrix [36]. As for the partial inductance matrix symmetry can be used to fill the **P**-matrix in an efficient manner.

- *The Resistance Matrix,* **R**
  The volume cell resistances are calculated from the volume cell discretization shown in Fig. 3.23 using (3.49). Since no resistive coupling exists between the volume cells the resulting **R**-matrix is a diagonal matrix. For the example in Fig. 3.22 the resistance matrix is

$$\mathbf{R} = \begin{bmatrix} R_{\alpha\alpha} & 0 & 0 \\ 0 & R_{\beta\beta} & 0 \\ 0 & 0 & R_{\gamma\gamma} \end{bmatrix} \tag{3.53}$$

  where the notation $R_{xx}$ is used for the resistance for volume cell $x$.

- *The Excess Capacitance of Dielectric Cell Matrix,* $\mathbf{C}_e$
  For dielectric cells the excess capacitance is calculated using (3.36) and the volume cell discretization of the dielectric structure. As for the resistance matrix no cross couplings exist among the excess capacitances which results in a diagonal $\mathbf{C}_e$-matrix. The three conductor geometry in Fig. 3.22 contains no dielectric areas which results in an empty $\mathbf{C}_e$-matrix. The dielectric inclusion in the PEEC model is further discussed in [25, 36].

- *Connectivity Matrix,* **A**
  To be able to formulate and solve the PEEC equations in both the time and frequency domain a *Connectivity Matrix* is needed that describes the connection of the partial inductances to the PEEC nodes. The entries in the **A**-matrix are created using the following rules :

  1. Each row corresponds to one volume cell/partial inductance.
  2. Each column corresponds to one PEEC node.
  3. The entry -1 at row $m$ and column $n$ in **A** indicates that the current direction in volume cell $m$ is from node $n$.
  4. The entry 1 at row $m$ and column $n$ in **A** indicates that the current direction in volume cell $m$ is into node $n$.

  This results in the **A**-matrix for the example in Fig. 3.22 according to

$$\mathbf{A} = \begin{bmatrix} -1 & 1 & 0 & 0 & 0 & 0 \\ 0 & 0 & -1 & 1 & 0 & 0 \\ 0 & 0 & 0 & 0 & -1 & 1 \end{bmatrix} \tag{3.54}$$

- *Node Reduction Matrix,* $\boldsymbol{R_V}$
  A second PEEC model information-matrix needed for the formulation of the circuit equations is the *Node Reduction Matrix*, $\mathbf{R_V}$. This matrix reduces multiple PEEC nodes at one geometrical point in a PEEC model to only one single PEEC node and performs the summation of the coefficients of potential contributions from each surface to one combined node coefficient of potential. Multiple PEEC nodes and/or surfaces at one geometrical point appear for 3D PEEC models and when 1D and 2D PEEC discretizations are put together. This problem is detailed in the included paper F, *3D PEEC Capacitance Calculations*. The entries in the $\mathbf{R_V}$ matrix are created using the following rules :

  1. Each row corresponds to one geometrical point before reduction.
  2. Each column corresponds to one geometrical point after reduction.
  3. The entry 1 at row $m$ and column $n$ in the $\mathbf{R_V}$ matrix indicates that the geometrical points $m$ and $n$ will be joint after the reduction.

  The example in Fig. 3.24 has no multiple PEEC nodes. Consider, as an example, to join node two with node three and node four with node five in the three conductor structure would result in a PEEC model for a bent conductor geometry with a $\mathbf{R_V}$ matrix written as

$$\mathbf{R_V} = \begin{bmatrix} 1 & 0 & 0 & 0 \\ 0 & 1 & 0 & 0 \\ 0 & 1 & 0 & 0 \\ 0 & 0 & 1 & 0 \\ 0 & 0 & 1 & 0 \\ 0 & 0 & 0 & 1 \end{bmatrix} \tag{3.55}$$

**Frequency Domain Circuit Equations for the Solution of PEEC Models**

The full-wave solution of PEEC models require the correct representation of the retarded electric- and magnetic- field couplings, see (3.39). The individual retardation terms are included in the off-diagonal entries in the partial inductance- and partial coefficient of potential- matrices resulting in complex matrix entries.

**Admittance Method Circuit Equations** The circuit equations in the Admittance method are built by using the PEEC cell in Fig. 3.25 and formulated as matrix equations using the previously defined matrices. In Fig. 3.25 the magnetic and electric coupling terms, $V_m^L$ and $V_i^C$ respectively, have been replaced by its frequency domain correspondence and the summations are over $N$ capacitive and $M$ inductive cells. Further, $V_{C_x}$ denotes voltage over *pseudo-capacitance* $C_x = \frac{1}{P_{xx}}$ and $Y_{ij}$ is a possible lumped circuit component connected between node $i$ and $j$.

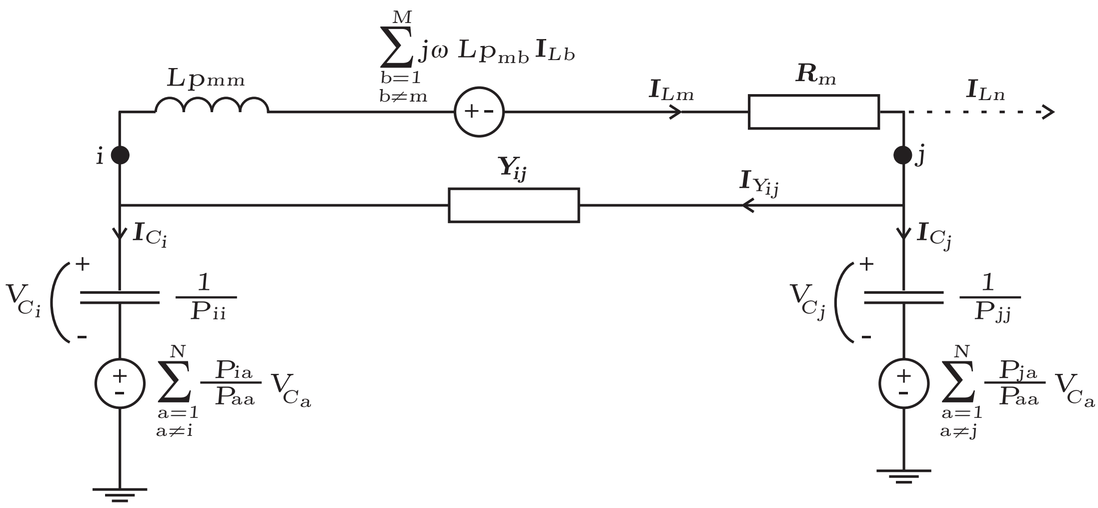


*Figure 3.25: A PEEC one-cell used in the development of the Admittance method circuit equations.*

The circuit equations are collected in three steps :

1. Kirchoff's voltage law is applied to the inductive branch in Fig. 3.25 resulting in

$$V_i - j\omega\, Lp_{mm}\, I_{Lm} - \sum_{b=1, b\neq m}^{M} j\omega\, Lp_{mb}\, I_{Lb} - R_m\, I_{Lm} - V_j = 0 \tag{3.56}$$

This equation can be written in matrix form as

$$-\mathbf{AV} \;-\; (\mathbf{R} + j\omega\mathbf{L})\, \mathbf{I}_L = \mathbf{V}_S \tag{3.57}$$

where $\mathbf{V}_S$ is a voltage source excitation.

2. Kirchoff's current law (KCL) is applied to each node. For example, KCL for node $j$ can be written as

$$I_{Lm} = I_{Ln} + I_{Y_{ij}} + I_{Cj} \tag{3.58}$$

and further expanded as

$$I_{Lm} = I_{Ln} + (V_j - V_i)Y_{ij} + j\omega C_{jj} V_{C_j} \tag{3.59}$$

This equation can be written in matrix form as

$$\mathbf{Y}_L\mathbf{V} \ + \ j\omega\mathbf{F}\mathbf{V}_c \ - \ \mathbf{A}^T\mathbf{I}_L = \mathbf{I}_S \tag{3.60}$$

in which $\mathbf{I}_S$ is a current source excitation vector, $\mathbf{Y}_L$ is an admittance matrix describing the lumped components, and $\mathbf{F}$ is a $N \times N$ diagonal matrix containing the admittances of the pseudo-capacitances, ie. entries according to

$$F_{nn} = C_{nn} \tag{3.61}$$

3. The potentials at the nodes are expressed using its constituents parts as, for instance, for node $j$ as

$$V_j = V_{C_j} + \sum_{a=1, a\neq j}^{N} \frac{P_{ja}}{P_{aa}} V_{C_a} \tag{3.62}$$

This equation can be written in matrix form as

$$-\mathbf{V} \ + \ \mathbf{S}\mathbf{V}_c = 0 \tag{3.63}$$

in which $\mathbf{S}$ is a $N \times N$ matrix containing the retarded electric field couplings with (complex) elements of the type

$$S_{ij} = \frac{p_{ij}}{p_{jj}} \tag{3.64}$$

The matrix equations described in (3.57), (3.60) and (3.63) can be reformulated to solve for the node potentials $\mathbf{V}$ and charges $\mathbf{q}$, or inductor currents $\mathbf{I}_L$ according to

$$\begin{bmatrix} -\mathbf{A} & -(\mathbf{R} + j\omega\mathbf{L}) \\ j\omega\mathbf{P}^{-1} + \mathbf{Y}_L & -\mathbf{A}^T \end{bmatrix} \begin{bmatrix} \mathbf{V} \\ \mathbf{I}_L \end{bmatrix} = \begin{bmatrix} \mathbf{V}_S \\ \mathbf{I}_S \end{bmatrix} \tag{3.65}$$

$$\mathbf{V} = \mathbf{P}\,\mathbf{q} \tag{3.66}$$

Using the previously defined matrices it is possible to construct the admittance matrix for the PEEC model as

$$\mathbf{Y} = (\mathbf{A}^T(\mathbf{R} + j\omega\mathbf{L} - j\omega^{-1}\mathbf{C}_e)^{-1})\mathbf{A} + j\omega(\mathbf{R_V}^T\,\mathbf{P}^{-1}\,\mathbf{R_V}) + \mathbf{Y}_L \tag{3.67}$$

from which the node potentials $\mathbf{V}$ are found by solving

$$\mathbf{V} = \mathbf{Y}^{-1}\mathbf{I}_S \tag{3.68}$$

Eq (3.67) and (3.68) is referred to as the Admittance method in this thesis. In (3.67) the $\mathbf{C}_e$ matrix, used to model dielectric cells, and the $\mathbf{R_V}$ matrix, used to remove multiple nodes and surfaces, have been included. The volume cell currents can then be calculated using post-processing as

$$\mathbf{I}_L \;=\; (\mathbf{R} + j\omega\mathbf{L})^{-1}(-\mathbf{AV} - \mathbf{V}_S) \tag{3.69}$$

(3.67) can be used for all types of PEEC models simply by excluding the unwanted partial elements. For instance, the admittance method for $(L_p, P)$PEEC models is written and solved as

$$\mathbf{V} = (\mathbf{A}^T\,(j\omega\mathbf{L})^{-1}\,\mathbf{A} + j\omega(\mathbf{R_V}^T\,\mathbf{P}^{-1}\,\mathbf{R_V}))^{-1}\,\mathbf{I}_S \tag{3.70}$$

**Modified Nodal Analysis (MNA) Method** Using a MNA method all the node potentials and inductive branch currents are calculated at the same time. The system matrix that is created is larger than for the Admittance Method but is also more sparse and the use of sparse matrix solvers are possible. The MNA method described here is derived from the Admittance matrix formulation in (3.65) by using the following matrix properties

$$j\omega\mathbf{P}^{-1} = j\omega\mathbf{F}\mathbf{S}^{-1} \tag{3.71}$$

$$j\omega\mathbf{F}\mathbf{S}^{-1} = j\omega{\mathbf{S}^{-1}}^T\mathbf{F} \tag{3.72}$$

resulting in a system of equations according to

$$\begin{bmatrix} -\mathbf{A} & -(\mathbf{R} + j\omega\mathbf{L}) \\ & \\ j\omega\mathbf{F} + \mathbf{S}^T\mathbf{Y}_L & -\mathbf{S}^T\mathbf{A}^T \end{bmatrix} \begin{bmatrix} \mathbf{V} \\ \\ \mathbf{I}_L \end{bmatrix} = \begin{bmatrix} \mathbf{V}_S \\ \\ \mathbf{S}^T\mathbf{I}_S \end{bmatrix} \tag{3.73}$$

In this formulation, the node potentials $\mathbf{V}$ and volume cell currents $\mathbf{I}_L$ are given without the computationally heavy inversion of the coefficient of potential matrix $\mathbf{P}$ in contrast to the Admittance method described in the previous section. This formulation is referred to as the MNA method in this thesis.

### Time Domain Circuit Equations for the Solution of PEEC Models

The time domain equations for the solution of PEEC model problems can be derived in the same way as for the frequency domain. The difference is the inclusion of the time retardation that is expressed as a complex part in the partial mutual couplings for frequency domain models, (3.74), while for time domain PEEC models the retardation is written as a finite time delay, (3.75) (the two equations displays the induced voltage in cell $\alpha$ due to the magnetic field coupling with cell $\beta$).

$$V_{\alpha\beta} = j\omega Lp_{\alpha\beta}\; I_\beta\; e^{-j\omega\tau_{\alpha\beta}} \tag{3.74}$$

$$v_{\alpha\beta} = Lp_{\alpha\beta}\,\frac{di_\beta(t - \tau_{\alpha\beta})}{dt} \tag{3.75}$$

The two following sections details the time domain solution of quasi-static PEEC models using the previously defined Admittance matrix- and MNA- formulation.

**Admittance Method Circuit Equations** For quasi-static time domain PEEC models the time domain circuit equations using the Admittance method can be written as

$$\begin{bmatrix} -\mathbf{A} & -(\mathbf{R}+\mathbf{L}\frac{d}{dt}) \\ \mathbf{P}^{-1}\frac{d}{dt}+\mathbf{Y}_L & -\mathbf{A}^T \end{bmatrix} \begin{bmatrix} \mathbf{V} \\ \mathbf{I}_L \end{bmatrix} = \begin{bmatrix} \mathbf{V}_S \\ \mathbf{I}_S \end{bmatrix} \tag{3.76}$$

similar to [56]. Discretizing matrix (3.76) in time by using the Backward Euler (BE) scheme yields

$$\begin{bmatrix} -\mathbf{A} & -(\mathbf{R}+\mathbf{L}\frac{1}{dt}) \\ \mathbf{P}^{-1}\frac{1}{dt}+\mathbf{Y}_L & -\mathbf{A}^T \end{bmatrix} \begin{bmatrix} \mathbf{V}_n \\ \mathbf{I}_{nL} \end{bmatrix} = \begin{bmatrix} \mathbf{V}_S-\mathbf{L}\frac{1}{dt}\mathbf{I}_{n-1_L} \\ \mathbf{I}_S+\mathbf{P}^{-1}\frac{1}{dt}\mathbf{V}_{n-1} \end{bmatrix} \tag{3.77}$$

Which can be formulated to a single equation to calculate the current PEEC node voltages, $\mathbf{V}_n$, as

$$\begin{aligned} \mathbf{V}_n \;=\; & \left[\mathbf{P}^{-1}\frac{1}{dt}+\mathbf{Y}+\mathbf{A}^T\left(\mathbf{R}+\mathbf{L}\frac{1}{dt}\right)^{-1}\mathbf{A}\right]^{-1} \\ & \left[\mathbf{I}_S+\mathbf{P}^{-1}\frac{1}{dt}\mathbf{V}_{n-1}-\mathbf{A}^T(\mathbf{R}+\mathbf{L}\frac{1}{dt})^{-1}(\mathbf{V}_S-\mathbf{L}\frac{1}{dt}\mathbf{I}_{n-1})\right] \end{aligned} \tag{3.78}$$

And the volume cell currents can be calculated using post-processing as

$$\mathbf{I}_n = -\left[\mathbf{R}+\mathbf{L}\frac{1}{dt}\right]^{-1}\left[\mathbf{V}_S-\mathbf{L}\frac{1}{dt}\mathbf{I}_{n-1}-\mathbf{A}\mathbf{V}_n\right] \tag{3.79}$$

**Modified Nodal Analysis (MNA) Method** For quasi-static time domain PEEC models, the TD-MNA system can be written as

$$\begin{bmatrix} -\mathbf{A} & -(\mathbf{R}+\mathbf{L}\frac{d}{dt}) \\ \mathbf{F}\frac{d}{dt}+\mathbf{S}^T\mathbf{Y}_L & -\mathbf{S}^T\mathbf{A}^T \end{bmatrix} \begin{bmatrix} \mathbf{V} \\ \mathbf{I}_L \end{bmatrix} = \begin{bmatrix} \mathbf{V}_S \\ \mathbf{S}^T\mathbf{I}_S \end{bmatrix} \tag{3.80}$$

Discretizing matrix (3.80) in time by using the Backward Euler (BE) scheme yields

$$\begin{bmatrix} -\mathbf{A} & -(\mathbf{R}+\mathbf{L}\frac{1}{dt}) \\ \mathbf{F}\frac{1}{dt}+\mathbf{S}^T\mathbf{Y}_L & -\mathbf{S}^T\,\mathbf{A}^T \end{bmatrix} \begin{bmatrix} \mathbf{V}_n \\ \mathbf{I}_{nL} \end{bmatrix} = \begin{bmatrix} \mathbf{V}_S-\mathbf{L}\frac{1}{dt}\mathbf{I}_{n-1_L} \\ \mathbf{S}^T\mathbf{I}_S+\mathbf{F}\frac{1}{dt}\mathbf{V}_{n-1} \end{bmatrix} \tag{3.81}$$

where for a fixed time step, $dt$, the leftmost block only has to be calculated once.

It is noted that for quasi-static time domain PEEC models only the previous voltages, $\mathbf{V}_{n-1}$, and currents, $\mathbf{I}_{n-1L}$ have to be stored to calculate the current ones. For full-wave TD PEEC models, accounting for the individual retardation between the surface and volume cells, even more instances of voltages and currents needs to be stored, resulting in storage and computationally heavy calculations. The system of ordinary differential equations (ODEs) describing the quasi-static PEEC model is transformed into a system of neutral delay differential equations (NDDEs) [73, 74] for the full-wave case. The full-wave formulation require the separation of the self (instantaneous) and mutual (retarded) couplings in the previous matrix formulations resulting in

$$\mathbf{L} = \mathbf{L}_S + \mathbf{L}_M \tag{3.82}$$

$$\mathbf{S} = \mathbf{S}_S + \mathbf{S}_M \tag{3.83}$$

for the MNA method where the subscript $S$ and $M$ indicate self and mutual terms respectively. The resulting system of NDDEs is in the following form

$$\begin{cases} \mathbf{C}_0\,\mathbf{y}\prime(t) + \mathbf{G}_0\,\mathbf{y}(t) + \mathbf{C}_1\,\mathbf{y}\prime(t-\tau) + \mathbf{G}_1\,\mathbf{y}(t-\tau) = \mathbf{B}\,\mathbf{u}(t, t-\tau), & t > t_0 \\ \mathbf{y}(t) = \mathbf{g}(t), & t \leq t_0 \end{cases} \tag{3.84}$$

where the matrices $\mathbf{C}_0$, $\mathbf{G}_0$, $\mathbf{C}_1$, $\mathbf{G}_1$, and $\mathbf{B}$ are real-valued and unrelated to previous matrix notations and the retarded couplings must be interpreted in an operator sense. The separation of self- and mutual- terms results in an extended right hand side in the corresponding equation system, since the mutual couplings are considered to be known (since they are related to past current and voltage values), and require constant re-evaluation for each time step. The TD modeling of PEECs is further investigated in [75, 76, 77].

**PEEC model complexity reduction**

Model reduction for PEEC models can be obtained from the original electromagnetic model previously referred to as $(L_p, P, R, \tau)$PEEC by simply excluding the unwanted PEEC model elements [7, 8, 78, 79, 80]. The exclusion of time retardation, resulting in a $(L_p, P, R)$PEEC model, enables the usage of commercial circuit solvers like SPICE and has proven to be efficient for EM analysis except for prediction of electromagnetic radiation when retardation plays an important role [52, 54]. Model complexity reduction is further discussed in the included paper A, *Simplified PEEC Models for PCB Structures and Comparison to Experimental Data*.

**PEEC model order reduction**

The basic idea of model order reduction (MOR) techniques is to reduce the size of a system described by circuit equations by only describing the dominant behavior of the original system [81]. Within quasi-static PEEC modeling the PRIMA algorithm [82] has been used with good results as shown in [83, 84].

### 3.3.6 Matrix solution

For frequency domain full wave PEEC models the off diagonal terms in the $\mathbf{L}$ and $\mathbf{P}$ matrices are complex to account for the retardation. Thus, a complex solution in terms of node voltages and/or volume cell currents is obtained. The more simple Admittance method creates a dense system matrix resulting in a more time consuming solution process. The MNA method system matrix is sparse and suitable sparse solver package can be used for the solution of the currents and voltages in an efficient manner.

### 3.3.7 Back end / Graph viewer

The Back End / Graph viewer is basically a post-processor used for viewing and manipulation of PEEC model results and can be used to :

- Calculate branch currents when using the Admittance method.
- Display and print resulting node voltages and branch currents.
- Calculate electric and magnetic field strengths for the test object at given locations.

### 3.3.8 Stability of PEEC models

In Fig. 3.10, presenting a general flowchart for PEEC based EM simulations, the two conditions **Stable** and **Unstable** are represented. The reasons are the instabilities that can be observed in the solution of PEEC time- and frequency-domain simulations. The instabilities are observed as spurious resonances of large amplitudes in both the time- and frequency-domain, see Fig. 3.26 for time domain example. The problem is typical for integral equation methods and thus not specific for the PEEC method.

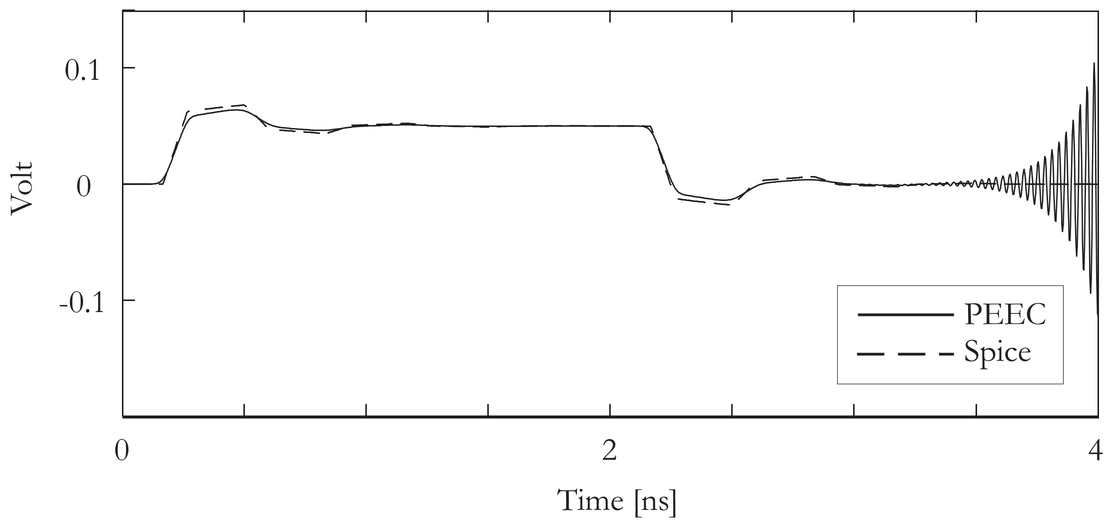


*Figure 3.26: Example of 'Late time instability' in a TD PEEC simulation.*

The instabilities in the PEEC method can be traced back to the :

- Discretization of the integral equation [85, 86] (both time- and frequency-domain PEEC models).
- The numerical technique used for the time integration [75] (only time domain PEEC models).

Both these problems have been discussed in the literature and actions have been proposed to stabilize PEEC models. The most important additions for stabilizing the basic PEEC formulation are discussed in the following sections.

### +PEEC Formulation

The most important addition to stabilize PEEC models is the +PEEC formulation detailed in [70]. The +PEEC formulation suggests a refined calculation of the partial elements to obtain a better phase response in the +PEEC model than in the basic PEEC model. The formulation utilizes a partitioning of the volume- and surface-cells for both self and partial mutual element calculations. This results in the new partial inductance calculation according to

$$L^{+}_{p_{ij}} = \frac{\mu}{4\pi}\frac{1}{a_i a_j}\sum_{k=1}^{M_i}\sum_{kk=1}^{N_i}\sum_{q=1}^{M_j}\sum_{qq=1}^{N_j} e^{-j\beta R_{k,kk,q,qq}} \int_{a_k}\int_{l_{kk}}\int_{a_q}\int_{l_{qq}} \frac{d\vec{l}_{kk}\cdot d\vec{l}_{qq}}{R}\, dl_{qq}\, da_q\, dl_{kk}\, da_k \tag{3.85}$$

to be compared with the original formulation (with the retardation term included)

$$L_{p_{ij}} = e^{-j\beta R_{ij}} \frac{\mu}{4\pi}\frac{1}{a_i a_j}\int_{a_i}\int_{a_j}\int_{l_i}\int_{l_j}\frac{d\vec{l}_j\cdot d\vec{l}_i}{R}\, da_i\, da_j \tag{3.86}$$

In (3.85) the two inductive cells have been partitioned into $M \times N$ subcells with a maximum dimension $\Delta$ according to

$$\Delta = \frac{c}{n\, f_e} \tag{3.87}$$

where $c = 3 \cdot 10^8$, $n$ is varied and $f_e$ corresponds to the extended frequency range upper limit. The extended frequency range is calculated from the maximum frequency, $f_{max}$, in the active frequency range as

$$f_e \approx 50\, f_{max} \tag{3.88}$$

This gives a good phase representation for frequencies corresponding to $50 f_{max}$ and results in a more stable PEEC model without introducing additional number of unknowns. The key issue in the +PEEC formulation is not to improve the PEEC model in the active frequency region, instead, the behavior in the extended frequency region is considered. More specifically, the input impedance of FD-PEEC models in the extended frequency range is considered to ensure passivity of the corresponding PEEC models. A negative input impedance in the active or extended frequency range implies a nonphysical (or active) PEEC model prone for instabilities in the time domain. The +PEEC formulation improves the behavior in the extended frequency range and in the possible time domain solution.

The same procedure (partitioning) as described above is also applied for the calculation of the partial coefficients of potential to improve stability for PEEC models.

### Parallel Damping Resistors

To further stabilize PEEC models in the extended frequency range a parallel damping resistor can be used in conjunction with the +PEEC formulation, resulting in the +RPEEC formulations. The basic PEEC model including the parallel damping resistor is shown in Fig. 3.27.

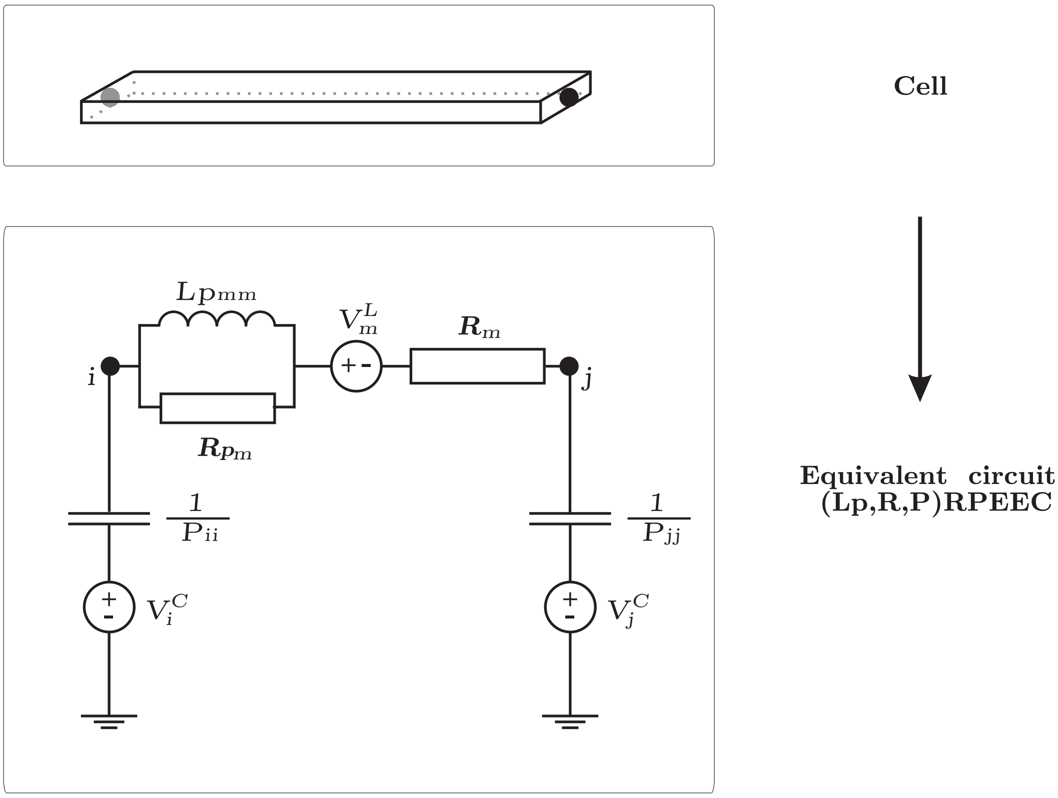


*Figure 3.27: PEEC model for conductor including parallel damping resistor to improve stability.*

The inclusion of the parallel resistance, $R_{p_m}$ in Fig. 3.27, introduces losses in the PEEC model that can improve the stability without increasing the number of unknowns. The value of the parallel damping resistance is calculated for each cell according to

$$R_{p_m} = k\,\omega_{max}\,Lp_{mm} \tag{3.89}$$

where $\omega_{max} = 2\,\pi\,f_{max}$ and $k\ =\ 10, ..., 100$ depending on the problem [70].

### PEEC model stability analysis

The two previous sections details actions that can improve stability that is taken before the final equation system, that is to be solved, is constructed. After construction of the final equation system, simple mathematical analysis of the system matrix gives important information on the stability of the PEEC model. As detailed in [86], the system matrix, $M(z)$, for a small $(L_p, P, \tau)$PEEC problem is constructed and the locations of the roots of $\det M(z)$ is studied. If no roots are located in the right half plane the system matrix is invertible in the right half plane and the PEEC model is stable. The system matrix is reproduced in (3.90) for clarity using the notations for partial elements from previous sections.

$$M(z) = \begin{bmatrix} \frac{z}{p_{11}} & 0 & 0 & -\frac{p_{12}}{p_{11}} e^{-\tau_1 z} + 1 & \frac{p_{12}}{p_{11}} e^{-\tau_1 z} - \frac{p_{13}}{p_{11}} e^{-\tau_2 z} \\ 0 & \frac{z}{p_{22}} & 0 & \frac{p_{12}}{p_{22}} e^{-\tau_1 z} - 1 & 1 - \frac{p_{23}}{p_{22}} e^{-\tau_1 z} \\ 0 & 0 & \frac{z}{p_{33}} & \frac{p_{13}}{p_{33}} e^{-\tau_2 z} - \frac{p_{23}}{p_{33}} e^{-\tau_1 z} & \frac{p_{23}}{p_{33}} e^{-\tau_1 z} - 1 \\ -1 & 1 & 0 & z\, L_{p_{11}} & z\, e^{-\tau_L z}\, z\, L_{p_{12}} \\ 0 & -1 & 1 & z^{\tau_L z} L_{p_{12}} & z\, L_{p_{22}} \end{bmatrix} \tag{3.90}$$

It was found that for a model with zero delays, i.e. setting $\tau_1 = \tau_2 = \tau_L = 0$ in (3.90), all the roots of det $M(z)$ lie on the imaginary axis and the system is inherently stable. When introducing delays in the model some of the roots could be located in the right half-plane causing an unstable nonphysical model.

The system analysis described above is possible, but not practical for large PEEC models due to the computational effort required in the analysis. However, the analysis gives us insight and information on the complex stability problems PEEC models are subjected to.

#### Time integration methods

The solution of TD-PEEC models involves the construction and solution of the corresponding TD equations as detailed above. The stability-actions detailed in the previous sections can produce stable PEEC models *in combination* with a well suited time integration technique for the type of equations arising for PEEC models. Commonly used time integration techniques are the:

- Forward Euler.
- Backward Euler.
- Lobatto III-C[75].

Where the Backward Euler and Lobatto III-C is to prefer over the Forward Euler [75, 76] due to stability reasons.

This section on '*Stability of PEEC models*' has shortly introduced the stability problems associated with PEEC models. Much work is performed within this area and recent, unpublished, work has shown that the correlation between time- and frequency-domain PEEC models can be further used to overcome the stability problems.

### 3.3.9 Concluding remarks

This chapter has introduced some practical aspects of EM modeling using the PEEC method. For in-depth studies of each area the referred scientific articles should be reviewed.

# Chapter 4

# Thesis Summary

## 4.1 Summary of Contributions

This section gives a brief summary of the papers included in this thesis.

### 4.1.1 Paper A - **Simplified PEEC Models for PCB Structures and Comparison to Experimental Data**

Author: J. Ekman.
Reproduced from: Proc. of Progress in Electromagnetic Research Symposium, PIERS 2001, page 431, Osaka, Japan, July 2001.

This paper describe a technique to obtain simple $(L_p, P, R)$PEEC models for one layer PCB structures. The idea is to use a discretization strategy to facilitate the use of closed form equations to calculate the partial elements. The connection of touching partitions, at the same PEEC model nodes, are made through the use of small resistances to exclude the manual summation of the partial self capacitance to each node. This results in simplified partial element equivalent circuits useful in a design or analyzing process. The method only requires three equations for the partial element $(L_p, C)$ calculations and a student PSpice version as the solver. This makes the PEEC method an accessible EM simulation technique requiring only a freeware circuit simulation program as the solver.

### 4.1.2 Paper B - **Experimental Verification of PEEC Based Electric Field Simulations**

Author: J. Ekman.
Reproduced from: Proc. of 2001 IEEE International Symposium on EMC, pages 351–355, Montreal, Canada, August 2001.

EM simulations can be used to predict emission and immunity levels of electronic components and systems. This require in the PEEC method the use of post-processing equations to translate the system currents and voltages (circuit variables) into field variables, $\vec{E}$ and

$\vec{H}$. The disadvantage with the use of post-processing is the extra amount of work and the increased total computation time for the PEEC model analysis. A recent proposed technique describes and electric field sensor that can be included in the basic PEEC circuit simulation and deliver the emitted electric field at multiple user-specified locations. The benefits are the elimination of the post-processing related work and possible error sources. The electric field sensor is a special PEEC one-cell that is one-way coupled with the test object, i.e. the test object is coupled to the sensor but the sensor in not coupled to the test object. Several numerical test were carried out comparing post-processing and the sensor formulation. It was found that results obtained using the electric field sensor are sensible to the geometric shape of the sensor. The reasons are thought to be numerical problems involved in the computation of mutual partial elements for widely separated cells and the impact of the fixed discretization of the sensor for a wide variety of frequencies. At this stage the post-processing is to be preferred even though the amount of work increases considerably.

### 4.1.3 PAPER C - **Integral Order Selection Rules for a Full Wave PEEC Solver**

Authors: G. Antonini, J. Ekman, A. Orlandi.
Reproduced from: Proc. of the 15th Zurich Symposium on EMC, pages 431–436, Zurich, Switzerland, February 2003.

The task of computing partial elements fast and accurately is very important to facilitate correct EM modeling using the PEEC method. Since even for seemingly 'small' problems the number of partial elements can exceed several millions and inaccuracies can result in problems, as found in the included *Paper B*. The recent introduction of the nonorthogonal PEEC method will increased the use of numerical integration routines, to calculate partial elements, in PEEC based EM solvers. The increased use is due to the surface and volume cell discretizations in the nonorthogonal PEEC method consists of nonorthogonal cells for which existing analytical solutions for the calculation of the partial elements cannot be used. When using numerical integration for the calculation of partial elements the accuracy is proportional to the time consumed by the numerical routines. This paper introduces *The fast multi-function method*, (FMF)PEEC, in which the accuracy in the numerical integration routines, thus the accuracy in the mutual partial elements, are chosen depending on a mutual coupling factor. The speed up by using the *fast multi-function method* is in the order of 30 for realistic simulations.

### 4.1.4 PAPER D - **Nonorthogonal PEEC Formulation for Time- and Frequency-Domain EM and Circuit Modeling**

Authors: A. E. Ruehli, G. Antonini, J. Esch, J. Ekman, A. Mayo, A. Orlandi.
Reproduced from: IEEE Transactions on EMC, vol. 45, no. 2, pages 167–176, May 2003

The extension from the orthogonal to the nonorthogonal PEEC method is a major advancement of the technique and facilitates the modeling of complex structures, improves accuracy by reducing the use of staircase-approximations, and reduces the number of cells in the PEEC model discretizations. The paper details the basic integral equations for nonorthogonal geometries and the evaluation of the partial elements using global and local coordinate systems. Since the nonorthogonal formulation is consistent with the PEEC model for rectangular geometries the two formulations can be mixed to gain optimal performance. Among several numerical experiments 3D PEEC model simulations were compared against 2D transmission line PowerSpice simulations with very good agreement.

### 4.1.5 Paper E - **A Comparative Study of PEEC Circuit Elements Computation**

Authors: G. Antonini, J. Ekman, A. Ciccomancini Scogna, A. E. Ruehli.

Reproduced from: Proc. of IEEE International Symposium on EMC, 2003, Istanbul, Turkey, May 2003.

The fast and accurate computation of PEEC circuit elements, partial inductances and coefficients of potential, is one of the most challenging problems within PEEC modeling. Recently the fast multipole method (FMM) has been applied to the PEEC method in the frequency domain. In this paper the evaluation of PEEC elements is performed by means of two methods: a matrix version of the hybrid FMMPEEC method and the *fast multi-function approach*, (FMF)PEEC, detailed in the included *Paper C*. Implementation issues are addressed and discussed. The accuracy of both the methods are clarified and validated via the analysis of several case studies. Both the methods offers very good speed up and flexibility in the partial element calculations suitable for the calculation of nonorthogonal PEEC partial elements.

### 4.1.6 Paper F - **3D PEEC Capacitance Calculations**

Authors: J. Ekman, G. Antonini, A. Orlandi.

Reproduced from: Proc. of the IEEE International Symposium on EMC, 2003, Boston, USA, August 2003.

For certain problem classes within EM modeling a 3D current flow needs to be accounted for. The extension from one and two dimensional PEEC models to full three dimensional modeling is mainly in the calculation of the partial coefficients of potentials. This is due to the fact that in 3D PEEC models multiple surfaces share the same PEEC model node and the total node coefficient of potential needs to be computed from the multiple surface coefficients of potential. This can result in increasing, or even excessive, computation times if this problem is neglected. The paper presents three different techniques to compute the node coefficient of potential using local or global reduction matrices or a weighting mean value procedure. By using the local reduction matrix approach or the weighted mean value procedure the node coefficient of potential matrix is obtained using less calculations and matrix operations resulting in considerable time savings. The impact of using the different formulations are shown by comparing node coefficients of potential and by experiments.

## 4.2 Conclusions

This thesis contributes with PEEC model advancements and improvements to facilitate EM modeling of realistic structures using the PEEC method.

*In Paper A, C, E, and F*, the calculation of the partial elements are given special attention due to the great importance in PEEC model based EM solvers. More specifically, *Paper A* suggests a discretization strategy where the flexibility in the PEEC cell aspect ratios and PEEC model reductions are used to obtain simplified calculations of PEEC model partial elements using analytic expressions. The paper also displays the simplicity in using reduced PEEC models for EM modeling. *Paper C* introduces the *The fast multi-function method*, FMF(PEEC), and establishes guidelines for the use of numerical integration techniques, in the evaluation of the partial elements, to minimize the total calculation time. The method is further used and refined in *Paper E* where the *Fast multipole method* is introduced within partial element calculations. Both the methods offers very good speed up and flexibility in the partial element calculations suitable for the calculation of nonorthogonal PEEC partial elements. *Paper F* focuses on the calculation of node partial coefficients of potential for PEEC models. The paper presents three different techniques where speed up or accuracy is obtained using local or global reduction matrices or a weighting mean value procedure. By using the local reduction matrix approach or the weighted mean value procedure the coefficient of potential matrix is obtained using less calculations and matrix operations resulting in considerable time savings.

*Paper B* applies a new technique, an electric field sensor, to calculate the radiated electric field from a printed circuit board. The technique is appealing since it allows the calculation of the field during simulation, and thereby excludes the traditional use of post-processing tools, and the introduced number of unknowns are kept at a minimum. It was found that the direct technique is sensible to the geometry of the sensor and that post-processing is to be preferred even though the amount of work increases considerably.

In *Paper D* the nonorthogonal PEEC method is detailed in theory and practice. The extension from orthogonal to nonorthogonal cells facilitates the modeling of complex structures, improves accuracy by reducing the use of staircase-approximations, and reduces the number of cells in the PEEC model discretizations. Among several numerical experiments 3D PEEC model simulations were compared against 2D transmission line PowerSpice simulations with very good agreement.

## 4.3 Future Development of the PEEC Method

The work conducted so far has resulted in several interesting areas concerning future advancements of the PEEC method. They can be summarized as follows :

- The efficient calculation of the partial elements need further investigation due to the introduction of the nonorthogonal PEEC method for which the analytical formulas can not be used.
- Discretization strategies for improving stability and accuracy have been shown to

be a very interesting area. Work conducted so far indicates the need for PEEC method grid generators taking into account specific PEEC features.

- Model order reduction techniques for solving large quasi-static PEEC models have shown to be very effective. However, the use within full wave PEEC modeling have, to my knowledge, never been explored and thus needs to.
- By subdividing capacitive- and inductive cells the PEEC model stability can be improved. The basic effect needs to be further investigated in theory and practice and guidelines could be developed to obtain further control over the stability of PEEC models.
- The calculation of the retardation term in both the time- and frequency domain can be done using different approaches. Work performed so far indicates that different approaches have impact on PEEC model accuracy and stability and needs further investigation.
- The usage of the fast $O(N^2)$ time domain approach to predict the $O(N^3)$ frequency domain response for PEEC models is an interesting and unexplored field within PEEC model speed up.
- Preliminary studies indicate the importance of high accuracy in the partial element values to assure PEEC model stability. This needs further investigation before it is possible to introduce this third factor to consider in the stability of the general PEEC formulation.

# References


[1] T. Hubing, "Standardization, industrial and research trends in EMC", presented at *Int. Symposium on EMC*, opening session, Sorrento, Italy, September 2002.

[2] Directive 89/336/EEC, "Electromagnetic Compatibility (EMC) Directive 89/336/EEC", The Council of the European Communities.

[3] T. Williams, *EMC for Product Designers*. Third edition, Butterworth-Heinemann, 2001.

[4] IEC50 (161): (BS4727 : Pt 1 : Group 09) Glossary of electrotechnical, power, telecommunication, electronics, lightning and colour terms: Electromagnetic compatibility.

[5] Michael Styrefors, Microbit, Kalix, Sweden, private communication, 2002.

[6] M. N. O. Sadiku, *Numerical Techniques in Electromagnetics*. CRC Press, Inc. 1992.

[7] W. P. Pinello, A. C. Cangellaris, and A. Ruehli, "Prediction of Differential- and Common-Mode Noise in High-Speed Interconnects With the Partial Element Equivalent Circuit Technique", in: *Proc. of the IEEE Int. Symposium on EMC*, pages 940–955, Denver, CO, USA, 1998.

[8] W. Pinello, A. C. Cangellaris, and A. E. Ruehli, "Hybrid Electromagnetic Modeling of Noise Interactions in Packaged Electronics Based on the Partial-Element Equivalent-Circuit Formulation", *IEEE Transactions on Microwave Theory and Techniques*, 45(10):1889–1896, October 1997.

[9] HUGO, Human Model dataset 3.0, Computer Simulation Technology, Germany 2003.

[10] B. Archambeault, C. Brench, and O. Rahami, *EMI/EMC Computational Modeling Handbook*. Kluwer Academic Publishers, 1998.

[11] K. S. Yee, "Numerical Solution of Initial Value Problems Involving Maxwell's Equations in Isotropic Media", *IEEE Transations on Antennas and Propagation*, 14:302–307, 1966.

[12] D. M. Sullivan, *Electromagnetic Simulation Using the FDTD Method*. John Wiley & Sons, Inc. , 2000.

[13] J. Jin, *The Finite Element Method in Electromagnetics.* John Wiley & Sons, New York, USA, 1993.

[14] W. Cheney and D. Kincaid, *Numerical Analysis.* Second edition, ISBN 0-534-33892-5, 1996.

[15] C. Johnson, *Numerical Solution of Partial Differential Equations by the Finite Element Method.* Studentlitteratur, ISBN 91-44-25241-2, 1987.

[16] J. Carlsson, *Computation of EMC Properties of Slots and Printed Circuit Boards.* Ph.D Dissertation, Chalmers University of Technology and SP Swedish National Testing and Research Institute, Sweden, 1998.

[17] R. F. Harrington, *Field Computation by Moment Methods.* Robert E. Krieger, Malabar, FL, 1987.

[18] A. F. Peterson, S. L. Ray, and R. Mittra, *Computational Methods for Electromagnetics.* IEEE Press, New York, USA, 1998.

[19] G. J. Burke and A. J. Poggio, *Numerical electromagnetics code (NEC) - Method of Moments, Part I: NEC Program Description - Theory.* Research report, Lawerence Livermore Laboratory, Livermore, CA. 1981.

[20] G. J. Burke and A. J. Poggio, *Numerical electromagnetics code (NEC) - Method of Moments, Part II: Program Description - Code.* Research report, Lawerence Livermore Laboratory, Livermore, CA. 1981.

[21] http://www.nec2.org/ (2003-03-14).

[22] A. E. Ruehli, "Inductance Calculations in a Complex Integrated Circuit Environment", *IBM Journal of Research and Development*, 16(5):470–481, September 1972.

[23] P. A. Brennan and A. E. Ruehli, "Efficient Capacitance Calculations for Three-Dimensional Multiconductor Systems", *IEEE Transactions on Microwave Theory and Techniques*, 21(2):76–82, February 1973.

[24] A. E. Ruehli, "Equivalent Circuit Models for Three-Dimensional Multiconductor Systems", *IEEE Transactions on Microwave Theory and Techniques*, 22(3):216–221, March 1974.

[25] J. E. Garrett, *Advancements of the Partial Element Equivalent Circuit Formulation.* Ph.D. Dissertation, The University of Kentucky, 1997.

[26] D. K. Cheng, *Fundamentals of Engineering Electromagnetics.* Addison-Wesley Publishing Company, 1994.

[27] T. A. Jerse, *A Hybrid Technique for Efficiently Estimating Common Mode Currents in Transmission-line Structures.* Ph.D. Dissertation, The University of Kentucky, 1994.

[28] L. W. Nagel, *SPICE2: A Computer Program to Simulate Semiconductor Circuits.* Memorandum No. M520, May 1975.

[29] E. Chiprout and A. E. Ruehli, "The Importance of Retardation in PEEC Models for Electrical Interconnect and Package (EIP) Applications", in: *Proc. of the IEEE Topical Meeting on Electrical Performance and Electronic Packaging*, pages 232–234, Portland, OR, USA, 1995.

[30] G. Wollenberg and A. Görisch, "Analysis of 3-D Interconnect Structures with PEEC Using SPICE", *IEEE Transactions on EMC*, 41(4):412–417, November 1999.

[31] P. A. Brennan, N. Raver, and A. E. Ruehli, "Three-Dimensional Inductance Computations with Partial Element Equivalent Circuits", *IBM Journal of Research and Development*, 23(6):661–668, November 1979.

[32] E. B. Rosa, "The Self and Mutual Inductance of Linear Conductors", *Bulletin of the National Bureau of Standards*, 4(2):301–344, 1908.

[33] F. Grover, *Inductance Calculations: Working Formulas and Tables.* Van Nostrand 1946.

[34] C. Hoer and C. Love, "Exact Inductance Equations for Rectangular Conductors With Applications to More Complicated Geometries", *Journal of Research of the National Bureau of Standards – C. Engineering and Instrumentation*, 69C(2):127–137, 1965.

[35] A. E. Ruehli, *An Integral Equation Equivalent Circuit Solution to a large class of interconnect systems.* Ph.D. Dissertation, The University of Vermont, USA, 1972.

[36] A. E. Ruehli, "Circuit Models for Three-Dimensional Geometries Including Dielectrics", *IEEE Transactions on Microwave Theory and Techniques*, 40(7):1507–1516, July 1992.

[37] H. Heeb and A. E. Ruehli, "Approximate Time-Domain Models of Three-Dimensional Interconnects", in: *Proc. of the IEEE Int. Conference on Computer-Aided Design*, pages 201–205, Santa Clara, CA, USA, 1990.

[38] H. Heeb and A. E. Ruehli, "Three-dimensional interconnect analysis using partial element equivalent circuits", *IEEE Transactions on Circuits and Systems*, 39:974-982, November 1992.

[39] H. Heeb, S. Ponnapalli, and A. E. Ruehli, "Frequency Domain Microwave Modeling Using Retarded Partial Element Equivalent Circuits", in: *Proc. of the IEEE Int. Design Automation Conference*, pages 702–706, Dallas, TX, USA, 1993.

[40] A. E. Ruehli, J. Garrett, and C. R. Paul, "Circuit Models for 3D Structures with Incident Fields", in: *Proc. of the IEEE Int. Symposium on EMC*, pages 28–31, Dallas, Tx, USA, August 1993.

[41] A. E. Ruehli, G. Antonini, and A. Orlandi, "Extension of the Partial Element Equivalent Circuit Method to Non Rectangular Geometries", in: *Proc. of the Int. Symposium on EMC*, pages 728–733, Seattle, Washington, USA, August 1999.

[42] G. Antonini, A. Ruehli, and J. Esch, "Nonorthogonal PEEC Formulation for Time and Frequency Domain Modeling", in: *Proc. of the Int. Symposium on EMC*, pages 728–733, Minneapolis, MN, USA, August 2002.

[43] A. E. Ruehli and H. Heeb, "Challanges and Advances in Electrical Interconnect Analysis", in: *Proc. of the IEEE Int. Design Automation Conference*, pages 460–465, Anaheim, CA, USA, 1992.

[44] A. E. Ruehli, "Circuit Oriented Electromagnetic Solutions in the Time and Frequency Domain", *IEICE Transactions on Communications*, E80-B(11):1594–1603, November 1997.

[45] A. Chiprout *et al.*, "Simulating 3-D Retarded Interconnect Models using Complex Frequency Hopping (CFH)", in: *Proc. of the IEEE Int. Conference on Computer-Aided Desing*, pages 66–72, Santa Clara, CA, USA, 1993.

[46] H. Heeb *et al.*, "Three Dimensional Circuit Oriented Electromagnetic Modeling for VLSI Interconnects", in: *Proc. of the IEEE Int. Conference on Computer Design*, pages 218–221, Cambridge, MA, USA, 1992.

[47] V. Jandhyala *et al.*, "Coupled Electromagnetic-Circuit Simulation of Arbitrarily-Shaped Conducting Structures using Triangular Meshes", in: *Proc of the Int. Symposium on Quality Electronic Design*, pages 38–42, San Jose, CA, USA, 2002.

[48] A. E. Ruehli, "Cicruit Oriented Electromagnetic Solutions in the Time and Frequency Domain", *IEICE Transactions on Communications*, 80-B(11):1594–1603, November 1997.

[49] A. E. Ruehli and H. Heeb, "Retarded Models for PC Board Interconnects - or How the Speed of Light Affects Your SPICE Circuit Simulation", in: *Proc. of the IEEE Int. Conference on Computer-Aided Design.* pages 70–73, Los Alamitos, CA, USA, 1991.

[50] G.-L. Li and Z.-H. Feng, "Consider the Losses of Dielectric in PEEC", in: *Proc. of the Int. Conference on Microwave and Millimeter Wave Technology*, pages 793–796, Beijing, China, 2002.

[51] A. E. Ruelhi and A. C. Cangellaris, "Application of the Partial Element Equivalent Circuit (PEEC) Method to Realistic Printed Circuit Board Problem", in: *Proc. of the IEEE Int. Symposium on EMC*, pages 182–197, Denver, CO, USA, 1998.

[52] H. Heeb, A. Ruelhi, J. Janak, and S. Daijavad, "Simulating Electromagnetic Radiation of Printed Circuit Boards", in: *Proc. of the IEEE Int. Conference on Computer-Aided Design*, pages 392–395, Santa Clara, CA, USA, 1990.

[53] A. E. Ruehli *et al.*, "Comparision of Differential and Common Mode Response for Short Transmission Line using PEEC Models", in: *Proc. of the IEEE Topical Meeting on Electrical Performance and Electronic Packaging*, pages 169–171, Napa, CA, USA, 1996.

[54] A. C. Cangellaris, W. Pinello, and A. E. Ruehli, "Circuit-Based Description and Modeling of Electromagnetic Noise Effects in Packaged Low-Power Electronics", in: *Proc. of the Int. Conference on Computer Design*, pages 136–142, Austin, TX, USA, 1997.

[55] A. E. Ruehli, C. Paul, and J. Garrett, "Inductance Calculations using Partial Inductances and Macromodels", in: *Proc. of the Int. Symposium on EMC*, pages 23–28, Atlanta, GA, USA, 1995.

[56] G. Antonini, "Full Wave Analysis of Power Electronic Systems Through a PEEC State Variable Method", in: *Proc. of the IEEE Int. Symposium on Industrial Electronics*, pages 1386–1391, July 2002.

[57] G. Antonini and S. Cristina, "EMI design of power drive system cages using the PEEC method and genetic optimization techniques", in: *Proc. of the IEEE Int. Symposium on EMC*, pages 156–160, Montréal, Canada, 2001.

[58] G. Antonini and A. Orlandi, "Lightning-induced Effects on Lossy MTL Terminated on Arbitrary Loads: A Wavelet Approach", *IEEE Transactions on EMC*, 42(2), May 2000.

[59] G. Antonini, S. Cristina, and A. Orlandi, "PEEC Modeling of Lightning Protection Systems and Coupling to Coaxial Cables", *IEEE Transactions on EMC*, 40(4:2):481–491, November 1998.

[60] P. Restle, A Ruehli, and S. G. Walker, "Dealing with Inductance in High-Speed Chip Design", in: *Proc. of the IEEE Int. Design Automation Conference*, pages 904–909, New Orleans, LA, USA, 1999.

[61] J. Ekman and O. Andersson, *A Graphical User Interface for PEEC*. Project Report, Dep. of Computer Science and Electrical Engineering, Luleå University of Technology, 2003.

[62] A. E. Ruehli and P. K. Wolff, "Inductance Computations for Complex Three-Dimensional Geometries", in: *Proc. of the IEEE Int. Symposium on Circuits and Systems*, vol. 1, pages 16–19, New York, NY, 1981.

[63] A. E. Ruelhi, P. A. Brennan, and H. W. Young, "Recent Progress in Capacitance Computation Methods", in: *Proc. of the IEEE Int. Symposium on Circuits and Systems*, pages 135–138, Phoenix, AZ, USA, 1975.

[64] B. J. Rubin and B. Singh, "Study of Meander Line Delay in Circuit Boards", *IEEE Transactions on Microwave Theory and Techniques*, 48(9):1452–1460, September 2000.

[65] K. M. Coperich, A. E. Ruelhi, and A. Cangellaris, "Enhanced Skin Effect for Partial Element Equivalent Circuit (PEEC) Models", in: *Proc. of the IEEE Topical Meeting on Electrical Performance and Electronic Packaging*, pages 189–192, San Diego, CA, USA, 1999.

[66] G. Antonini, *Techniche Circuitali per la Risoluzione di Problemi di Compatibilitá Elettromagnetica.* Ph.D. Dissertation, University of Rome 'La Sapienza', Italy, 1998.

[67] G. Antonini, A. Orlandi, and A. Ruehli, "Analytical Integration of Quasi-Static Potential Integrals on Nonorthogonal Coplanar Quadrilaterals for the PEEC Method", *IEEE Transactions on EMC*, 44(2):399–403, May 2002.

[68] J. Ekman, *Experimental verification of PEEC based electric field simulations.* Master's thesis, Luleå University of Technology, Sweden, 1999.

[69] A. E. Ruelhi and P. A. Brennan, "Capacitance Models for Integrated Circuit Metallization Wires", *IEEE Journal of Solid-State Circuits*, SC-10(6):530–536, December 1975.

[70] J. Garrett, A.E. Ruehli, and C.R. Paul, "Accuracy and Stability Improvements of Integral Equation Models using the partial element equivalent circuit PEEC approach", *IEEE Transactions on Antennas and Propagation*, 46(12):1824–1831, December 1998.

[71] C. Ho, A. Ruehli, and P. Brennan, "The Modified Nodal Approach to Network Analysis", *IEEE Transactions on Circuits and Systems*, pages 504–509, June 1975.

[72] L. M. Wedepohl and L. Jackson, "Modified Nodal Analysis: An Essential Addition to Electrical Circuit Theory and Analysis", *Engineering Science and Eduction Journal*, pages 84–92, June 2002.

[73] C. T. H. Baker, C. A. H. Paul, and D. R. Willé, Issues on the Numerical Solution of Evolutionary Delay Differential Equations. *Numerical Analysis Report No. 28*, University of Manchester, April 1994.

[74] A. Bellen, N. Guglielmi, and A. Ruehli, "Methods for Linear Systems of Circuit Delay Differential Equations of Neutral Type", *IEEE Transactions on Circuits and Systems*, 46:212–216, January 1999.

[75] A. Bellen, H. Heeb, U. Miekkala, and A. E. Ruehli, "Stable Time Domain Solutions for EMC Problems using PEEC Circuit Models", in: *Proc. of the IEEE Int. Symposium on EMC*, pages 371–376, Chicago, IL, USA, 1994.

[76] W. Liniger and A. E. Ruehli, "Time Domain Integration Methods for Electric Field Integral Equations", in: *Proc. of the 1995 Zurich Symposium on EMC*, pages 209–214, Zurich, Switzerland, 1995.

[77] J. Cullum, A. E. Ruehli, and T. Zhang, "A Method for Reduced-Order Modeling and Simulation of Large Interconnects Circuits and its Application to PEEC Models with Retardation", *IEEE Transactions on Circuits and Systems*, 47(4):261–273, April 2000.

[78] A. E. Ruehli, "Partial Element Equivalent Circuit (PEEC) Method and its Application in the Frequency and Time Domain", in: *Proc. of the IEEE Int. Symposium on EMC*, pages 128–133, Santa Clara, CA, USA, 1996.

[79] J. Cullum, A. E. Ruehli, and T. Zhang, " Model Reduction for PEEC Models Including Retardation", in: *Proc. of the IEEE Topical Meeting on Electrical Performance and Electronic Packaging*, pages 287–290, West Point, NY, USA, 1998.

[80] W. Pinello, A. Cangellaris, and A. E. Ruehli, "Transient Electromagnetic Analysis and Model Complexity Reduction Using the Partial Element Equivalent Circuit Formulation", in: *Proc. of the IEEE MTT-S Int. Microwave Symposium*, pages 63–66, Denver, CO, USA 1997.

[81] N. Marques *et al.*, "A Mixed Nodal-Mesh Formulation for Efficient Extraction and Passive Reduced-Order modeling of 3D Interconnects", in: *Proc. of the IEEE Int. Design Automation Conference*, pages 297–302, San Francisco, CA, USA, 1998.

[82] A. Odabasioglu, M. Celik, and L. Pileggi, "Prima: Passive Reduced-order Interconnect Macromodeling Algorithm", in: *Proc. of the Int. Conference on Computer Aided-Design*, pages 58–65, San Jose, CA, USA, 1997.

[83] E. Vialardi and F. G. Canavero, "Macromodeling of Electrical Interconnects and Packages via PEEC Approach", in: *Proc. of the Int. Symposium on EMC*, pages 3–8, Sorrento, Italy, 2002.

[84] K. Gala *et al.*, "Inductance Model and Analysis Methodology for High-Speed On-Chip Interconnect", *IEEE Transactions on Very Large Scale Integration (VLSI) Systems*, 10(6):730–745, December 2002.

[85] A. Cangellaris, W. Pinello, and A. E. Ruehli, "Stabilization of Time Domain Solutions of EFIE based on Partial Element Equivalent Circuit Models", in: *Proc. of the IEEE Int. Symposium on EMC*, pages 966–969, New York, NY, USA, 1997.

[86] H. Heeb, U. Miekkala, and A. E. Ruehli, "Stability of Discretized Partial Element Equivalent EFIE Circuit Models", *IEEE Transactions on Antennas and Propagation*, 43(6):553–559, June 1995.

# Part II

# Paper A

# Simplified PEEC Models for PCB Structures and Comparison to Experimental Data

**Authors:**
Jonas Ekman

**Reformatted version of paper originally published in:**
Proceedings of the Progress in Electromagnetic Research Symposium, PIERS 2001, Osaka, Japan, July 2001.

# Simplified PEEC Models for PCB Structures and Comparison to Experimental Data

Jonas Ekman

**Abstract**

In this paper a technique to obtain simple Partial Element Equivalent Circuit (PEEC) models for single layer PCB structures is presented. The partial elements are easily calculated using modified versions of closed form equations. The input impedance of a single layer PCB and the reflection coefficient for a 9 element log-periodic dipole antenna measured using a network analyzer are compared against simplified PEEC model simulations. It is shown that the simplified PEEC models show good agreement for single layer PCB structures.

# 1 Introduction

The PEEC method was developed by Ruehli [1, 2, 3] and is based on the conversion of the Mixed Potential Integral Equation (MPIE) to the circuit domain. By using a specialized discretization, the original structure is converted into a network of lumped inductances, capacitances and resistances, entitled partial elements. The capacitive and inductive couplings are modelled using partial mutual elements which results in a electromagnetic correct model where additionally discrete components like transmission lines and voltage/current sources are easily included. The partial elements are calculated either by using numerical integration techniques or simplified closed form equations. The resultant equivalent circuits are solved with, for example, conventional circuit solvers like SPICE [4] where the same equivalent circuit can be used to obtain results in the time and frequency domain.

The calculation of the partial elements involves the evaluation of double surface and volume integrals. These integrals are often solved using numerical integration resulting in increased computation time and susceptibility to numerical errors. By using closed form equations [1, 2] for the partial elements the PEEC method grows to an accessible EM simulation technique requiring only a general circuit simulation program as the 'solver'. But, for a full-wave solution, time retardation must be included to account for finite travel times between the inductive and capacitive partitions and a specialized solver has to be used [5].

A technique to produce simplified PEEC models for i.e. printed antennas and circuit board layouts is presented. A discretization procedure is employed to facilitate the use of closed form equations to calculate the partial elements. The connection of touching partitions, at the same PEEC model nodes, are made through the use of small resistances to exclude the manual summation of the partial self capacitance to each node. This results in simplified partial element equivalent circuits useful in a design or analyzing process. This technique facilitates the development of the equivalent circuits and has been used to analyze several PCB structures, and the results have been compared to measurements.

# 2 Derivation of the PEEC Model

The starting point for the theoretical derivation is the summation of the electric field, $\vec{E}$, in a multiconductor system expressed in terms of the vector magnetic potential $\vec{A}$ and the scalar electric potential $\Phi$ as

$$\vec{E}(\vec{r},t) = -\frac{\partial}{\partial t}\vec{A}(\vec{r},t) - \nabla\Phi(\vec{r},t) \tag{1}$$

For a system containing $K$ conductors the free-space Green's function electromagnetic potentials are given by

$$\vec{A}(\vec{r},t) = \sum_{k=1}^{K} \frac{\mu}{4\pi}\int_{v_k} \frac{\vec{J}(\vec{r}\prime,t\prime)}{|\vec{r}-\vec{r}\prime|}dv_k \tag{2}$$

and

$$\Phi(\vec{r},t) = \sum_{k=1}^{K} \frac{1}{4\pi\varepsilon}\int_{v_k} \frac{q(\vec{r}\prime,t\prime)}{|\vec{r}-\vec{r}\prime|}dv_k \tag{3}$$

where

$$t\prime = t - \frac{|\vec{r}-\vec{r}\prime|}{v} \tag{4}$$

denotes the retardation time in the medium with propagation speed $v$. The charge density $q$ considers both the bound charges and the charges bounded in the dielectric regions. The expression for the current density $\vec{J}$ must be modified [6] to include the conduction current density $\vec{J}_C$ and the polarization current density in the dielectric medium according to

$$\vec{J} = \vec{J}_C + \varepsilon_o(\varepsilon_r - 1)\frac{\partial\vec{E}}{\partial t} \tag{5}$$

The total electric field at the surface of a conductor, $\vec{E}(\vec{r},t)$, can be found by combining (1), (2), (3) resulting in

$$\begin{aligned}\frac{\vec{J}(\vec{r},t)}{\sigma} &+ \sum_{k=1}^{K}\frac{\mu}{4\pi}\int_{v_k}\frac{\partial}{\partial t}\frac{\vec{J}(\vec{r}\prime,t\prime)}{|\vec{r}-\vec{r}\prime|}dv_k \\ &+ \sum_{k=1}^{K}\varepsilon_o(\varepsilon_r-1)\frac{\mu}{4\pi}\int_{v_k}\frac{\partial^2}{\partial t^2}\frac{\vec{E}(\vec{r}\prime,t\prime)}{|\vec{r}-\vec{r}\prime|}dv_k \\ &+ \sum_{k=1}^{K}\frac{1}{4\pi\varepsilon_o}\nabla\left[\int_{v_k}\frac{q(\vec{r}\prime,t\prime)}{|\vec{r}-\vec{r}\prime|}dv_k\right] = 0\end{aligned} \tag{6}$$

To solve the system of equations in (6), the current and charge densities are discretized into volume and surface cells respectively, Fig. 1. Each current volume cell conducts a constant current between the nodes and each charge surface cell represents a constant node charge.

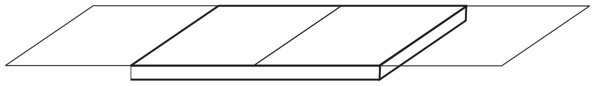

*Figure 1: Volume cell with two surface cells.*

Applying the Galerkin method [7], $K$ equations are obtained for the $K$ volume cells of the structure. The interpretation of these equations as the resistive, inductive and capacitive voltage drop in a closed loop [8] leads to the structure of the equivalent circuit for a PEEC cell as shown in Fig. 2.

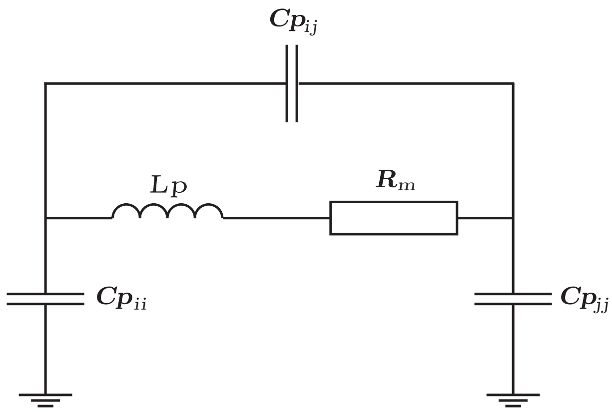


*Figure 2: Schematic description of a quasi-static PEEC cell.*

In Fig. 2, $R_m$ is the volume cell dc resistance calculated as

$$R_m = \frac{l_m}{a_m \cdot \sigma} \tag{7}$$

where $l_m$ is the cell length in the direction of the current flow, $a_m$ is the cell cross-section and $\sigma$ is the conductivity of the specific material. $Lp$ is the partial inductance calculated as

$$Lp_{mn} = \frac{\mu}{4\pi\, a_m a_n} \int_{a_m} \int_{a_n} \int_{l_m} \int_{l_n} \frac{d\vec{l_m} \cdot d\vec{l_n}}{|\vec{r} - \vec{r\prime}|} da_m \, da_n \tag{8}$$

If $(n = m)$, (8) represents the partial self inductance of the $m$:th cell. And if $(n \neq m)$, (8) represents the partial mutual inductance between the $m$:th and the $n$:th cell. Cp is the partial capacitance that can be calculated from the coefficients of potential $P_{ij}$, see further [9], where

$$P_{ij} = \frac{1}{4\pi\epsilon} \frac{1}{a_{si} a_{sj}} \int_{a_{si}} \int_{a_{sj}} \frac{1}{|\vec{r} - \vec{r\prime}|} da_{si} da_{sj} \tag{9}$$

If $(i = j)$ in (9), the partial self coefficient of potential of the $j$:th surface cell is calculated. And if $(i \neq j)$, (9) represents the partial mutual coefficient of potential between the $i$:th and the $j$:th surface cell.

For PEEC models where dielectric regions must be considered, the PEEC method has been extended through the use of dielectric cells [6].

# 3 Simplified PEEC Models

If the partial elements are calculated using (8) and (9) numerical integration techniques has to be used for the general case. But for simple orthogonal structures, like single layer PCB structures, it is possible to use only three closed form equations for the calculations. This makes the PEEC method an accessible EM simulation technique requiring only a general circuit simulation program like SPICE as the solver. The PEEC method can now be used for example in undergraduate courses to facilitate the understanding of EM theory or as an aid in a design process.

The approach is to try to discreticise the PCB structures into parallel rectangular surface and rectangular parallelepiped volume cells, which is required for the closed form equations. This is accomplished by (1) using two nodes at every corner geometry to separate the different partitions, x- and y-directed, (2) by connecting the two corner nodes by a small resistance. This is illustrated in Fig. 3 where two nodes have been placed in the corner separating one x-directed and one y-directed inductive partition. Without these nodes the resulting capacitive partition is L-shaped and the coefficient of potential needs to be summarized to obtain the combined node potential coefficient and the mutual coefficients. In a SPICE-like circuit solver, the two nodes can be connected through a small resistance to 'reduce' the two nodes to one and the summation is performed by the circuit solver.

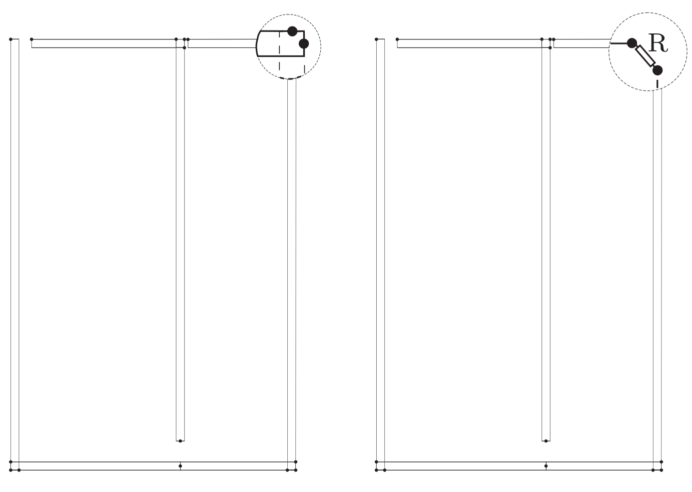


*Figure 3: Inductive partition for PCB example circuit in Fig. 6. Indicating the two nodes used to separated two inductive partitions (left) and the connection of the nodes through a small resistance (right).*

This result in an simplified EM model of the original circuit with easy calculated partial elements from closed form equations. All partial self and mutual coefficients of potentials (capacitive elements) are calculated using one single equation, and for the partial self and mutual inductive elements two equations are used.

# 4 Equations for Partial Element Calculations

In this section a complete set of equations for the calculation of the partial elements are presented. The equations are originally published in [1, 2, 10, 11, 12] for three-dimensional structures but have been modified to fit the single layer PCB structures considered in this paper.

## 4.1 Partial self inductance

When calculating the partial self inductance of a volume cell, (10) [1] has been used. Using the notations in Fig. 4 and the following normalizations $u = \frac{l}{w}$ and $\omega = \frac{t}{w}$ the partial self inductance of a $10 \times 1 \times 0.05$ mm ($l \times w \times t$) cell becomes 6.96 nH.

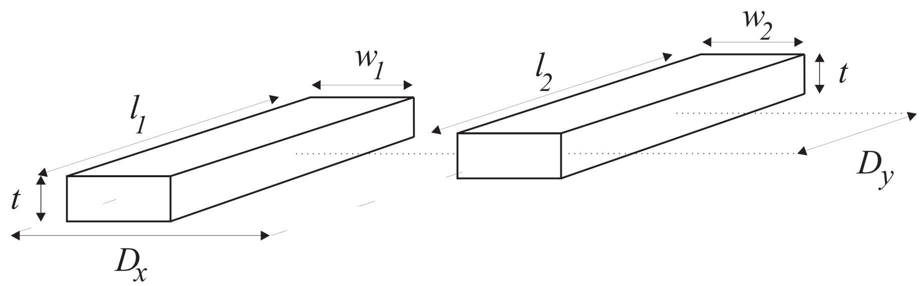


*Figure 4: Notations for partial inductance calculations.*

## 4.2 Partial mutual inductance

The partial mutual inductance between two inductive partitions correspond to the magnetic field coupling in the PEEC model. For the calculations (11) is used with the notations from Fig. 4. (11) was originally published in [12], but is presented in a modified form suitable for single layer PCB's.

Using the cell from the previous section, the mutual inductance between two volume cells with a center to center distance of 0 and 10 mm ($D_x$, $D_y$) is 0.94 nH.

## 4.3 Partial coefficients of potential

Due to a central difference approximation used in the theoretical derivation of the PEEC method, the surface cells are shifted half a cell length with respect to the the volume cells,

$$\begin{aligned}\frac{Lp_{ii}}{l} &= \frac{2\mu}{\pi}\{\frac{\omega^2}{24u}\left[\ln(\frac{1+A_2}{\omega})-A_5\right]+\frac{1}{24u\omega}\left[\ln(\omega+A_2)-A_6\right] \\ &+\frac{\omega^2}{60u}(A_4-A_3)+\frac{\omega^2}{24}[\ln(\frac{u+A_3}{\omega})-A_7]+\frac{\omega^2}{60u}(\omega-A_2)+\frac{1}{20u}(A_2-A_4) \\ &+\frac{u}{4}A_5-\frac{u^2}{6\omega}\tan^{-1}(\frac{\omega}{uA_4})+\frac{u}{4\omega}A_6-\frac{\omega}{6}\tan^{-1}(\frac{u}{\omega A_4})+\frac{A_7}{4} \\ &-\frac{1}{6\omega}\tan^{-1}(\frac{u\omega}{A_4})+\frac{1}{24\omega^2}\left[\ln(u+A_1)-A_7\right]+\frac{u}{20\omega^2}(A_1-A_4) \\ &+\frac{1}{60\omega^2 u}(1-A_2)+\frac{1}{60u\omega^2}(A_4-A_1)+\frac{u}{20}(A_3-A_4) \\ &+\frac{u^3}{24\omega^2}\left[\ln(\frac{1+A_1}{u})-A_5\right]+\frac{u^3}{24\omega}\left[\ln(\frac{\omega+A_3}{u})-A_6\right] \\ &+\frac{u^3}{60\omega^2}\left[(A_4-A_1)+(u-A_3)\right]\}\end{aligned} \tag{10}$$

where

$$\begin{array}{ll} A_1=\sqrt{1+u^2} & A_2=\sqrt{1+\omega^2} \\ A_3=\sqrt{\omega^2+u^2} & A_4=\sqrt{1+\omega^2+u^2} \end{array} \quad A_5=\ln(\tfrac{1+A_4}{A_3}) \quad A_6=\ln(\tfrac{\omega+A_4}{A_1}) \quad A_7=\ln(\tfrac{u+A_4}{A_2})$$

$$\begin{aligned} Lp_{km} &= \frac{\mu}{4\pi}\frac{1}{w_1 w_2}\sum_{i=1}^{4}\sum_{j=1}^{4}(-1)^{i+j}[\frac{b_j^2 a_i}{2}\ln(a_i+\rho_{ij})] \\ &+\frac{a_i^2 b_j}{2}\ln(b_j+\rho_{ij})-\frac{\rho_{ij}}{6}(b_j^2+a_i^2)]\end{aligned} \tag{11}$$

where

$$\rho_{ij}=\sqrt{a_i^2+b_j^2}$$

$$\begin{array}{ll} a_1=D_x-\frac{l_1}{2}-\frac{l_2}{2} & a_2=D_x+\frac{l_1}{2}-\frac{l_2}{2} \\ a_3=D_x+\frac{l_1}{2}+\frac{l_2}{2} & a_4=D_x-\frac{l_1}{2}+\frac{l_2}{2} \end{array}$$

$$\begin{array}{ll} b_1=D_y-\frac{w_1}{2}-\frac{w_2}{2} & b_2=D_y+\frac{w_1}{2}-\frac{w_2}{2} \\ b_3=D_y+\frac{w_1}{2}+\frac{w_2}{2} & b_4=D_y-\frac{w_1}{2}+\frac{w_2}{2} \end{array}$$

as indicated in Fig. 1. The capacitive couplings between the surface cells are calculated using the concept of coefficients of potential, $P_{ij}$ from (9). If no delay times between the surface cells are considered, lumped capacitances can be used to model the coupling. But, for finite delay times coupled sources are used [13] together with the coefficient of potential representation. For alternative capacitive representations see [9].

(12) [2] is used to calculate both the partial self and mutual coefficients of potentials. For the self term, with the notations from Fig. 5, use $a_x = b_x, a_y = b_y$ and $d_x = d_y = 0$.

$$\begin{aligned} ps_{ij} &= \frac{1}{4\pi\varepsilon}\frac{1}{a_x a_y b_x b_y} \\ &\quad \sum_{k=1}^{4}\sum_{m=1}^{4}(-1)^{m+k}[\frac{b_m^2 a_k}{2}\ln(a_k+\rho_{km}) \\ &\quad +\frac{a_k^2 b_m}{2}\ln(b_m+\rho_{km}) - \frac{\rho_{km}}{6}(b_m^2+a_k^2)] \end{aligned} \tag{12}$$

where

$$\rho_{km} = \sqrt{a_k^2 + b_m^2}$$

$$\begin{array}{ll} a_1 = d_x - \frac{a_x}{2} - \frac{b_x}{2} & a_2 = d_x + \frac{a_x}{2} - \frac{b_x}{2} \\ a_3 = d_x + \frac{a_x}{2} + \frac{b_x}{2} & a_4 = d_x - \frac{a_x}{2} + \frac{b_x}{2} \end{array}$$

$$\begin{array}{ll} b_1 = d_y - \frac{a_y}{2} - \frac{b_y}{2} & b_2 = d_y + \frac{a_y}{2} - \frac{b_y}{2} \\ b_3 = d_y + \frac{a_y}{2} + \frac{b_y}{2} & b_4 = d_y - \frac{a_y}{2} + \frac{b_y}{2} \end{array}$$

For a surface cell of 10×1 mm the self coefficient of potential is 6.34 pF$^{-1}$. The mutual coefficient of potential between two 'touching' 10×1 mm surface cells is 1.22 pF$^{-1}$ and between a 10×1 mm and a 5×1 mm surface cell, 1.66 pF$^{-1}$.

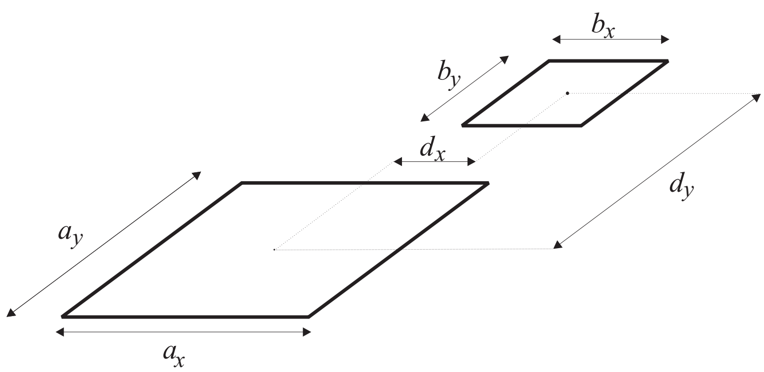


*Figure 5: Notations for coefficients of potential calculation.*

# 5 Experiments

The technique described has been used to analyze PCB structures such as dipoles, LPDA's and patch antennas where the discretized partition ratios has been; $0.03 < \frac{T}{W} < 0.1$ and $5 < \frac{L}{W} < 100$.

Simple Java programs have been used to generate the resulting circuit-files and a SPICE solver has been used for the simulations. In the experiments, the dielectric material has not been take into account, except for the LPDA where an effective $\varepsilon_r$ have been used [14].

The upper frequency limits for the experiments are set by the largest PEEC model cell length where 10 cells per shortest wavelength is a rule of thumb to use. For more complicated PEEC models other parameters including conductor shape and proximity to other conductors can influence the discretization.

## 5.1 Half wavelength dipole

The calculated partial elements from the previous sections can be used to simulate the resonance frequency for a simple half-wavelength dipole. If each arm of the dipole is modelled using five 10 mm volume cells, the resulting 100 mm dipole would have a theoretical resonance frequency of 1.5 GHz. If the inductive and capacitive couplings are realized using mutual elements only between the 'touching' volume/surface cells the resonance frequency is predicted to 1444 MHz. Further simulations made on the $\frac{\lambda}{2}$ dipole indicates that a finer discretization, the inclusion of all mutual elements and the retardation factor improve the accuracy of the PEEC model.

## 5.2 One layer PCB circuit

In Fig. 7 the simulated input impedance for the PCB structure in Fig. 6 connected to a 0.1m long 50 $\Omega$ coax cable is compared with network analyzer measurements.

The model consists of 15 self and 18 mutual partial inductances and 13 self and 156 mutual partial capacitances calculated using (10)-(12). The agreement compared to measurements are good up to about 1 GHz. Tests performed on the dipole indicates that for higher frequencies a finer discretization would improve the accuracy of the model.

## 5.3 LPDA

In Fig. 9 the reflection coefficient for the nine element log-periodic dipole antenna (LPDA), Fig. 8, printed on a 1.6mm thick dielectric plate is compared to network analyzer measurements.

This is a more complicated geometry and the model consists of 246 self and a maximum of 34308 mutual partial inductances and 196 self and a maximum of $(196^2 - 196)$ mutual partial capacitances. For this PEEC model, the unmodified three-dimensional equations from [1, 2, 10, 11, 12] was used with the proposed discretization strategy. The

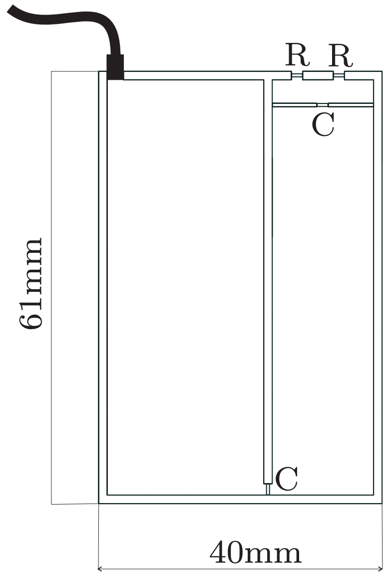


*Figure 6: PCB test circuit.*

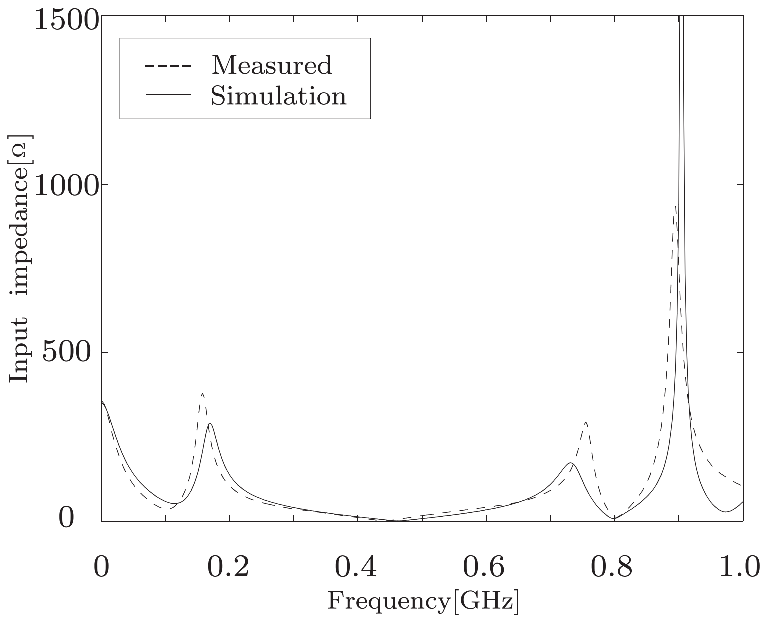


*Figure 7: Input impedance for PCB test circuit.*

3D equations must be used because the LPDA has antenna elements on both sides of the dielectric substrate. The model accurately predicts two LPDA resonance peeks at 800 and 1125 MHz but fails to predict the magnitude of the reflection coefficient at lower frequencies. To model the LPDA at higher frequencies a finer discretization could improve the accuracy of the model. An important factor to improve the result for the LPDA could be the inclusion of the retardation. Since the retardation introduce a neutral damping

[6] in the PEEC model the simulated low frequency region of the reflection factor could be improved. And, since the dielectric regions are of more importance for this structure, the use of dielectric cells could improve the accuracy instead the use of an effective $\varepsilon_r$.

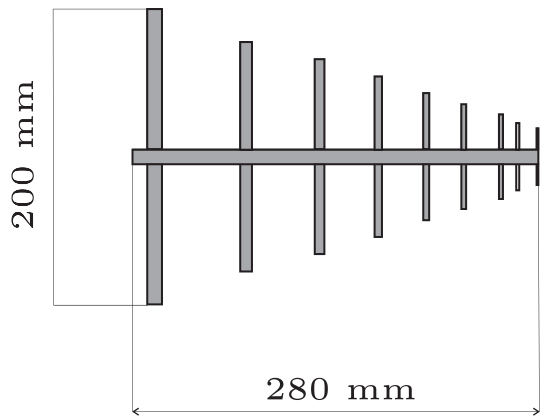


*Figure 8: Log-periodic dipole antenna (LPDA).*

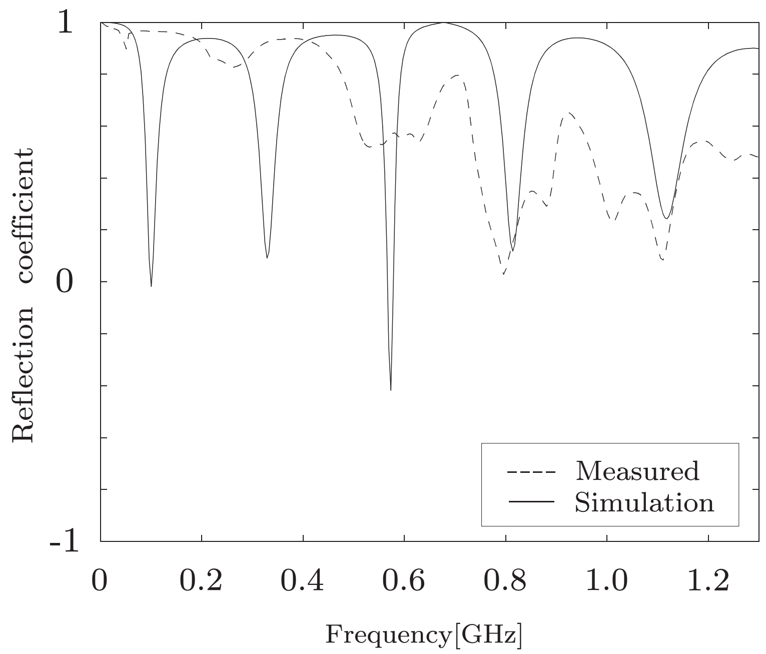


*Figure 9: Reflection coefficient for 9 element LPDA.*

# 6 Conclusions

The proposed method to generate simplified PEEC models for PCB structures have been verified by comparing simplified PEEC model simulations against measurements for several prototype PCB's. The agreement is very good for the investigated single layer PCB's where the PEEC models are obtained using (10)-(12). For more complicated geometries, like the presented 9 element LPDA, the accuracy is not that good. It is possible that the simplifications are to extensive for two layer structures.

# References


[1] A. E. Ruehli, "Inductance Calculations in a Complex Integrated Circuit Environment", *IBM Journal of Research and Development*, 16(5):470–481, September 1972.

[2] P. A. Brennan and A. E. Ruehli, "Efficient Capacitance Calculations for Three-Dimensional Multiconductor Systems", *IEEE Transactions on Microwave Theory and Techniques*, 21(2):76–82, February 1973.

[3] A. E. Ruehli, "Equivalent Circuit Models for Three-Dimensional Multiconductor Systems", *IEEE Transactions on Microwave Theory and Techniques*, 22(3):216–221, March 1974.

[4] L. W. Nagel, *SPICE2: A Computer Program to Simulate Semiconductor Circuit.* Memorandum No. M520, May 1975.

[5] A. Görisch and G. Wollenberg, "Analysis of 3-D Interconnect Structures with PEEC Using SPICE", *IEEE Transactions on EMC*, 41(4):412–417, November 1999.

[6] A. E. Ruehli, "Circuit Models for Three-Dimensional Geometries Including Dielectrics", *IEEE Transactions on Microwave Theory and Techniques*, 40(7):1507–1516, July 1992.

[7] M. N. O. Sadiku, *Numerical Techniques in Electromagnetics.* CRC Press, Inc. 1992.

[8] J. E. Garrett, *Advancements of the Partial Element Equivalent Circuit Formaulation*, Ph.D. Dissertation, The University of Kentucky, 1997.

[9] P. A. Brennan and A. E. Ruehli, "Capacitance Models for Integrated Circuit Metallization Wires", *IEEE Journal of Solid State Circuits*, 10(6):530–536, December 1975.

[10] P. A. Brennan, N. Raver, and A. E. Ruehli, "Three-Dimensional Inductance Computations with Partial Element Equivalent Circuits", *IBM Journal of Research and Development*, 23(6):661–668, November 1979.

[11] J. Garrett, C. Paul, and A. E. Ruehli, "Inductance Calculations using Partial Inductances and Macromodels", in: *Proc. of the IEEE Int. Symp. on Electromagnetic Compatibility*, pages 23–28, New York, NY, 1995.

[12] A. E. Ruehli and P. K. Wolff, "Inductance Computations for Complex Three-Dimensional Geometries", in: *Proc. of the IEEE Int. Symp. on Circuits and Systems*, vol. 1, pages 16–19, New York, NY, 1981.

[13] H. Heeb and A. E. Ruehli, "Approximate Time-Domain Models of Three-Dimensional Interconnects", in: *Proc. of the IEEE Int. Conference on Computer Design*, pages 201–205, Los Alamitos, CA, USA, 1990.

[14] S. Jenvey and U. Lundgren, "A Comparison of Measured and Simulated Current Distributions on a Printed Log-Periodic Antenna", in: *Proc. of the Nordic Antenna Symposium*, Lund, Sweden, 2000.

# Paper B

# Experimental Verification of PEEC Based Electric Field Simulations

**Authors:**
Jonas Ekman

**Reformatted version of paper originally published in:**
Proceedings of the 2001 IEEE International Symposium on EMC, Montreal, Canada, August 2001.

# Experimental Verification of PEEC Based Electric Field Simulations

Jonas Ekman

**Abstract**

Two methods to simulate the radiated electric field for printed circuit boards using Partial Element Equivalent Circuit (PEEC) models has been investigated. First, different types of PEEC models have been used with post-processing algorithms to calculated the radiated electric field in a traditional manner. Then, a newly proposed electric field sensor direct incorporated in the PEEC simulations have been used for the same task. Calculated and simulated field strengths for a simple PCB are compared against measurements taken in an anechoic EMC chamber. It is shown that the post-processing equations compares better to measurements then the electric field sensor.

## 1 Introduction

Due to international EMC regulations and to ensure functionality, product developers use numerical simulations of electromagnetic properties of printed circuit board layouts and other complicated structures prior to construction. To detect non compliance at this point in a product cycle is valuable since appropriate actions now can improve the EM characteristic in a very cost effective way. There are a variety of EM simulation techniques, one more suitable then the others for a specific problem. Since the Partial Element Equivalent Circuit (PEEC) method is based on an integral equation formulation this technique is ideal for 'open air' problems like radiations from PCB´s. The PEEC method was developed by Ruehli[1, 2, 3] and is based on the conversion of the Mixed Potential Integral Equation (MPIE) to the circuit domain. By using a specialized discretization, the original structure is converted into a network of discrete inductances, capacitances and resistances, called partial elements. This results in a electromagnetic accurate model where additionally discrete components like transmission lines and voltage/current sources are easily included. The partial elements are calculated either by using numerical integration techniques or simplified closed form solutions. The resultant equivalent circuit can be solved with a conventional circuit solver like SPICE[4], where the same equivalent circuit can be used to obtain results in both the time and frequency domain.

The calculation of the radiated fields for circuit variable based EM simulation techniques like the PEEC method is done in two steps. First, the PEEC model is used to solve for the currents in the volume cells. Second, the calculated currents are used in a post-processing tool that calculates the field components. This introduce an extra amount of work for the user and additional error sources for the result, hence it is desirable to exclude this extra step. The newly proposed electric field sensor [5] is then an appealing solution. The sensor is a special PEEC one-cell that is coupled to the test object using mutual partial elements, and the radiated field strength can be plotted direct after a successful PEEC model analysis. In this paper the proposed sensor and full and simplified PEEC models using post-processing algorithms have been compared to measurements taken in an anechoic chamber for the radiated electric field strength of a simple PCB.

## 2 Derivation of the PEEC Model

The starting point for the theoretical derivation is the equation for the sources of electric field at any point in a conductor

$$\vec{E} = \vec{E}^i + \vec{E}^s \tag{1}$$

where $\vec{E}^i$ and $\vec{E}^s$ is the incident and scattered electric field respectively. This equation can be rewritten using the current density $\vec{J}$, conductivity $\sigma$, vector magnetic potential $\vec{A}$ and the scalar electric potential $\Phi$, resulting in

$$\frac{\vec{J}(\vec{r},t)}{\sigma} = \vec{E}^i + \left[-\frac{\partial}{\partial t}\vec{A}(\vec{r},t) - \nabla\Phi(\vec{r},t)\right] \tag{2}$$

For a system containing $K$ conductors the free-space Green's function potentials are given by

$$\vec{A}(\vec{r},t) = \sum_{k=1}^{K} \frac{\mu}{4\pi}\int_{v_k} \frac{\vec{J}(\vec{r}\prime,t\prime)}{|\vec{r}-\vec{r}\prime|}dv_k \tag{3}$$

and

$$\Phi(\vec{r},t) = \sum_{k=1}^{K} \frac{1}{4\pi\varepsilon}\int_{v_k} \frac{q(\vec{r}\prime,t\prime)}{|\vec{r}-\vec{r}\prime|}dv_k \tag{4}$$

where $t\prime$ denotes the retardation time in the medium with propagation speed $v$ and calculated as

$$t\prime = t - \frac{|\vec{r}-\vec{r}\prime|}{v} \tag{5}$$

The charge density $q$ considers both the bound charges and the charges bounded in the dielectric regions. The expression for the current density $\vec{J}$ must be modified [6] to include the conduction current density $\vec{J_C}$ and the polarization current density in the dielectric medium according to

$$\vec{J} = \vec{J_C} + \varepsilon_o(\varepsilon_r - 1)\frac{\partial\vec{E}}{\partial t} \tag{6}$$

Combining (2), (3), (4) and setting the incident field, $\vec{E}^i$, to zero results in (7) if the field point is inside a conductor

$$\frac{\vec{J}(\vec{r},t)}{\sigma} + \sum_{k=1}^{K} \frac{\mu}{4\pi} \int_{v_k} \frac{\partial}{\partial t} \frac{\vec{J}(\vec{r}\prime,t\prime)}{|\vec{r}-\vec{r}\prime|} dv_k$$
$$+ \sum_{k=1}^{K} \varepsilon_o(\varepsilon_r - 1) \frac{\mu}{4\pi} \int_{v_k} \frac{\partial^2}{\partial t^2} \frac{\vec{E}(\vec{r}\prime,t\prime)}{|\vec{r}-\vec{r}\prime|} dv_k \tag{7}$$
$$+ \sum_{k=1}^{K} \frac{1}{4\pi\varepsilon_o} \nabla \left[ \int_{v_k} \frac{q(\vec{r}\prime,t\prime)}{|\vec{r}-\vec{r}\prime|} dv_k \right] = 0$$

To solve the system of equations in (7), the current and charge densities are discretized into volume and surface cells respectively, Fig. 1. The current volume cells conducts the current between the nodes and the charge surface cells represent the node charge. Inside the cells the variables are constant.

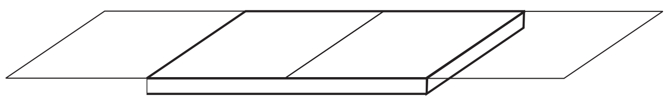

*Figure 1: Volume cell with two surface cells.*

Applying the Galerkin method [7] $K$ equations are obtained for the $K$ volume cells of the structure. The interpretation of these equations as a loop [8] results in the structure of the equivalent circuit for a PEEC one-cell, Fig. 2.

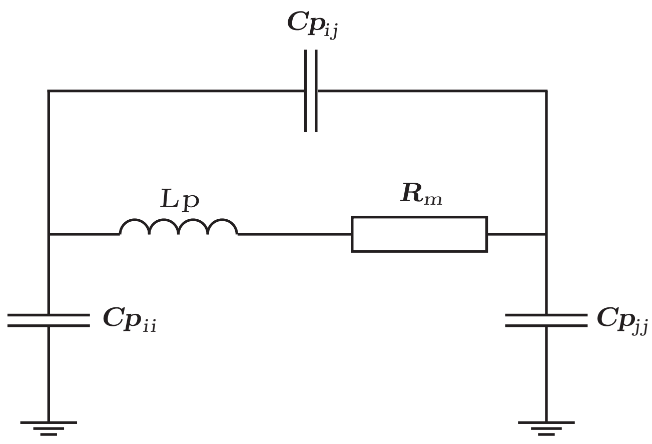


*Figure 2: Schematic description of a quasi-static PEEC cell.*

In Fig. 2, $Rm$ is the volume cell dc resistance calculated as

$$R_m = \frac{l_m}{a_m \cdot \sigma} \tag{8}$$

where $l_m$ is the volume cell length in the direction of the current flow, $a_m$ is the cell cross-section normal to the current flow and $\sigma$ is the conductivity of the specific material. Lp is the partial inductance calculated as

$$Lp_{mn} = \frac{\mu}{4\pi\, a_m a_n} \int_{a_m} \int_{a_n} \int_{l_m} \int_{l_n} \frac{d\vec{l_m} \cdot d\vec{l_n}}{|\vec{r} - \vec{r\prime}|} da_m\, da_n \tag{9}$$

If ($n = m$), (9) represents the self partial inductance of the $m$:th cell. And if ($n \neq m$), (9) represents the mutual partial inductance between the $m$:th and the $n$:th cell. $Cp$ is the partial capacitance that can be calculated from the coefficients of potential $P_{ij}$ [9]

$$P_{ij} = \frac{1}{\varepsilon_o a_{si} a_{sj}} \frac{1}{|\vec{r} - \vec{r\prime}|} \int_{a_{si}} \int_{a_{sj}} da_{si} da_{sj} \tag{10}$$

If ($i = j$), the coefficients of potential in (10) can be recalculated to the self partial coefficient of potential of the $j$:th surface cell. And if ($i \neq j$) the coefficients can be recalculated to the mutual partial coefficient of potential between the $i$:th and the $j$:th surface cell. For PEEC models where dielectric regions must be considered, the PEEC method has been extended through the use of dielectric cells [6].

# 3 Time Retardation

Time retarded PEEC models are be used to ensure accuracy for specific EM problems [10] and if the discretized structure is electrically large or the active frequency spectrum is high. The concept of time retardation can be seen in (3) where the vector magnetic potential $\vec{A}$ at point $\vec{r}$ at time $t$ is calculated from using the current densities $\vec{J}$ in all the discretized volume cells at a retarded time $t\prime$. To extend the PEEC model to be a full-wave solution of Maxwell's equations the representation of the mutual partial elements must be revised. In the proposed retarded PEEC model [11] all mutual partial capacitances are replaced by controlled current- and/or voltage-sources depending on the problem at hand. The mutual partial inductances can be represented in a similar way. The controlled sources are derived from basic circuit theory and the resultant equivalent circuit for a PEEC one-cell is given in Fig. 3.

The importance of time retardation for EM field simulations have been verified in the past[12] and the formulation described above will be used in this paper with a modified SPICE solver[5], capable of handling the finite time delays.

# 4 Post-processing Equations

For integral equation based EM models, post-processing equations are normally used to convert the calculated current and charge distributions in the structure to the radiated electric and/or magnetic field strengths. This is straightforward when the PEEC model is applied to Manhattan-type of PCB geometries[13]. The traces on PCB's are usually very

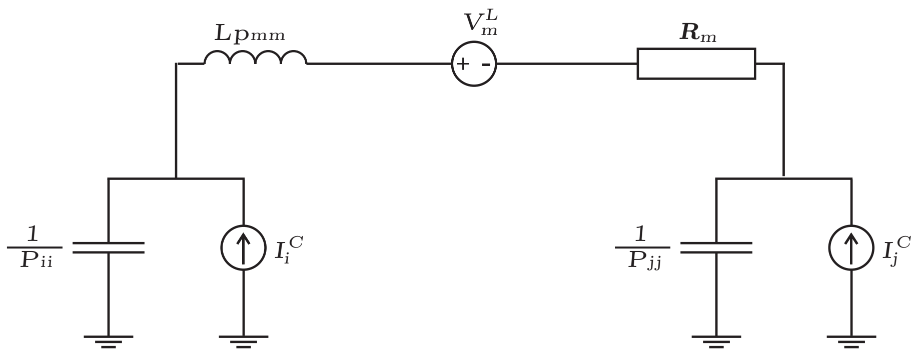


*Figure 3: Equivalent circuit model for PEEC volume cell m connecting node i and j. $V_m^L$ accounts for the retarded magnetic field coupling and $I_\alpha^C$ accounts for the retarded electric field couplings.*

narrow and thin in reference to the length and thus each volume cell can be seen as a wire of finite length with a well defined current flow given by the circuit solver for the PEEC model. One way to derive the radiated electric field from a wire is to start by using the rotation of the vector magnetic potential to describe the magnetic flux density, $\vec{B}(\vec{r},t)$. The resultant expression to describe time domain electric field intensities is expressed as (11).

$$\vec{E}(\vec{r},t) = \frac{\mu_o}{4\pi}\sum_N \int \left[\frac{\vec{j}(\vec{r}\prime,t\prime)\times\vec{r}}{r^3} + \frac{\frac{\delta\vec{j}}{\delta t}(\vec{r}\prime,t\prime)\times\vec{r}}{cr^2}\right] dv \tag{11}$$

where the summation is over each of the $N$ conducting volume cells of the discretized structure. (11) can be simplified for far field calculations by excluding the first term, $\propto \frac{1}{r^3}$, inside the brackets. This approximation have been used for the 3 m electric field calculations in this paper since the frequencies are high, $> 200$ MHz, and the distance to the observation point, $\vec{r}$, is large.

# 5 Electric Field Sensor

To be able to exclude the post-processing step in a electric field simulation would decrease the work load for the user and also minimize the potential for man made errors.

In a proposed solution [5] an electric field sensor is realized as a special PEEC one-cell where the partial self inductance of the sensor is excluded and the sensor is not coupled to the test object. But, the test object is coupled to the sensor in a normal fashion using partial mutual inductances and partial mutual coefficients of potentials. The electric field is calculated from the sensor end potentials(node potentials) and the induced voltage in the one-cell. This is a powerful formulation since it allows for sensors at indefinitely many locations in one single run. For instance, sensors could be placed around a test object in a sphere configuration to detect e-field maximums. The increase in unknowns are also acceptable, for a $n$ inductive and $m$ capacitive partitioned PEEC the additional coupling terms are $\leq (n+2m)$ for one single sensor. For each sensor two more nodes are also added to the system matrix.

The main drawback in the sensor formulation is the numerical difficulties arising when calculating the partial mutual couplings between the EUT and the sensor. Since the PEEC formulation require a very high accuracy in the calculated partial elements, the combination of:

1. large observation distances from the EUT (PEEC model) to the field point, in the order of meters.
2. the $\frac{\lambda}{10}$-rule for the discretization, requiring small cell dimensions in the PEEC model.

results in a complicated modeling situation. Even for distances no more than 3 m the inductive and capacitive couplings are very small. The length of the sensor was also shown to be a critical parameter. The 'calculated' field strengths differs significantly, in the order of $\pm 10$ dB, with the sensor length. In the simulations the sensor length, inductive partition, was set to no more then $\frac{\lambda_{min}}{10}$, according to established PEEC design rules. The sensor width and thickness were set to $\frac{1}{10}$ of the length.

# 6 Experimental Setup

The measurements were performed in an anechoic EMC chamber. The PCB was placed on a plastic table 1 m above the floor and fed using a Rohde & Schwartz SME03E signal generator. The radiated emissions were measured with a Chase BiLog antenna connected to a Rohde & Schwartz ESPC EMI test receiver. The absolute accuracy for the emission measurements performed at the test location has been estimated to $\pm$ 8 dB.

The PCB used in this paper, Fig. 4, is a $61 \times 40$ mm RC circuit with surface mounted components originally presented in [3]. The PEEC model, used in the simulations, consists of 15 inductive and 13 capacitive partitions. All the mutual coupling terms and conductor resistances are used but the dielectric medium was not considered.

The field strengths at a 1 and 3 meter distance from the PCB to the reference point at the antenna were measured. The observation point, $\vec{r}$, was shifted to four different locations centered and perpendicular to the PCB traces. The lower frequency limit, 200 MHz, is set to ensure far field conditions for the post-processing equation. The upper frequency limit, 1 GHz, is set by the PEEC model partitioning and the receiver antenna.

# 7 Results

Typical results for the calculated and simulated electric field strengths compared against measurements at a 1 and 3 meter distance can be seen in Fig. 5 and 6 respectively. As expected, the measurements and the two simulation techniques do not show perfect agreement. The sensor result is slightly better for near field simulations while the post-processing technique is better for far field calculation. The typical results shows also an underestimating of the electric field strength under 500 MHz and a overestimating

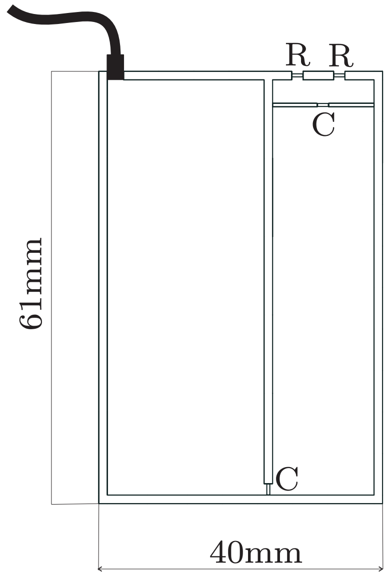


*Figure 4: Test circuit for which electric field intensity has been simulated and measured.*

at frequencies over 500 MHz. This has been observed before, for example in [12]. The tests has also shown that the length of the sensor is a critical parameter. By changing the sensor length, the field strength curve is either raised or lowered. Since the mutual inductive coupling terms between the PCB and the sensor are very small for a 3 m distance, the use of the sensor at a 10 m distance could introduce possible numerical problems.

# 8 Conclusions

The study performed has shown that the use of post-processing equations are more reliable then the use of the proposed electric field sensor. The possible reasons are the sensitivity to the sensor length and the potential numerical problem with the small coupling coefficients for far field prediction. This indicates that the sensor formulation has to be improved.

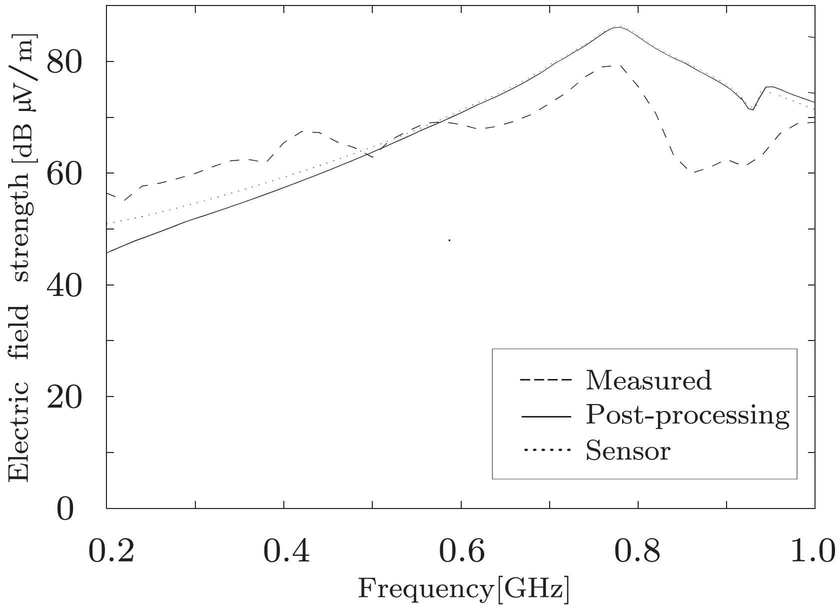


*Figure 5: Magnitude of electric field intensity at 1m.*

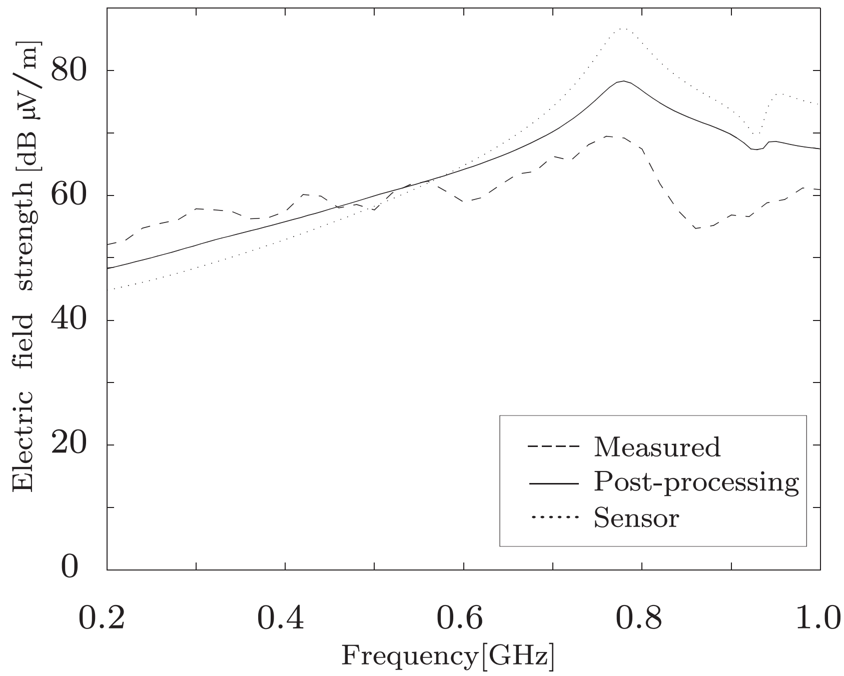


*Figure 6: Magnitude of electric field intensity at 3m.*

# References


[1] A. E. Ruehli, "Inductance Calculations in a Complex Integrated Circuit Environment", *IBM Journal of Research and Development*, 16(5):470–481, September 1972.

[2] P. A. Brennan and A. E. Ruehli, "Efficient Capacitance Calculations for Three-Dimensional Multiconductor Systems", *IEEE Transactions on Microwave Theory and Techniques*, 21(2):76–82, February 1973.

[3] A. E. Ruehli, "Equivalent Circuit Models for Three-Dimensional Multiconductor Systems", *IEEE Transactions on Microwave Theory and Techniques*, 22(3):216–221, March 1974.

[4] *The Design Center - Circuit Analysis Refrence Manual. Version 6.1.* MicroSim Corporation. July 1994.

[5] G. Wollenberg and A. Görisch, "Analysis of 3-D Interconnect Structures with PEEC Using SPICE", *IEEE Transactions on EMC*, 41(4):412–417, November 1999.

[6] A. E. Ruehli, "Circuit Models for Three-Dimensional Geometries Including Dielectrics", *IEEE Transactions on Microwave Theory and Techniques*, 40(7):1507–1516, July 1992.

[7] M. N. O. Sadiku. *Numerical Techniques in Electromagnetics*. CRC Press, Inc. 1992.

[8] J. Ekman. *Experimental Verification of PEEC Based Electric Field Simulations*, Master's thesis 1999:183, Luleå University of Technology, Sweden, May 1999.

[9] P. A. Brennan and A. E. Ruehli, "Capacitance Models for Integrated Circuit Metallization Wires", *IEEE Journal of Solid State Circuits*, 10(6):530–536, December 1975.

[10] A. E. Ruehli and E. Chiprout, "The Importance of Retardation in PEEC Models for Electrical Interconnect and Package (EIP) Applications", in: *Proc. of the IEEE 4th topical meeting on Electrical Performance of Electronic Packaging*, pages 232–234, New York, NY, USA, October 1995.

[11] A. E. Ruehli, "Circuit Oriented Electromagnetic Solutions in the Time and Frequency Domain", *IEICE Transactions on Communications*, 80-B(11):1594–1603, November 1997.

[12] A. E. Ruehli and H. Heeb, "Retarded Models for PC Board Interconnects - or How the Speed of Light Affects Your SPICE Circuit Simulation", in: *Proc. of the IEEE Int. Conference on Computer-Aided Design*, pages 70–73, Los Alamitos, CA, USA, 1991.

[13] A. E. Ruehli, "Simulating Electromagnetic Radiation of Printed Circuit Boards", in: *Proc. of the IEEE Int. Conference on Computer-Aided Design*, pages 392–395, Santa Clara, CA, USA. 1990.

# Paper C

# Integral Order Selection Rules for a full wave PEEC Solver

**Authors:**
Giulio Antonini[1], Jonas Ekman, Antonio Orlandi[1]

**Reformatted version of paper originally published in:**
Proceedings of the 15th Zurich Symposium on EMC, Zurich, Switzerland, February 2003.



[1]University of L'Aquila, Department of Electrical Engineering, Poggio di Roio, 67100 L'Aquila.

# Integration Order Selection Rules for a Full Wave PEEC Solver

G. Antonini, J. Ekman, A. Orlandi

**Abstract**

This paper proposes a technique to reduce the calculation time for the complex partial elements used in a retarded partial element equivalent circuit (rPEEC) frequency domain solver. The technique utilizes a thresholding scheme where strongly coupled PEEC cells are calculated with higher accuracy than the weakly coupled. Guidelines for limiting the order of integration used in the evaluation of the complex partial elements are presented. The trade-off between accuracy and computation time of the partial elements and the resulting PEEC system solution is investigated and displayed.

## 1 Introduction

For the analysis of electromagnetic field related problems a number of techniques are available. Each technique with its unique features that are suitable for a specific class of problems. For electromagnetic field problems where a circuit equivalent is sought the PEEC method is useful.

In the PEEC method, conductors are represented by partial circuit elements. The partial elements are lumped inductances, capacitances (calculated from the coefficients of potential) and resistances that have to be calculated based on the geometry of the problem. The conductor discretization and thus the number of partial elements are determined by the upper frequency limit of the model. Quasi-static partial elements can be used when retarded field couplings can be ignored, e.g. when the shortest wavelengths are long compared to the structure analyzed. When quasi-static PEEC models are used for orthogonal structures, the partial elements can be calculated using analytical expressions resulting in fast computation times. For complicated three-dimensional problems or when retarded couplings are of importance, for example in high frequency system analysis, the partial elements must be calculated using numerical integration methods. In these methods, the accuracy in the computed elements is determined by the order of approximation of the function being calculated. Increasing the order in the numerical integration routines and thus the accuracy, the calculation time increases considerably. This is of no importance when simple geometries are modelled using few partial elements. But, when the PEEC method is used to solve frequency domain full wave electromagnetic field problems, the partial elements have to be recalculated at each frequency to account for the retarded field couplings. This provides incentive to develop and use efficient algorithms to calculate the rPEEC partial elements.

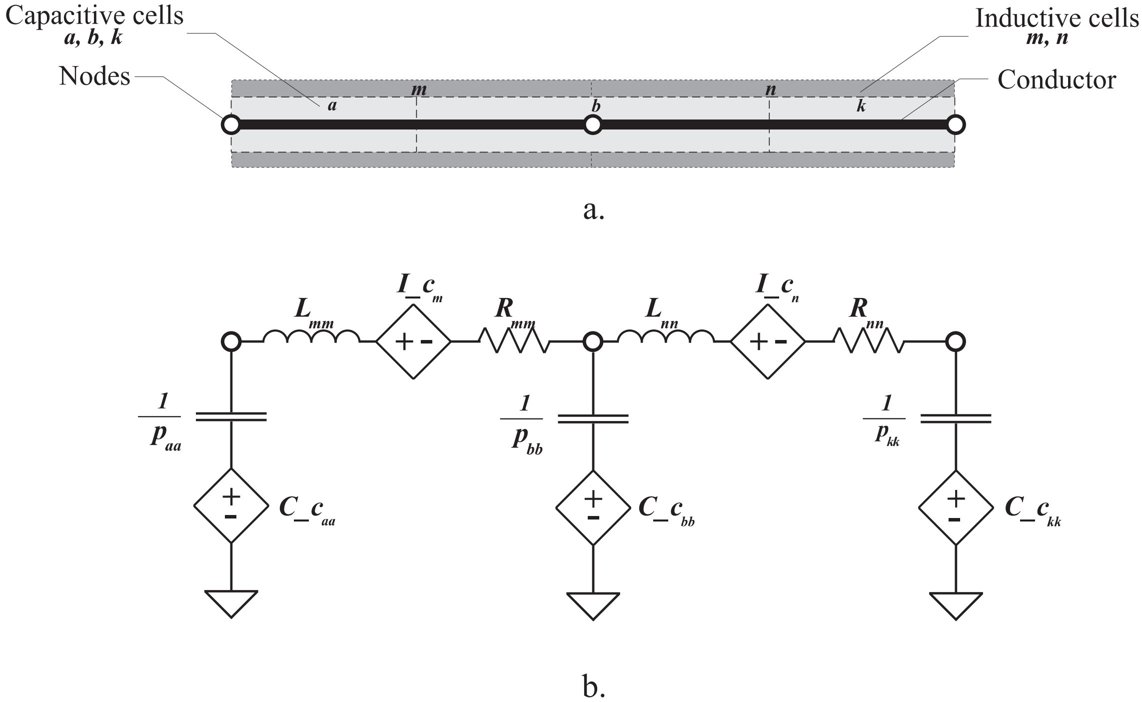


*Figure 1: PEEC two cell example.*

In this paper, guidelines for limiting the order of numerical integration used in the evaluation of the rPEEC partial elements depending on their mutual coupling magnitude are presented. The guidelines are implemented in a PEEC full wave solver. Two case studies confirm the proposed approach provides a good trade-off between accuracy and computation time in the evaluation of the rPEEC partial elements.

# 2 The PEEC Method

The PEEC method originates in partial inductance calculations used for interconnect problems from the early 1970s [1]. The transition from a design tool to the full wave method involves (1) the capacitive representation [2], (2) the inclusion of time retardation [3] and (3) the dielectric formulation [4]. The research performed now reflects on the engineering subject, and thus involves stability analysis [5], speed up [6] and model reduction techniques [7].

## 2.1 Basic theory

The theoretical derivation starts from the expression of the electric field by using the scalar and vector potentials, (1).

$$\vec{E}(\vec{r}) = -j\omega\mu\vec{A} - \nabla\phi \tag{1}$$

If the field point, $\vec{r}$, is on the surface of a conductor and the definitions of the potentials are used with the free space Green's function, $G(\vec{r}, \vec{r\prime})$, (1) can be written as

$$\begin{aligned} \vec{E}^i(\vec{r}) &= \frac{\vec{J}(\vec{r})}{\sigma} + j\omega\mu \int_{v\prime} G(\vec{r}, \vec{r\prime}) J(\vec{r\prime}) dv\prime \\ &+ \frac{\nabla}{\varepsilon_0} \int_{v\prime} G(\vec{r}, \vec{r\prime}) q(r\prime) dv\prime \end{aligned} \tag{2}$$

where $E^i$ is an external applied electric field. This integral equation and the concept of partial elements are the base of the PEEC method. For a more complete theoretical derivation see for example [8].

If the PEEC method is applied to a perfect conductor, solid black in Fig. 1a, the corresponding PEEC two cell consist of partial self inductances, $L_{\alpha\alpha}$, the volume cell DC resistance, $R_{\alpha\alpha}$ between the nodes and the partial self coefficients of potential to each node, $P_{\beta\beta}$, according to Fig. 1b. To account for the retarded electric and magnetic field couplings between the capacitive and inductive partitions, controlled current or voltage sources can be used, $C\_c$ and $I\_c$ in Fig. 1b, respectively. As can be noted from the figure, the capacitive cells, light grey in Fig. 1a, are shifted with regard to the inductive cells, dark grey in Fig. 1a, by half a cell length. This is due to a central difference approximation in the theoretical derivation.

The advantages with the PEEC method become visible in the simple example in Fig. 1. As noted, the method transforms the electromagnetic field problem to a circuit representation and offers a combined solution making it easy to include additional circuit elements such as transmission lines and power sources. The method also offers a great deal of flexibility in the calculation of the partial elements (accuracy and speed), macro-modeling techniques can be used to simplify large problems and the direct coupling to the physics give a good insight to the problem.

## 2.2 Calculating partial elements

All calculations of the complex partial inductances and coefficients of potential are based on (3) and (4), respectively.

$$Lp_{mn} = \frac{\mu \cos\theta}{4\pi s_m s_n} \iiint_{v_m} \iiint_{v_n} \frac{e^{-j\beta|r_m - r_n|}}{|r_m - r_n|} \, dv_n \, dv_m \tag{3}$$

$$P_{ab} = \frac{1}{4\pi\varepsilon s_a s_b} \iint_{s_a} \iint_{s_b} \frac{e^{-j\beta|r_a - r_b|}}{|r_a - r_b|} \, ds_a \, ds_b \tag{4}$$

in which $\theta$ is the angle between the inductive volume cell currents, $s_{m,n}$ are the cross-section in the direction of the currents and $s_{a,b}$ are the area of the charge surface cells. From these formulations a number of analytical equations and approximative formulas have been developed. The expression for the complex partial inductance (3), a double volume integral, can for example be converted to a double surface integration [8], (5), or to a double contour integral [9], (6), for the quasi-static coplanar case.

$$Lp_{mn} = \frac{\mu \cos\theta}{4\pi w_m w_n} \iint_{s_m} \iint_{s_n} \frac{e^{-j\beta|r_m - r_n|}}{|r_m - r_n|} \, ds_n \, ds_m \tag{5}$$

$$Lp_{mn} = -\frac{\mu \cos\theta}{4\pi s_m s_n} e^{-j\beta|r_{c\_c}|} \cdot \sum_{m=1}^{4} \sum_{n=1}^{4} \int_{l_m} \int_{l_n} |r_m - r_n| \, (u_n \cdot u_m) \, dl_n \, dl_m \tag{6}$$

in which $w_{m,n}$ are the widths of the current volume cells, $r_{c\_c}$ is the center to center distance for the surface cells and $u_{m,n}$ are the outward normal vectors to the surface cells [9]. The same conversion can be made for the coefficients of potential, (4). The evaluation of (5) and (6) and the corresponding expressions for the coefficients of potential are performed, in this paper, using different order of Gauss-Legendre integration (GLi). The GLi method is a generalization of the Newton-Cotes formula, shown in (7), using weights, $w$, and not equally spaced abscissas, $\alpha, \beta$, to achieve greater accuracy.

$$\int_0^1 \int_0^1 f(\alpha, \beta) \, d\alpha \, d\beta \approx \sum_{i=0}^{n} \sum_{j=0}^{n} w_i \, w_j \, f(\alpha_i, \beta_j) \tag{7}$$

This method allows the user to choose the number of points, $n$ in (7), used in the method thus influencing the accuracy and the speed of the computation.

## 2.3 Solving PEEC full wave models

After discretizising the structure into nodes and calculating the corresponding partial elements the PEEC model has to be solved in term of node voltages and/or branch currents. This can be done for the simplest case when no retardation is considered in a SPICE like solver. But for a retarded PEEC model, not supported by SPICE, a full wave solver has to be used. In the time domain this corresponds to solving a large set of delayed differential equations. For the frequency domain, a large system of equations including complex elements has to be solved. The partial elements are calculated for each frequency and stored in matrices to facilitate the solution of the PEEC system. From these matrices, the PEEC system admittance matrix, $\mathbf{Y}$, can be formed according to (8).

$$\mathbf{Y} = (\mathbf{A}^T(\mathbf{R} + j\omega\mathbf{L})^{-1})\mathbf{A} + j\omega\mathbf{P}^{-1} \tag{8}$$

in which $\mathbf{R}$ is the volume cell resistance matrix, $\mathbf{P}$ is the partial coefficient of potential matrix , $\mathbf{L}$ is the partial inductances matrix and $\mathbf{A}$ is the connectivity matrix describing the connection of the partial elements. Using this method, the PEEC model is excited using a current vector, $\mathbf{I}$, in which the $n$th place indicates a current injected into the $n$th PEEC model node. The node voltages, $\mathbf{V}$, are then found by solving, $\mathbf{V} = \mathbf{Y}^{-1}\mathbf{I}$. If the PEEC model branch currents and node voltages are required, the modified nodal analysis (MNA) formulation can be used, see [5].

# 3 Integration Order Selection

The developed PEEC full wave solver is formulated according to the admittance matrix method and uses LU decomposition [10] to solve the complex set of equations. A performance test of the solver was performed on a standard laptop, P3/750MHz/256RAM. In the test, the total calculation time of the complex partial mutual elements using $5^{th}$ order, $(n = 5)$, GLi in the surface formulation (4) and (5) and the corresponding system solution time, using LU decomposition, are considered. The result is displayed in Fig. 2 and indicates that both the calculation- and solution time must be improved to make the solver applicable to analysis of systems containing more than 1 000 nodes.

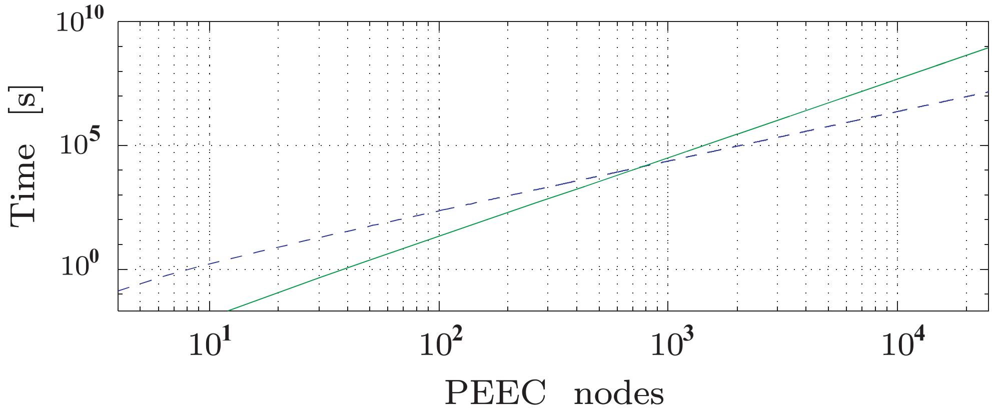


*Figure 2: Complex partial mutual element calculation time, dashed, and solution time for the resulting complex system, solid, per frequency.*

A survey on accuracy and calculation time of complex mutual partial elements, at DC, for the surface formulation using different order of GLi was also performed as shown in Table I. In the table, the complex partial elements for the zero thickness geometries in Fig. 3 are compared. The accuracy is given as the relative error, defined as

$$e_r = \frac{|P_{S8} - P|}{|P_{S8}|} \tag{9}$$

in which $P_{S8}$ is the magnitude of the partial element calculated using the reference case, surface formulation using $8^{th}$ order of GLi (indicated S8), and $P$ is the magnitude of the present partial element calculation. The speed up is defined as the ratio of the CPU times, $\frac{C_{S8}}{C}$ , where $C_{S8}$ is the required CPU time to calculate the partial element using the reference case, surface formulation using $8^{th}$ order of GLi, and $C$ is the CPU time for the present calculation. The tabulated values are strongly correlated to the specific geometry of the problem but give an estimate on the speed up and accuracy achieved with the different orders of GLi.

To improve the speed of the developed solver the focus is on the evaluation of the partial elements since the solution time can be decreased using, for example, an iterative solver or a more efficient matrix library.

*Table 1: Speed up and accuracy for geometries in Fig. 3.*

| Order of GLi | Speed up | Rel. error, $e_r$ a. | b. |
|---|---|---|---|
| $S1$ | 73.5 | 0.1026 | 0.1379 |
| $S2$ | 57.2 | 0.02135 | 0.002450 |
| $S3$ | 30.0 | 0.002726 | 0.000057 |
| $S4$ | 13.1 | 0.000379 | 0 |
| $S5$ | 6.10 | 0.000804 | 0 |
| $S6$ | 3.10 | 0.000619 | 0 |
| $S7$ | 1.70 | 0.000310 | 0 |
| $S8$ - *Ref* | 1 | 0 | 0 |

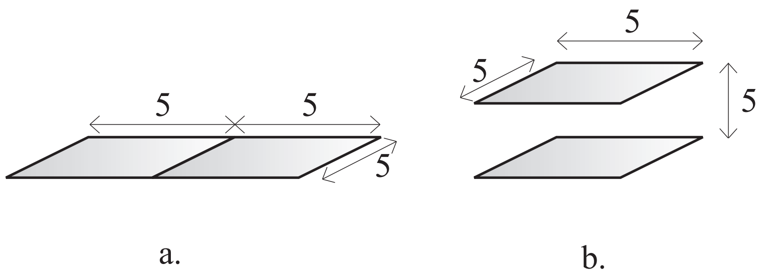


*Figure 3: Test geometries for Table 1 comparisons, dimensions in mm.*

To speed up the evaluation of the partial elements a selection rule of different integration strategies (surface and contour) and order $n$ of GLi is developed. This rule resorts on the fact that mutual partial elements for closely coupled cells must be calculated using a greater accuracy than for weakly coupled, similar to [11] and [12]. The selection is based on the magnitude of the static coupling coefficients $Kp_{ij}$ and $Kl_{ij}$ defined as

$$Kp_{ij} = \frac{p_{0ij}}{\sqrt{p_{0jj} \cdot p_{0ii}}} \tag{10a}$$

$$Kl_{ij} = \frac{l_{0ij}}{\sqrt{l_{0jj} \cdot l_{0ii}}} \tag{10b}$$

where $l_{0ij}$ and $p_{0ij}$ are the quasi-static partial elements calculated using analytical formulas. The selection rule calls for the definition of the coupling limits, by means of the values $K_{min}$, $K_1$,..., $K_{max}$. Depending in which interval the coefficients in (10) fall, suitable integration strategy and order is selected. The logic stepping of the procedure is represented in Table II and can be summarized as follows:

1. Set the calculation routines, choose from (3), (5) and (6) for the complex partial inductance evaluation. Choose the order of GLi used in the routines for each coupling limit, $K_{min}, .., K_{max}$.

*Table 2: General selection rule.*

| Lower coupling limits | | Coupling coefficient | | Upper coupling limits | | Order of Gli |
|---|---|---|---|---|---|---|
| $K_{min}$ | $>$ | $Kl_{ij}$ or $Kp_{ij}$ | | | $\rightarrow$ | $n_{min}$ |
| $K_1$ | $>$ | $Kl_{ij}$ or $Kp_{ij}$ | $\geq$ | $K_{min}$ | $\rightarrow$ | $n_{min+1}$ |
| .. | $>$ | $Kl_{ij}$ or $Kp_{ij}$ | $\geq$ | .. | $\rightarrow$ | $n$ |
| $K_{max}$ | $>$ | $Kl_{ij}$ or $Kp_{ij}$ | $\geq$ | $K_2$ | $\rightarrow$ | $n_{max-1}$ |
| | | $Kl_{ij}$ or $Kp_{ij}$ | $\geq$ | $K_{max}$ | $\rightarrow$ | $n_{max}$ |

2. Calculate two coupling matrices, $\mathbf{P}_0$ and $\mathbf{L}_0$, for partial coefficient of potential and partial inductances using quasi-static analytical formulas.

3. Start frequency looping.

4. Before each complex partial mutual element is calculated, use $\mathbf{P}_0$ and $\mathbf{L}_0$ to estimate the coupling magnitude, $Kp_{ij}$ and $Kl_{ij}$ respectively, and thus what routine to use, as defined in the first stage.

The proposed name for the method detailed above is *The fast multi-function method*, (FMF)PEEC, due to the utilization of different functions for partial element calculations for predefined coupling limits.

*Table 3: Thresholds and corresponding routines used for* rPEEC *tests.*

| *Test* | *Speed up* | *Coupling limits* | $< 0.01$ | *0.01-0.05* | *0.05 - 0.15* | *0.15 - 0.25* | $> 0.25$ |
|---|---|---|---|---|---|---|---|
| *Dipole* | *Ref* | *Ref* | S8 | S8 | S8 | S8 | S8 |
| | 6 | Test 1 | S5 | S5 | S5 | S5 | S5 |
| | 31 | Test 2 | S2 | S3 | S3 | S4 | S5 |
| | 8.8 | Test 3 | - | S5 | S5 | S5 | S5 |
| | 28 | Test 4 | C3 | C3 | C4 | C5 | S5 |
| *PIFA* | *Ref* | *Ref* | S5 | S5 | S5 | S5 | S5 |
| | 4 | Test 5 | S2 | S2 | S3 | S4 | S5 |
| | 6 | Test 6 | S2 | S2 | S2 | S4 | S4 |
| | 6 | Test 7 | A | A | A | A | A |

# 4 Validation and Refinements

## 4.1 Half wavelength dipole

As first test, the input current of a half-wavelength dipole is computed. The dipole dimensions are, (L x W x T), 200 x 1 x $20e^{-3}$ mm including a 2 mm air gap between the two arms resulting in a theoretical resonance frequency of 750 MHz. The dipole was discretized into 20 cells per conductor, giving an upper frequency limit of approximately 3 GHz when using 20 cells per wavelength.

The first test was performed using the thresholds and routines according to Table 3. The abbreviations in the table are S for surface formulation and C for contour formulation with the corresponding order of GLi indicated. The simulation of the reference test, Ref in Table 3 using the surface formulation with $8^{th}$ order GLi, took approximately 20 h for 500 frequencies.

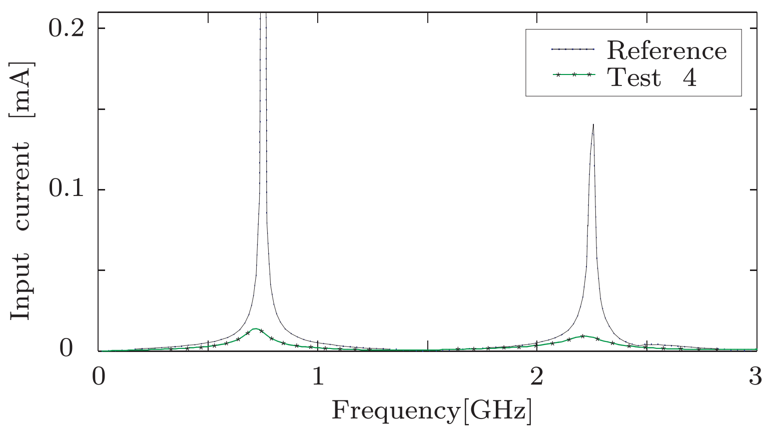


*Figure 4: Half wavelength dipole input current.*

The following tests indicated a considerable speed up but a decrease in accuracy in the input impedance when mixing the surface and the contour formulation as shown in Fig. 4. This can be explained from the fact that the complex contour formulation only considers a center to center cell distance when evaluating the exponential term in (6). This results in 'unmatched' delays for the whole system and a smoothing of the system response. This was confirmed by using the surface formulation with the center to center approximation mixed with the original formulation. The dipole was also simulated, in Test 3, without the mutual elements [12, 11] with a coupling magnitude, (10), less then 0.01. This exclusion of retarded couplings results in a speed up but also to a more undamped system response since time delays that includes a natural damping in the system are excluded. The speed up that the scheme, using the conditions for Test 2, offers is a factor of 31 with good agreement to the reference case up to the upper frequency limit, see Fig. 5. Further tests indicated that the speed up is kept when increasing the discretization and thus increasing the upper frequency limit.

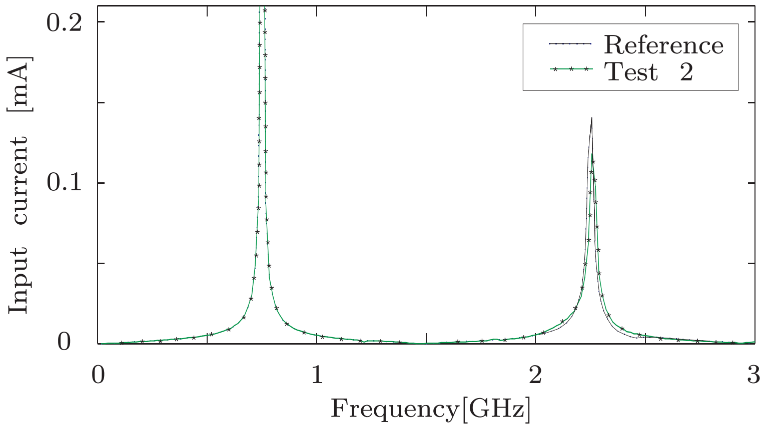


*Figure 5: Half wavelength dipole input current.*

## 4.2 Planar inverted F antenna (PIFA)

As second test, the resonance frequencies for the 900 / 1800 MHz planar inverted F antenna in Fig. 6 were modelled. The antenna consists of two antenna patches connected through a LC resonator circuit located 6 mm above a ground plane [13].

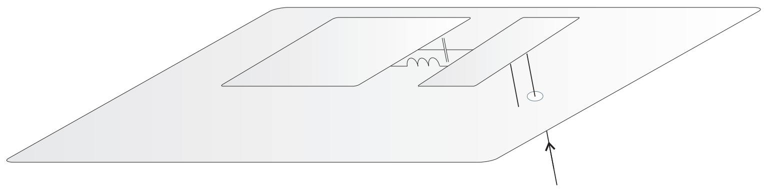

*Figure 6: Planar Inverted F Antenna (PIFA).*

This structure was modelled using 2.5 mm square cells for the zero thickness antenna patches, 20×20 and 10×20 mm. In the 100×50 mm, zero thickness ground plane, 5 mm square cells were used. The PIFA was simulated up to 2.5 GHz using the thresholds and routines according to Table 3. For Test 7, specified in Table III, all mutual partial elements where calculated using analytic expressions, indicated with A in Table III, using a center to center approximation for the evaluation of the complex exponential term in (3) - (6). The result for one PIFA simulation, Test 7, is shown in Fig. 7 where the reflection coefficient of the antenna, $S_{11}$ with reference to 50 Ω, is displayed and compared against a full wave finite integration technique (FIT) simulation using CST Microwave Studio [14]. The two resonance frequencies at 900 and 1800 MHz were found exactly in the PEEC simulation while the FIT is 7% off for the higher resonance. For Test 7 the simulation time is 8 min/freq. for a discretization that consist of 418 capacitive nodes. This total solution time is strongly dependant on the matrix manipulation routines used and can be further improved by using a more efficient matrix library. The speed up is typically a factor four to six for the performed tests when comparing to the reference case not using

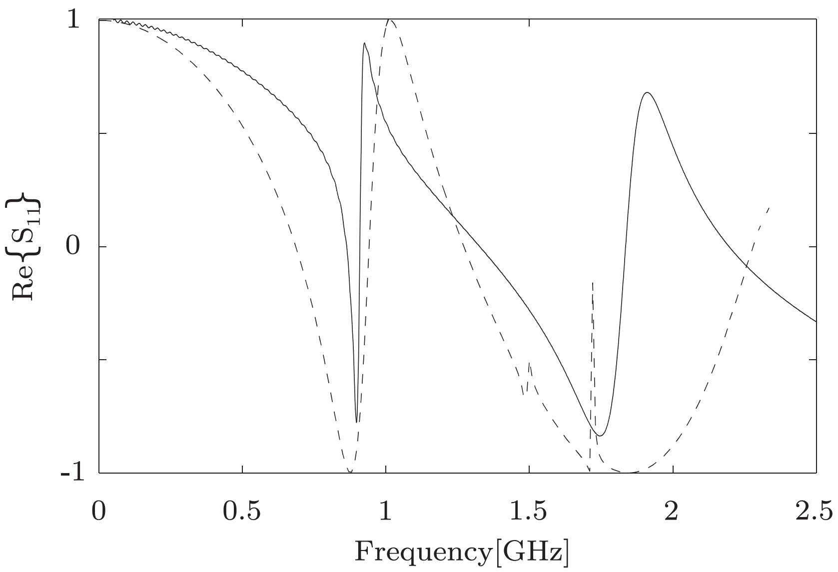


*Figure 7: $S_{11}$ for PIFA. Comparison for CST software (solid) and PEEC (dashed).*

the proposed thresholding scheme. The smoothing of the system response is also noted for the PIFA as for the dipole when mixing the surface and contour formulation, Fig. 4.

# 5 Conclusions

The proposed *The fast multi-function method* to speed up the evaluation of the rPEEC partial elements in a PEEC full wave frequency domain solver has been successfully implemented. It has been shown that using a thresholding scheme where 2 to 5 point GLi is used to calculate the complex partial elements provides the best trade-off between accuracy and speed for these antenna examples. The speed up is typically a factor of 31, comparing the reference case with Test 2 and a factor of five when comparing Test 1 and Test 2. It was also noted that mixing different techniques for the partial element calculation can decrease the accuracy in the solution.

# References


[1] A. E. Ruehli, "Inductance Calculations in a Complex Integrated Circuit Environment", *IBM Journal of Research and Development*, 16(5):470–481, September 1972.

[2] P. A. Brennan and A. E. Ruehli, "Efficient Capacitance Calculations for Three-Dimensional Multiconductor Systems", *IEEE Transactions on Microwave Theory and Techniques*, 21(2):76–82, February 1973

[3] A. E. Ruehli and H. Heeb, "Retarded Models for PC Board Interconnects - or How the Speed of Light Affects Your SPICE Circuit Simulation", in: *Proc. of the IEEE Int. Conference on Computer-Aided Design*. pages 70–73, Los Alamitos, CA, USA, 1991.

[4] A. E. Ruehli, "Circuit Models for Three-Dimensional Geometries Including Dielectrics", *IEEE Transactions on Microwave Theory and Techniques*, 40(7):1507–1516, July 1992.

[5] A. E. Ruehli, U. Miekkala, and H. Heeb, "Stability of Discretized Partial Element Equivalent EFIE Circuit Models, *IEEE Transactions on Antennas and Propagation*, 43(6): 553–559, June 1995.

[6] G. Antonini, A. Orlandi, and A. E. Ruehli, "Speed-Up of PEEC Method by Using Wavelet Transform", in: *Proc. of the IEEE Int. Symp. on EMC*, Washington, DC, USA, August 2000.

[7] R. D. Slone, W. T. Williams, and Z. Bai, "Using Partial Element Equivalent Circuit Full Wave Analysis and Pade Via Lanczos to numerically Simulate EMC Problems", in: *Proc. of the IEEE Int. Symp. on EMC*, Washington, DC, USA, August 2000.

[8] J. E. Garrett, A. Ruehli, and C. R. Paul, "Accuracy and Stability Improvements of Integral Equation Models Using the Partial Element Equivalent Circuit (PEEC) Approach", *IEEE Transactions on Antennas and Propagation*, 46(12):1824–1832, December 1998.

[9] G. Antonini, A. Orlandi, and A. Ruehli, "Analytical Integration of Quasi-Static Potential Integrals of Nonorthogonal Coplanar Quadrilaterals for the PEEC Method", *IEEE Transactions on EMC*, 44(2):399–403, May 2002.

[10] Matrix TCL Pro 2.0, (2002-02-28), http://www.techsoftpl.com/matrix/index.htm.

[11] F. Sabath and H. Garbe, "Prediction Errors due to Ignoring Field Coupling on Printed Circuit Boards", in: *Proc. of the* 12$^{th}$ *Int. Zurich Symp. on EMC*, Zurich, Switzerland, February 1997.

[12] F. Sabath and H. Garbe, "Prediction of Computation Errors due to Ignoring Coupling between Signal Traces", in: *Proc. of the IEEE Int. Symp. on EMC*, Austin, TX, USA, August 1997.

[13] G. K. H Lui and R. D. Murch, "Compact Dual-Frequency PIFA Design Using LC Resonators", *IEEE Transactions on Antennas and Propagation*, 49(7):1016–1019, July 2001.

[14] CST Microwave Studio, (2002-02-28), http://www.cst.de.

# Paper D

# Nonorthogonal PEEC Formulation for Time- and Frequency-Domain EM and Circuit Modeling

**Authors:**
A. E. Ruehli[1], G. Antonini[2], J. Esch[1], J. Ekman, Anita Mayo[1], A. Orlandi[2]

**Reformatted version of paper originally published in:**
*IEEE Transactions on EMC*, vol. 45, no. 2, May 2003.



[1]IBM TJ Watson Research Center, Yorktown, New York, USA.
[2]University of L'Aquila, Department of Electrical Engineering, Poggio di Roio, 67100 L'Aquila.

# Nonorthogonal PEEC Formulation for Time- and Frequency-Domain EM and Circuit Modeling

A. E. Ruehli, G. Antonini, J. Esch, J. Ekman, A. Mayo, A. Orlandi

**Abstract**

Electromagnetic solvers based on the Partial Element Equivalent Circuit (PEEC) approach have proven to be well suited for the solution of combined circuit and electromagnetic problems. The inclusion of all types of SPICE circuit elements is possible. Due to this, the approach has been used in many different tools. Most of these solvers have been based on a rectangular or Manhattan representation of the geometries. In this paper we systematically extend the PEEC formulation to the case of nonorthogonal geometries since many practical electromagnetic problems require a more general formulation. Importantly, the model given in this paper is consistent with the classical PEEC model for rectangular geometries. Examples illustrating the application of the approach are given for both the time and frequency domain.

## 1 Introduction

The need for practical computational tools and techniques as well as models for realistic EMC and Electrical Interconnect and Package (EIP) problems has increased drastically over the last few years with the faster speed of digital electronic chips and with the increased frequencies in todays RF circuits. In response to this progress in technologies, electromagnetic (EM) modeling techniques and EM solvers have also made progress at an impressive pace. This has resulted in specialized versions of the modeling techniques. Solvers are tailored for a specific class of problems, which allows increased efficiency. An EM modeling approach must be classified as suitable for a particular application range e.g. electrical machines, scattering problems, waveguide analysis or, again, EMC or EIP problems. Even the EMC and the EIP classes can be further subdivided into subproblems for which a particular solution approach yields the best results [1]. In this paper we consider the surface and volume integral equation based Partial Element Equivalent Circuit (PEEC) technique applied to heterogeneous combined circuit and EMC and/or EIP problems. Examples of other approaches for mixed EM-circuit problems are given for the TLM method in [2] and for the FDTD technique in [3].

The PEEC approach has evolved over the years with a focus toward EMI and EIP problems. In the beginning, full wave solutions were not necessary for many aspects of the problems and the quasi-static solutions were used. They are still in use, for capacitance [4, 5, 6] and inductance ($L_p$)PEEC problems [7]-[12]. With the increase in the speed and frequency ranges of the VLSI chips, higher frequency solutions became necessary. This made the use of more consistent models necessary and many variants of

PEEC models were devised for different applications [13]-[22]. A clear and easy notation has been devised to differentiate between the many different possible PEEC models. As an example, the notation $(L_p, P, R, \tau)$PEEC means that the model includes partial inductance $L_p$, coefficients of potential $P$, resistance $R$ and delays $\tau$. For a specific application, other combinations of elements may be more suitable. The delays in time are equivalent to a complex term in the mutual partial elements, phase shift, in the frequency domain as is apparent from the Laplace transform where $\mathcal{L}f(t-\tau) = F(s)\,e^{-s\tau}$. The PEEC method can be applied in both the time and the frequency domain very much like a typical SPICE type circuit solver where the option *.ac* leads to a frequency domain analysis while *.tran* corresponds to a time domain analysis. Time domain models are used extensively for modeling VLSI circuits and chips while frequency domain models are used for RF type applications.

In this paper, we focus on a systematic extension of the PEEC solution for nonorthogonal geometries in both the time and the frequency domain. Early on in the history of PEEC models, simplified nonorthogonal geometries where modelled in terms of rectangular bars with arbitrary orientations [9, 11, 12, 23]. Very recently, new approaches have been presented for nonorthogonal PEEC models using triangular cells with other approaches e.g. [21, 24, 25]. In this paper we further develop the quadrilateral or hexahedral formulation presented in [26, 27]. The quadrilateral and hexahedral shapes are used to represent the different conductors as well as dielectric regions. Quadrilateral surface cells have been used successfully for EM modeling using the integral equation solution approach e.g. [28, 29].

Importantly, the new general formulation retains all the properties of the orthogonal PEEC method. In fact, it is intriguing that the topology of the resultant general PEEC circuit model is exactly the same for rectangular and nonorthogonal geometries provided that triangular cells are not used [30]. For example, triangular surface cells need three basis functions rather than two as is the case for rectangular as well as quadrilateral surface cells. Hence, the new approach in this paper retains the flexibility of the conventional orthogonal PEEC approach, and importantly, properties like *full-wave* and *full-spectrum*. The *full-wave* aspects refers to the fact that up to a high frequency limit all modes of propagation are calculated. The *full-spectrum* label means that the method does not have a low frequency limit as is the case for many other EM methods. The PEEC solution is valid down to and including a *dc* solution which is very important for the modeling of time domain problems. This is in part why the *full-wave* model is practically the same as the quasi-static model with the exception of the delays or retardation provided that the appropriate circuit elements are included in the model. Further, the PEEC model has been extended to accurately include models for dielectrics [13, 22] and also scattering or incident fields [31]. The nonorthogonal extension in this paper can be applied to all aspects of modeling like $(L_p, R)PEEC$ inductance models or other reduced models. Example applications for the nonorthogonal approach are arbitrary shaped printed circuit antennas or the modeling of connectors including their EMI radiation. Other EMC and EIP applications point to the strength of the method. For example, the method has been applied for the modeling of high voltage towers [15], and the analysis of printed circuit boards e.g. [16, 22, 26]. Also, comparisons with measurement and the solution with other techniques have been made [32, 33].

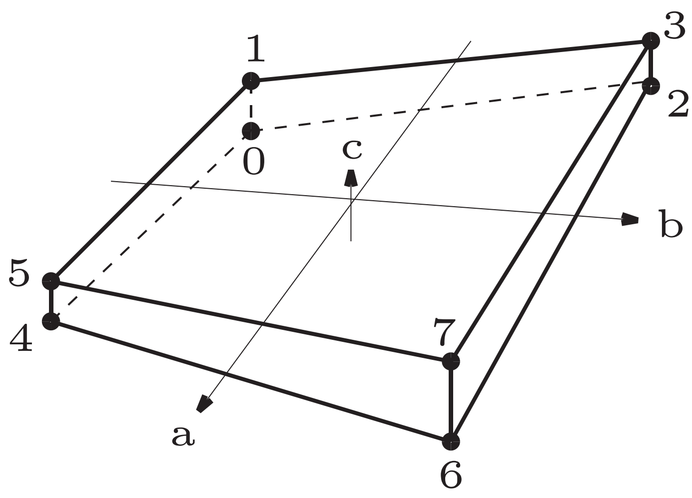


*Figure 1: Basic hexahedral cell with local coordinates.*

# 2 Nonorthogonal PEEC Model

## 2.1 Nonorthogonal formulation

In this Section we give an outline of the geometrical nonorthogonal extension to the PEEC method. The objects can be quadrilateral and/or hexahedral conductors or dielectrics which can be both orthogonal and/or nonorthogonal.

The formulation utilizes a *global* as well as a *local* coordinate system. The key *global* coordinate system uses the conventional Cartesian coordinates $x, y, z$ where a global vector $\vec{F}$ is of the form $\vec{F} = F_x\hat{x} + F_y\hat{y} + F_z\hat{z}$. Therefore, the global unit vectors $\hat{x}$, $\hat{y}$ and $\hat{z}$ are position independent. We mark a vector in the global coordinates as $\vec{r_g}$ for a clear distinction from the local coordinates. The *local* coordinates $a, b, c$ are used to separately represent each specific possibly nonorthogonal object. We call the unit vectors $\hat{a}, \hat{b}, \hat{c}$ so that they are not confused with circuit variables like voltage $v$ etc. Details for nonorthogonal coordinate systems can be found in several texts e.g. [34]. First, we very briefly introduce the local coordinate system we use for a hexahedral element shown in Fig. 1. The purpose of the local coordinates is to identify the location of any point belonging to the hexahedron in terms of the variables $a, b, c$ where $a \in [-1, +1]$ and where $a$ can mean $a = a, b, c$. The purpose of all this is to uniquely map a point $a, b, c$ into a point in the global coordinates $\vec{r_g}$. We accomplish this by specifying eight vectors $\vec{r_{gk}}$ where $k = 0, ..., 7$ with the coordinates $x_k, y_k, z_k$. It will be clear that the corners of the hexahedron are reached when $a, b, c = \pm 1$.

Next, we create clean assignment of the corner indices in Fig. 1 for the hexahedron using a binary code for the symbols $a, b, c$, where the -1 coordinates map into logical zeros, and +1 coordinates map into logical ones. The order of the logical variables is abc. Hence, for example, the binary code $abc = 011$ corresponds to the corner $a = 0$,

$b = 1$ and $c = 1$ and its decimal equivalent is 3 for corner 3 as can be verified in Fig. 1. This makes the assignment unique and easy to remember. As indicated above, all local coordinates have to relate back to the global $x, y, z$ coordinates. Therefore, a unique representation is needed for the mapping from a local point $a, b, c$ on an object to the global point $\vec{r_g}$. Mapping a point in the above hexahedron from a local coordinate point $a, b, c$ into a global coordinate point $x, y, z$ is described by

$$x = \sum_{k=0}^{7} N_k(a, b, c) x_k, \tag{1}$$

which is applied for $x = x, y, z$. The coefficients in (1) are given by

$$\begin{aligned}
N_0 &= 1/8(1-a)(1-b)(1-c)\\
N_1 &= 1/8(1-a)(1-b)(1+c)\\
N_2 &= 1/8(1-a)(1+b)(1-c)\\
N_3 &= 1/8(1-a)(1+b)(1+c)\\
N_4 &= 1/8(1+a)(1-b)(1-c)\\
N_5 &= 1/8(1+a)(1-b)(1+c)\\
N_6 &= 1/8(1+a)(1+b)(1-c)\\
N_7 &= 1/8(1+a)(1+b)(1+c)
\end{aligned} \tag{2}$$

where $a \in [-1, +1]$ and again $a = a, b, c$. The close relation to the binary variables is evident in (2).

With this, we are in a position to also express the tangential vectors with respect to the local coordinates as

$$\frac{\partial \vec{r_g}}{\partial a} = \frac{\partial x}{\partial a}\hat{x} + \frac{\partial y}{\partial a}\hat{y} + \frac{\partial z}{\partial a}\hat{z} \tag{3}$$

where the derivatives are found from (1) and (2). Finally, the magnitude of the tangential vector $h_a = \left|\frac{\partial \vec{r_g}}{\partial a}\right|$ where the position dependent unit vectors can be determined from $\hat{a} = \left(\frac{\partial \vec{r_g}}{\partial a}\right) \Big/ h_a$ where again $a = a, b, c$. With this we are prepared to formulate the geometrical aspects for the nonorthogonal PEEC circuit elements.

In the PEEC circuit solution, terminal or nodal variables are associated with each of the resultant circuit elements will be collected in an overall circuit solver vector of unknowns. The solution vector variables are quantities like the potentials $\vec{\Phi}$, and other conventional circuit variables like $i, \vec{v}, q$ where $\vec{i}$ are the currents, $\vec{v}$ the voltages, and $\vec{q}$ charges. If no other circuit elements are included, the solution vector used is $(\vec{\Phi}, \vec{i})^T$ as the only unknowns since this vector directly yields the most useful EM circuit output variables. Here we point out that in part, the inclusion of both $\vec{\Phi}$ and $\vec{i}$ is, responsible for the *full spectrum* property of the solution methodology such that the correct *dc* solution is obtained.

## 2.2 Basic integral equations for nonorthogonal geometries

The PEEC formulation uses an integral equation solution of Maxwell's equations based on the total electric field. An integral, or inner product, is used to reformulate each term of (10) into the circuit equations. This inner product integration converts each term into the fundamental form $\int \vec{E} \cdot dl = V$ where $V$ is a voltage or potential difference across the circuit element. It is evident that this transforms the sum of the electric fields in (4) into the Kirchoff's Voltage Law (KVL).

The starting point is the total electric field at or in the material which is

$$\vec{E}^i(\vec{r_g}, t) = \frac{\vec{J}(\vec{r_g}, t)}{\sigma} + \frac{\partial \vec{A}(\vec{r_g}, t)}{\partial t} + \nabla \phi(\vec{r_g}, t) \tag{4}$$

where $\vec{E}^i$ is a possible incident electric field, $\vec{J}$ is the current density in a conductor and $\vec{A}$ and $\phi$ are the electromagnetic vector and scalar potentials, respectively. As indicated above, the dielectric areas are taken into account as an excess current rather than a capacitance with the scalar potential using the volume equivalence theorem [35]. This is accomplished by adding and subtracting $\epsilon_0 \partial \vec{E}/\partial t$ in the Maxwell equation for $\vec{H}$, or

$$\nabla \times \vec{H}(\vec{r_g}, t) = \vec{J}(\vec{r_g}, t) + \epsilon_0(\epsilon_r - 1)\frac{\partial \vec{E}(\vec{r_g}, t)}{\partial t} + \epsilon_0 \frac{\partial \vec{E}(\vec{r_g}, t)}{\partial t} \tag{5}$$

Here, the current in (5) is written as a total current

$$\vec{J}(\vec{r_g}, t) = \vec{J_C}(\vec{r_g}, t) + \epsilon_0(\epsilon_r - 1)\frac{\partial \vec{E}(\vec{r_g}, t)}{\partial t} \tag{6}$$

where $\vec{J_C}$ is the conductor current and the remainder of the equations is the equivalent polarization current due to the dielectric.

The vector potential $\vec{A}$ is for a single conductor at the field point $\vec{r_g}$ given by

$$\vec{A}(\vec{r_g}, t) = \mu \int_{v\prime} G(\vec{r_g}, \vec{r_g}\prime)\vec{J}(\vec{r}\prime, t_d)dv\prime \tag{7}$$

where the retardation time is given by $t_d = t - \mid \vec{r_g} - \vec{r_g}\prime \mid /c$ which simply is the free space travel time between the points $\vec{r_g}$ and $\vec{r_g}\prime$. It is noted that in the formulation derived here, both the retardation and the Green's functions are free space quantities where

$$G(\vec{r_g}, \vec{r_g}\prime) := \frac{1}{4\pi} \frac{1}{\mid \vec{r_g} - \vec{r_g}\prime \mid} \tag{8}$$

The scalar potential is defined as

$$\phi(\vec{r_g}, t) = \frac{1}{\epsilon_0} \int_{v\prime} G(\vec{r_g}, \vec{r_g}\prime) q(\vec{r_g}\prime, d) dv\prime \tag{9}$$

Finally, using the above, we can formulate an integral equation for the electric field at a point $\vec{r_g}$ which is to be located either inside a conductor or inside a dielectric region. Starting from (4) with the externally applied electric field set to zero, and substituting

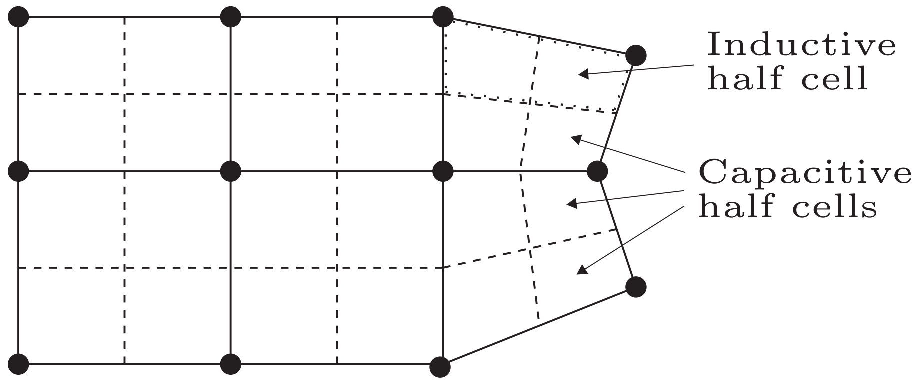


*Figure 2: Geometry with several quadrilateral elements.*

for $\vec{A}$ and $\phi$ from (7) and (9) respectively. For more details, please see any one of the PEEC papers e.g. [14, 20, 36, 37]. A derivation of the PEEC model with the rectangular, finite dielectrics is given in [13]. The final integral equation to be solved is

$$\begin{aligned} \hat{n} \times \vec{E}^i(\vec{r_g}, t) &= \hat{n} \times \left[ \frac{\vec{J}(\vec{r_g}, t)}{\sigma} \right] \\ &+ \hat{n} \times \left[ \mu \int_{v\prime} G(\vec{r_g}, \vec{r_g}\prime) \frac{\partial \vec{J}(\vec{r_g}\prime, t_d)}{\partial t} dv\prime \right] \\ &+ \hat{n} \times \left[ \epsilon_0(\epsilon_r - 1)\mu \int_{v\prime} G(\vec{r_g}, \vec{r_g}\prime) \frac{\partial^2 \vec{E}(\vec{r_g}\prime, t_d)}{\partial t^2} dv\prime \right] \qquad (10) \\ &+ \hat{n} \times \left[ \frac{\nabla}{\epsilon_0} \int_{v\prime} G(\vec{r_g}, \vec{r_g}\prime) q(\vec{r_g}\prime, t_d) dv\prime \right] \end{aligned}$$

where $\hat{n}$ is the surface normal to the body surfaces. Equation (10) is a time domain formulation which can easily be converted to the frequency domain by using the Laplace transform operator $s = \partial/\partial t$ and where the time retardation will transform to $e^{-s\tau}$ where $\tau$ is the delay time.

## 2.3 Discretization of conductor and dielectrics geometries

Section 2.2 shows the integral equation (10) which needs to be solved. In this Section we determine the discrete equivalent and the circuit elements for nonorthogonal geometries. The basic hexahedral element or object is shown in Fig. 1 and an example for the connection between quadrilateral and orthogonal surface elements is shown in Fig. 2. In PEEC we distinguish between inductive and capacitive cells and subdivisions where the inductive cells connect between the nodes and capacitive cells surround the nodes. The compatibility between quadrilateral and rectangular cells is apparent from Fig. 2. The bodies are joined together simply by joining the nodes where the adjoining half cells in

Fig. 2 combine into full cells. To represent the current flow in orthogonal cells, we use the convenient weighting function $J = I/(WT)$ where $I, J$ are the current and current density and $W, T$ are the cell width and thickness, respectively. For the general case, we assume also that the conductor cross section is subdivided into cells to take the Skin effect into account. This leads to the hexahedral elements in Fig. 1 for the nonorthogonal case. Since PEEC is an integral equation based formulation the usual volume filament (VFI) Skin effect models result automatically from the subdivision of the interiors of the conductors [36]. The generalization of the current distribution for nonorthogonal hexahedral cell shapes is given by

$$J_a = \frac{h_a}{\left|\frac{\partial \vec{r_g}}{\partial a} \cdot (\frac{\partial \vec{r_g}}{\partial b} \times \frac{\partial \vec{r_g}}{\partial c})\right|} I_a \tag{11}$$

where $J_b$ and $J_c$ can easily be found by permuting the indices. We call the quotient in (11) the weight $w_a$ which simplifies (11) to $J_a = w_a I_a$. We should note that all the above quantities are a function of the local position coordinates $a, b, c$. Next, we use an integral or inner product operator

$$V_a = \int_a \int_b \int_c w_a \hat{a} \cdot \vec{E} \left|\frac{\partial \vec{r_g}}{\partial a} \cdot (\frac{\partial \vec{r_g}}{\partial b} \times \frac{\partial \vec{r_g}}{\partial c})\right| da\, db\, dc \tag{12}$$

to integrate the terms of (10) where $\vec{E}(a, b, c)$ is the $\vec{E}$ field term to be integrated. We need to apply the inner product to each term in (10) to transform each term to a voltage drop across a circuit element in the KVL equation. Next, we integrate the right hand terms of the integral equation (10). After applying the inner product, the first element on the right hand side leads to the series resistance term in the form

$$R_a = \frac{1}{\sigma} \int_a \int_b \int_c \frac{{h_a}^2}{\left|\frac{\partial \vec{r_g}}{\partial a} \cdot (\frac{\partial \vec{r_g}}{\partial b} \times \frac{\partial \vec{r_g}}{\partial c})\right|} da\, db\, dc \tag{13}$$

The second right hand side term of (10), after applying (12) is a generalization of the partial inductance concept for nonorthogonal problems, or

$$Lp_{aa'} = \mu \int_a \int_b \int_c \int_{a'} \int_{b'} \int_{c'} (\hat{a} \cdot \hat{a}')\ h_{a'}\ \ G[\vec{r_g}(a, b, c); \vec{r_g}(a', b', c')]\ da'\, db'\, dc'\ h_a\ da\, db\, dc \tag{14}$$

The charge density is in general of a similar form as (11). Of course charge does not have a directional dependence, and the volume charge $q_v$ is given by

$$q_v(a, b, c) = \frac{1}{\left|\frac{\partial \vec{r_g}}{\partial a} \cdot (\frac{\partial \vec{r_g}}{\partial b} \times \frac{\partial \vec{r_g}}{\partial c})\right|} Q \tag{15}$$

where $Q$ is the total charge in the volume cell. For the conventional conductors, the charge will be restricted to the surface cells only. The gradient in (4) in the $\hat{a}$ direction evaluates to

$$\nabla \phi|_a = \frac{1}{h_a} \frac{\partial \phi}{\partial a} \tag{16}$$

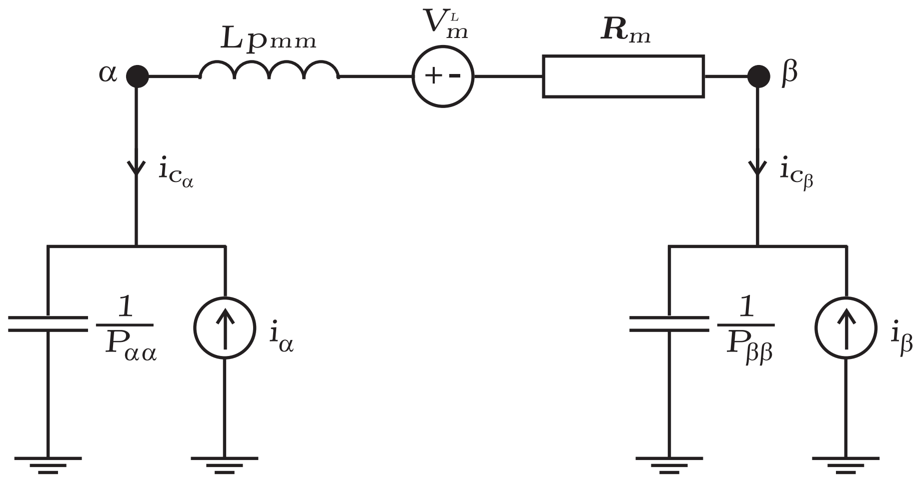


*Figure 3: PEEC model for one inductive branch of Fig. 1.*

To maintain symmetry for the circuit elements or coefficients we approximate the derivative, with an integrated average over the two corner cells corresponding to the derivative where the spacing is the projection in the $\hat{a}$ direction for the center to center distance $d_a$. This approximation implies that (16) simplifies to

$$\nabla\Phi|_a \approx \frac{1}{h_a\, d_a} \int \phi(a,b,c) dS_l \tag{17}$$

where $S_l$ is a surface in the appropriate surface direction(s). Finally, by inserting for the potential $\phi$ in (17) and by cancelling the appropriate terms, we get for the coefficients of potential

$$P_{aa'} = \frac{1}{\epsilon} \int_a \int_b \int_{a'} \int_{b'} G[\vec{r_g}(a,b,c); \vec{r_g}\prime(a',b',c')]\ da\prime\, db\prime\ da\, db \tag{18}$$

Here $a, b, a', b'$ are interpreted in a general sense for the appropriate cell orientations.

The PEEC circuit for one inductive branch is shown in Fig. 3. The top part of Fig. 1 consists of four inductive branches resulting in four KVL loops. Specifically, a KVL loop involves two nodes with the capacitances to infinity and a partial inductance in series with a resistor. Hence, the element shown for the bottom layer only of the element shown in Fig. 1 consists of four loops to infinity where the PEEC topology for the orthogonal and the nonorthogonal case are the same, with the exception of the circuit element values. Importantly, the same MNA circuit solver can be used for both separately as well as the mixed cases.

Similar to the orthogonal case, the dielectrics are represented with additional circuit elements. We define the excess capacitance of a dielectric cell $\gamma$ as

$$C_\gamma^+ := \epsilon_0(\epsilon_\gamma - 1) \Big/ \int_a \int_b \int_c \frac{{h_a}^2}{\left|\frac{\partial \vec{r_g}}{\partial a} \cdot \left(\frac{\partial \vec{r_g}}{\partial b} \times \frac{\partial \vec{r_g}}{\partial c}\right)\right|} dadbdc \tag{19}$$

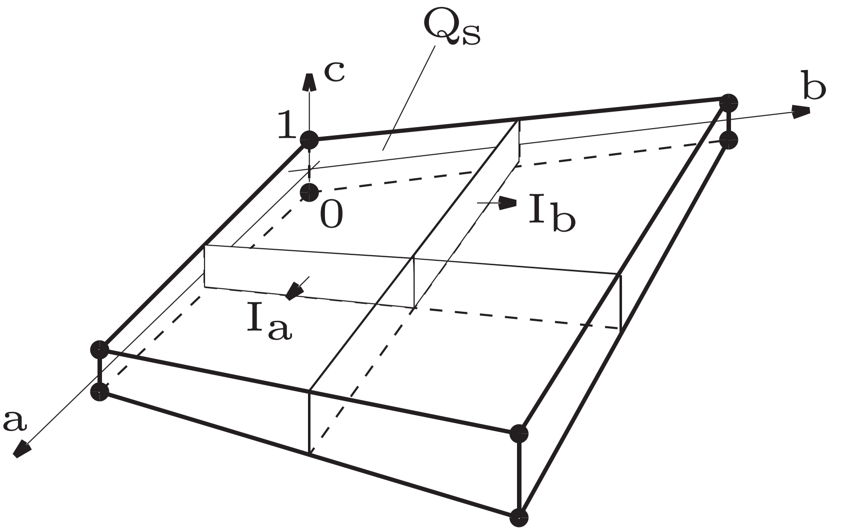


*Figure 4: PEEC model for top part of Fig. 1.*

where $\epsilon_\gamma$ is the dielectric constant of the dielectric cell. The equivalent circuit for the dielectric cell $\gamma$ is given by a partial inductance $Lp_{\gamma\gamma}$ in series to a capacitor $C^+_\gamma$ with the current $i = C^+_\gamma \frac{d(\Phi_a - \Phi_b)}{dt}$, where $\phi_a$ and $\phi_b$ are the potential at the two ends of the dielectric cell. This model for finite dielectrics is a very important part of the PEEC approach [13].

## 2.4 Continuity equation and Kirchoff's current law

It is important that the continuity equation is satisfied at the cell level for the currents and charges. Its differential form is given by $\nabla \cdot \vec{J} + \frac{\partial q}{\partial t} = 0$ where $\vec{J}$ is the current density and $q$ is the surface charge density. The continuity equation is applied at the location of each node. For this reason, we show the geometry of a corner in Fig. 4 corresponding to nodes 0 and 1 in Fig. 1. Since only one quarter of the elements surrounding the node is shown, we assume that the surface element in Fig. 4 may be connected to other similar surfaces along the a-c and the b-c surfaces. Hence, the volume for which the continuity equation is applied consists of the corners which are involved in the geometry surrounding the node(s). It is sufficient to consider only the corner elements, by ignoring the internal surfaces shown in Fig. 4, for simplicity.

Integrating the continuity equation over the corner yields

$$\int_v \nabla \cdot \vec{J} dv = -\frac{\partial}{\partial t} \int_v q \, dv = \int_s \vec{J} \cdot \hat{n} \, dS \tag{20}$$

where the divergence theorem [38] is used in the last step and where the vector $\hat{n}$ is normal to the surface $S$. The volume integral part pertains to the top and bottom $a - b$ surfaces corners connected to nodes 1 and 0 which are charged as indicated with $Q_s$ in Fig. 4. If the nodes 0 and 1 are shorted, then the charge density consists of two $\delta$-functions at the surfaces of the conductors with the surface charge $q(a,b,c)$ and the contributions at $c=\pm 1$ are

$$Q = \int_{a=-1}^{0}\int_{b=-1}^{0} q(a,b)\left|\frac{\partial \vec{r_g}}{\partial a}\times\frac{\partial \vec{r_g}}{\partial b}\right| da\, db \tag{21}$$

and where the surface charge can be found from (15) as $q_\pm(a,b) = Q_\pm / \left|\frac{\partial \vec{r_g}}{\partial a}\times\frac{\partial \vec{r_g}}{\partial b}\right|$. Inserting this into (21) yields the charges $Q_\pm$ on the corner surfaces.

Similarly, the currents associated with the corner nodes $0,1$ are flowing through the cross-sectional areas indicted by $I_a$ in the $a$ direction and $I_b$ in the $b$ direction. The current through the section of conductor cross-section for $I_a$ is given by

$$I_a = \int_{b=-1}^{0}\int_{c=-1}^{0} I_a\, w_a \hat{a}\cdot\left|\frac{\partial \vec{r_g}}{\partial b}\times\frac{\partial \vec{r_g}}{\partial c}\right| db\, dc \tag{22}$$

Again, the same relationship holds for the equation for the $b$ coordinate. Adding all terms pertaining to the continuity equation we get, for one corner only

$$\frac{dQ_+}{dt}+\frac{dQ_-}{dt}+I_a+I_b=0 \tag{23}$$

which can be recognized as the KCL. It is evident that the continuity equation is satisfied since the admittance part of the Modified Nodal Analysis (MNA) formulation method [39] is based on summing up all the current contributions at a node. Another important observation is that for systems which include retardation all the parts which belong to a node are mostly instantaneous, while the retardation must be included for all parts outside the volume. Since the partial inductances extend from one node to a neighbor node, we need to subdivide the partial inductances into two half-s were the part at the node is instantaneous and where the second part which belongs to a neighboring cell must include a retarded partial mutual inductance. It should be noted that this does not introduce additional unknowns and it improves the time domain stability [40].

# 3 Evaluation of Circuit Elements

One of the challenging subjects for the PEEC method is the evaluation of the circuit elements due to the high accuracy requirements for the dense structures which must be solved for EMI and EIP problems. This issue is worst for elements corresponding to cells which coincide or are in close physical proximity. Unfortunately, the early work in this field, like inductance calculations in power systems, had different less dense applications where more approximate results were acceptable [41]. For speed and accuracy reasons, we utilize a *multi-function* approximation approach for the coefficient evaluation which is based on analytical results as well as on numerical solutions. Further, the PEEC method poses another challenge for the coefficient evaluation due to the large aspect ratios in the size of the conductors as will be shown below in an example in Section 5. The evaluation of the partial inductances (14) for rectangular geometries has been the topic of many papers over the years e.g. [7, 9, 12, 42]. Further, the coefficients of potential (18) are available in closed form for all rectangular cells in [4] and for parallel rectangular cells in [43].

The evaluation of the coefficients for the nonorthogonal case is even more challenging. The zero thickness self term as well as coefficients which are in a plane have been considered in a recent paper [44]. In order to evaluate these coefficients for the general nonorthogonal case we use a combination of analytic integration and Gaussian quadrature. Specifically, for physically close cells, we first divide each hexahedral cell into a set of layers in the $c$ direction. The thickness of these layers is not uniform, but is determined by a compound Gaussian quadrature rule. Specifically, in the local coordinates the $k$:th layer is $a \in [-1, +1]$, $b \in [-1, +1]$, $c \in [c_{k-1}, c_k]$. The values of the $\{c_k\}$ are the values of the nodes in the 4 point Gaussian quadrature rule with $lvl$ levels of compounding. There are thus a total of $5(lvl)$ -1 layers in each inductive cell. The value of $lvl$ depends on the aspect ratios of the cell and the accuracy required.

Once each cell has been subdivided, then the evaluation of the integral (14) is reduced to the evaluation of $nz$ fourfold integrals of the form

$$L^s p_{aa'} = \mu \int_a \int_b \int_{a'} \int_{b'} (\hat{a} \cdot \hat{a}')\ h_{a'}\ \ G[\vec{r_g}(a, b, c); \vec{r_g}(a', b', c')]\ da'\ db'\ h_a\ da\ db \tag{24}$$

where $nz$ is the product of the number of layers in each cell. Each fourfold integral is the integral over two quadrilaterals. We evaluate these integrals by subdividing each quadrilateral into uniform rectangles in the local $a$ and $b$ directions. Assuming that we integrate a rectangular domain $R = a \in [-1, +1], b \in [-1, +1]$ into $nm$ subquadrilaterals $R_{ij} = (i-1)/n \leq a \leq i/n, (j-i)/m \leq b \leq j/m$. The subdivisions $n$ and $m$ are chosen to maintain a reasonable aspect ratio as well as the required accuracy. The evaluation of the partial self and near mutual inductances, (14), is more difficult than the potential coefficients due to inner product. For this, we subdivide each rectangular domain into two triangles for which an analytical formulation exists. On each triangle we approximate $\hat{a} \cdot \hat{a'} h_a h_{a'}$ by a linear function which agrees with its vales at the three vertices of the triangle. Importantly, an analytical formula for the product of a linear function and the Green's function exists for a triangle [45]. We perform the outer integration in (14) with respect to $a, b$ and $c$ by using a 9 point sixth order accurate product Gaussian quadrature rule. Once we have obtained an approximation $S_1$ to the integral in (14) using this method, we divide each cell into twice as many $c$ layers as before, that is we double $lvl$, and repeat the procedure, obtaining another approximation, $S_2$. Then, we use second order Richardson extrapolation to obtain our final estimate $S = (4S_2 - S_1)/3$.

# 4 General Circuit Solver Aspects

In this Section we consider a general purpose time and frequency domain solver implementation for the PEEC approach. As mentioned in Section 2, the full spectrum property in PEEC is obtained by using a combined solution vector $(\vec{\Phi}, i)^T$ in the time domain or frequency domain. This is based on the modified nodal analysis (MNA) circuit formulation [39] where $\vec{\Phi}$ is the potential and $\vec{i}$ are the cell and some branch currents. The zero potential $\phi = 0$ corresponds to the ground node 0 or node at an *infinite distance in space*. We found that the inclusion of the potentials as unknowns has proven to be very valuable as output quantities. For example for PC board plane to plane voltages

[33] are simply given by the potential difference between the closely located planes. Alternatively, if charges are desired $\vec{q}$ is required for some elements instead of $\vec{\Phi}$ then they can be included in the MNA as part of the solution vector e.g. Singhal and Vlach in [46]. Many practical problems consist of different SPICE type lumped circuit elements in addition to the PEEC model. These elements can easily be included in the circuit matrix using the usual MNA stamps [39, 47, 48] for both the time and frequency domain. These matrix stamps have been developed for a multitude of circuit elements. A PEEC computer program may consist of a model element generator and several circuit solvers for the time and the frequency domain. The elements of the equivalent circuits generated by the PEEC discretization are stamped into the MNA circuit matrix and then the resultant circuit is solved using a sparse matrix code. Over the years, other loop based approaches like the MLA [49] have been applied to the PEEC problems. Mixed circuit formulations including loop or mesh formulations have also been used since they can lead to efficient solution for some specialized problems [17, 50]. One of the present research topics is the speed up of the solution process. Non retarded $(L_p, P, R)PEEC$ and full wave solutions have been attempted using the Model Order Reduction (MOR) approaches for circuit which do not have a multitude of input/output connections and a moderate number of relevant eigenvalues e.g. [51]. This research is on-going especially in the area of $(L_p, R)PEEC$ models for on chip applications where $L_p^{-1}$ is used to limit the radius of coupling for the partial mutual inductances e.g. [42].

Much progress has been made very recently in the stable time solution of integral equation based full wave solutions. Early work, where mostly explicit numerical integration methods are employed is summarized in [52]. Since then, several researchers have shown that much more stable solutions can be obtained with implicit numerical integration methods e.g. [14, 53, 54, 55]. This implies that today, the stable transient analysis of large structures can be accomplished efficiently. It should be noted that the full-spectrum property is a very important aspect of the method for both the time and the frequency domain where the input spectrum often ranges from $dc$ to the maximum permissible frequency content.

The SPICE input language is an other aspect of an EM circuit solver which makes its use practical and easier to understand. The utility of this was well recognized early on and the SPICE syntax has been used in all the ″Ciao″ series of PEEC solvers e.g. [14]. We call the code based on the formulation in this paper IBMciao. We continued to enhance the language to include the description of the nonorthogonal conductors. This approach also allows a rapid combined time- and frequency-domain analysis which lead to a better understanding of the electrical and electromagnetic behavior of the systems, and helps the designer to gain insight into the way the various parameters of the system impact its overall performance. While the majority of the language used for the description of the various types of circuit elements is based, as much as possible, on the conventional SPICE language, some specialized syntax is used in company specific versions (e.g., Motorola's Mspice and IBM's PowerSpice) and commercial versions like PSpice and Hspice. One of the recommended enhancements in the basic SPICE language is an improved syntax for mutual inductances

```
Kname   Lname1   Lname2   <type>  number  <delay>
```

The new proposed option assigns directly the value of the mutual inductance rather than the transformer coupling factor $k = L12/\sqrt{L11L22}$ which is computationally expensive. More specifically, the default option could be that the coupling factor is assigned (in which case the assignment “k” for ”type” is optional), while for the case where the more desirable mutual inductance value is explicitly given the assignment “m” for “type” is required. The savings are evident for circuits with many mutual inductance like PEEC circuits. Also, the delay between the inductors allows the inclusion of retarded PEEC models in SPICE [20].

# 5 Numerical Experiments

We give several examples in this paper to illustrate the versatility of the approach.

## 5.1 Half wavelength dipole

As a first example we model a dipole shown in Fig. 5 with a length of 200 mm to compare with a well known results and to confirm the accuracy of the solution. Since the theoretical results are available for the lossless case we use a zero resistance $(L_p, P, \tau)PEEC$ model. The meshing we use is non-uniform with smaller cells towards the center gap as well as the ends of the dipole. At the center we introduced a gap of 2 mm. Results are given for two dipoles with different cross sections to show that in order to obtain a close agreement with the theoretical value, we had to resort to a very small, $1\mu m \times 1\mu m$, cross section. Our results in Fig. 6 correspond to the data with a magnitude of the impedance is 73.5Ω at resonance which agrees well with the theoretical value of 73.1Ω. The resonance frequency for this case is also very close, within a percent of the theoretical resonance frequency of 750 MHz.

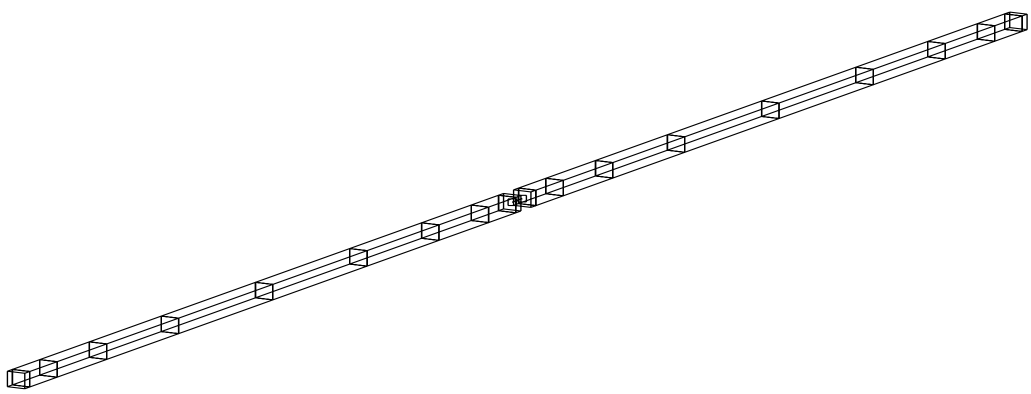

*Figure 5: $\frac{\lambda}{2}$ Dipole antenna with non-uniform meshing.*

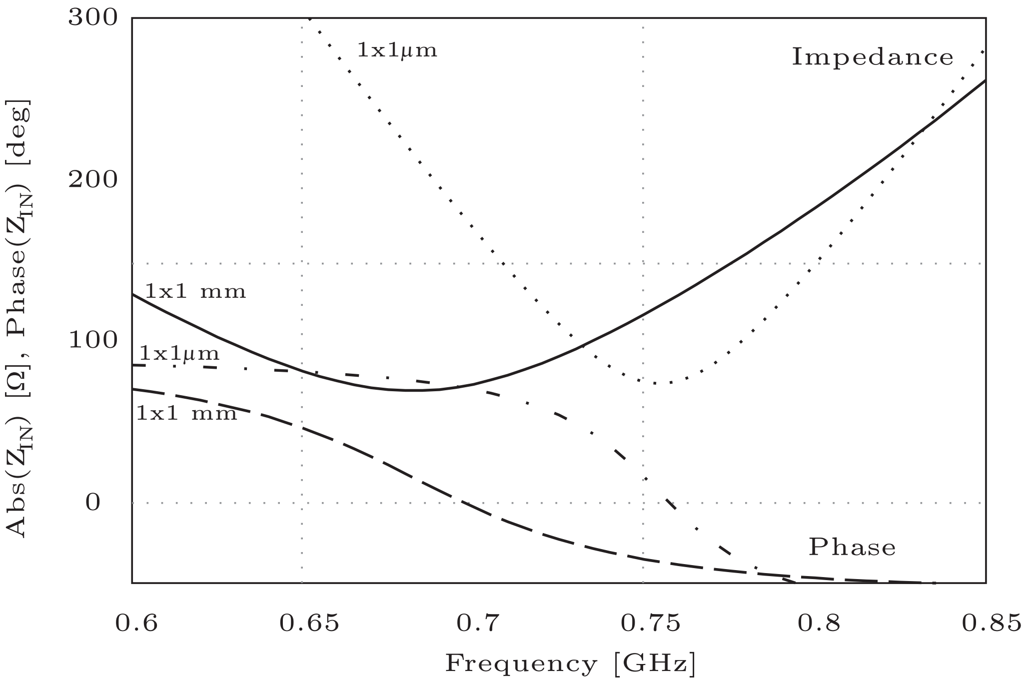


*Figure 6: Input impedance and phase for* $1 \times 1\,mm$*, and* $1 \times 1\,\mu m$ *lossless dipole.*

## 5.2 Lossy transmission line 1

The second example, a time domain Skin effect transmission line example shown in Fig. 7, is designed to give a comparison with an accurate SPICE type solution. This example also illustrates that accurate answers can be obtained even for very large cell aspect ratios. In this case, the cell thickness to length ratio is as large as 1:4750.

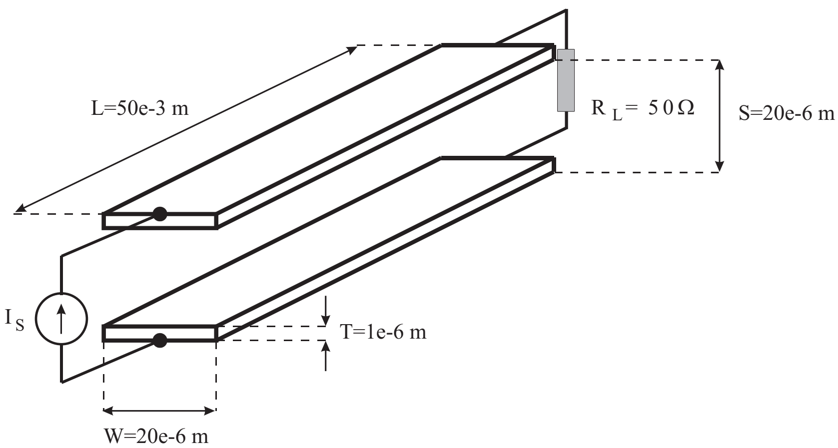


*Figure 7: Lossy transmission line 1 test setup.*

The cross-section is subdivided for the volume filament (VFI) Skin effect representation with 1 cell along the thickness and 10 cells along the width. The length is subdivided into 20 non-uniform cells where the cell size is decreasing towards the ends. In this comparison, we used the PowerSpice circuit solver which uses a method of characteristics based transmission line formulation [56]. Fig. 8 shows that the 3D PEEC model and the 2D transmission line SPICE solver give very close voltage waveforms at the beginning and the end of the line.

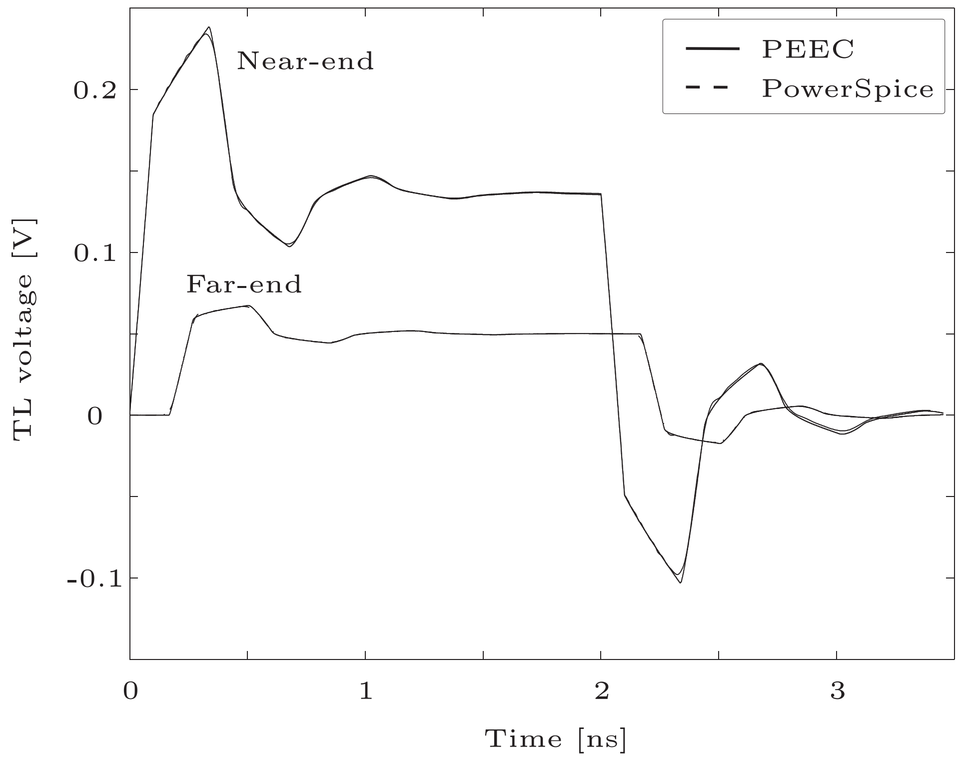


*Figure 8: Waveform comparisons for 3D PEEC and 2D transmission line solvers.*

## 5.3 Lossy transmission line 2

The new nonorthogonal formulation increases the number of electrical structures that can be analyzed using PEEC. Examples of nonorthogonal problems are wire bonds, diagonal or PC board interconnects and chip interconnects which are at an arbitrary angle. Unfortunately, very few well documented results exist in this class of problems today.

The volumetric hexahedral meshing for nonorthogonal structures is very complex. Most modern software toolkits available for meshing are designed for mechanical or hydraulic analysis where the mesh structures is based on hexahedra. Our hexahedral meshing is an extension of the original rectangular approach [36] and it is node based as is shown in Fig. 2 for a zero thickness structure. Four different sub-meshes are associated with this node based mesh: A quadrilateral surface mesh for the capacitive cells, and three hexadral volumetric meshes for the inductive cells in the local $\hat{a}$, $\hat{b}$ and $\hat{c}$ directions. To create these meshes, we use the local coordinates as described in Section 2.1. Fig. 9 illustrates this for a hexahedral block which is subdivided into two inductive cells for the front directed $\hat{a}$, and one along the right directed $\hat{b}$ and one along the top direction $\hat{c}$. Hence, there are three corner nodes in the $\hat{a}$ direction, and 2 corner nodes in the $\hat{b}$ and $\hat{c}$ directions.

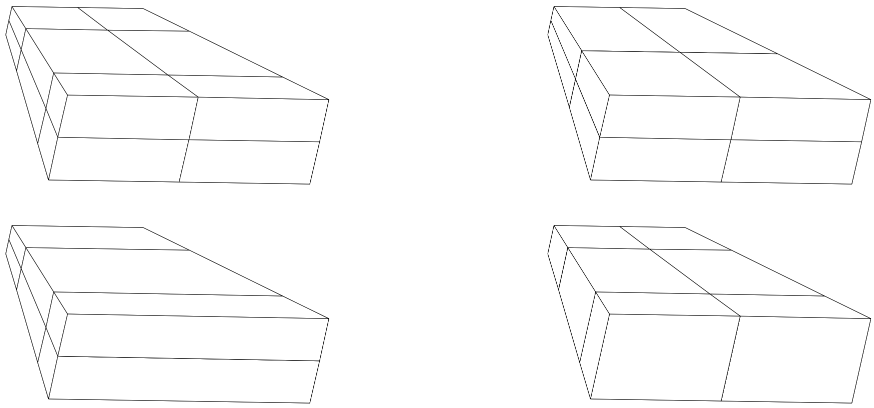

*Figure 9: Capacitive and inductive-resistive cells for a single nonorthogonal hexahedron. Upper-left: Capacitive surface cells; Lower-left: Inductive volume cells b-directed current (right); Upper-right: Inductive volume cells a-directed current (front); Lower-right: Inductive volume cells c-directed current (up).*

Computationally, the fast $O(N^2)$ time domain approach [14, 57] is always preferable and faster where applicable than the $O(N^3)$ frequency domain techniques. However, in the nonorthogonal case the runtime and memory usage of the analysis is impacted by the presence of the nonorthogonal elements due to the more complex element computations in the new formulation. In the orthogonal code, inductive coupling is confined to the currents in the same direction. This is no longer the case for arbitrary oriented conductors and more inductive cells will be coupled.

As a test of the nonorthogonal code, we modelled an short interconnect structure between a drive chip and a 50Ω resistive load shown in Fig. 10. The interconnect example consists of two lines above a ground plane with a nonorthogonal copper connection part embedded in air, or $\epsilon_r = 1$. The ground plane and the wires are 0.05mm thick with the exception of the upper connections which are 0.1mm thick. The width of all wires is 0.1mm with a 0.2mm spacing while more geometrical dimensions are shown Fig. 11. The only part not shown in this figure is the bend which starts at 6.0mm and ends at 8.0mm measured at the two corners where the wire bends. This is shown in Fig. 10. The spacing between the wires in the bend section is increased to 0.5mm. The two lines are driven differentially, by two current source pulses of the same magnitude and opposite directions in parallel with a 50Ω resistor. The sources have a common centered ground connected to the plane. The input waveform is a sine square wave shape with a rise time of 60ps, a fall time of 40ps and a pulse width of 0.7ns. Fig. 12 shows the results of a time domain analysis for the example in Fig. 10. The differential voltage-time waveforms are shown at the source as well as at the load. To approximately verify the solution, we used a Manhattan (rectangular) approximation of the geometry and the waveforms were slightly different as expected.

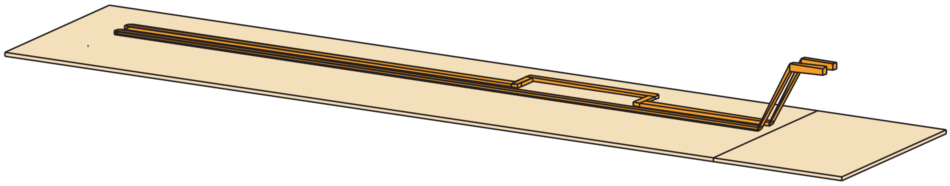

*Figure 10: Transmission line with nonorthogonal section.*

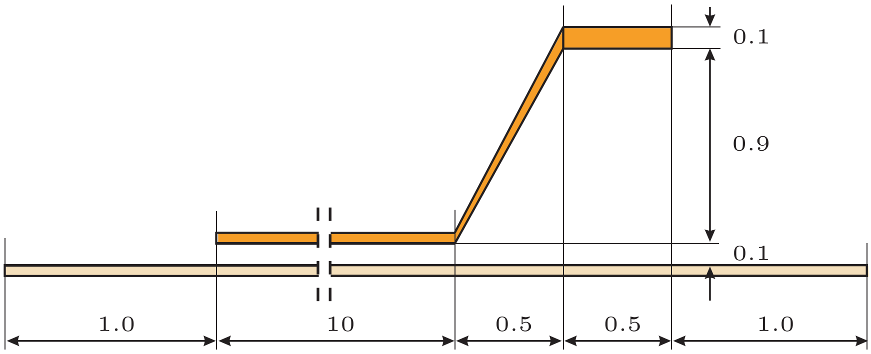


*Figure 11: Side view of differential connection (dimensions in mm).*

# 6 Conclusions

The formulation given in this paper extends the PEEC approach in a consistent way to general nonorthogonal geometries. Importantly, the approach converges to the rectangular formulation for orthogonal geometries. Further, like the original PEEC formulation it includes the volume filament (VFI) model for the Skin effect and a model for dielectric blocks. The examples in the paper show some of the versatility of the circuit oriented method. It is also shown that the ability to analyze in the time and frequency domain including other circuit elements leads to the best possible results for each problem at hand.

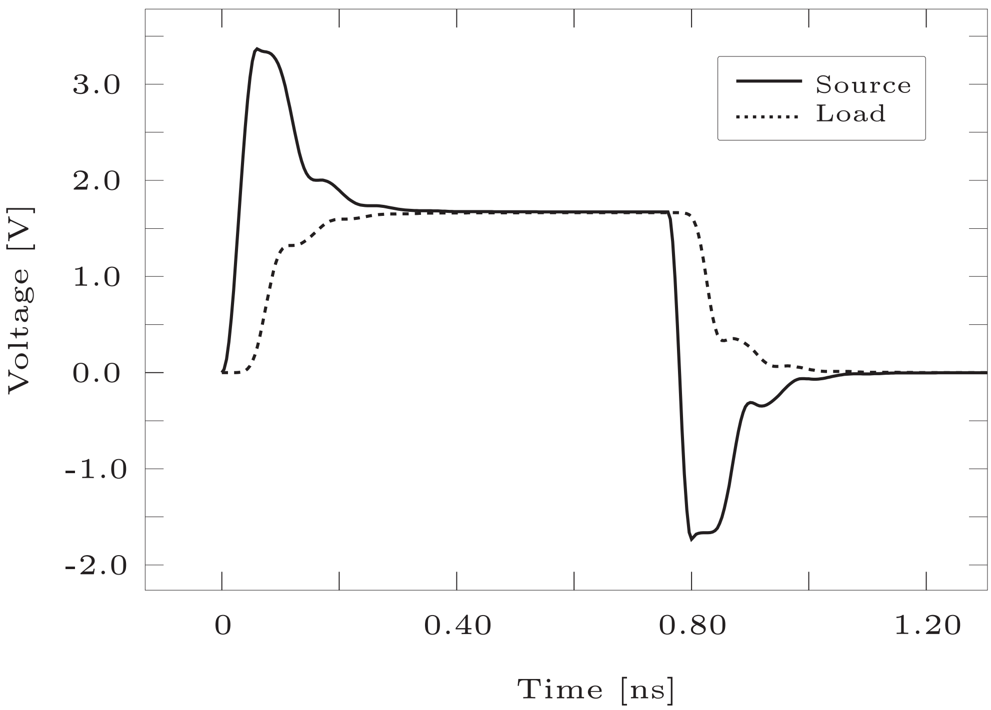


*Figure 12: Analysis results for structure in Fig. 10.*

# References


[1] B. Archambeault, O. Ramahi, and C. Brench, *EMI/EMC Computational modeling handbook*. KLUWER, 1998.

[2] C. Christopoulos, *An introduction to the Transmission-Line Modeling TLM method*. IEEE Press, 1992.

[3] W. Sui, *Time-domain computer analysis of nonlinear hybrid systems*. CRC Press, 2002.

[4] P. A. Brennan and A. E. Ruehli, "Efficient Capacitance Calculations for Three-Dimensional Multiconductor Systems", *IEEE Transactions on Microwave Theory and Techniques*, 21(2):76–82, February 1973.

[5] K. Nabors and J. White, "FastCap: A Multipole Accelerated 3D Capacitance Extraction Program", *IEEE Transactions on Computer Aided Design*. 10(11)1447–1459, 1991.

[6] Y. L. Le Coz and R. B. Iverson, "A stochastic algorithm for high speed capacitance extraction in integrated circuits", *IEEE Transactions om Microwave Theory and Techniques*, 40(7):1507–1516, July 1992.

[7] A. E. Ruehli, "Inductance Calculations in a Complex Integrated Circuit Environment", *IBM Journal of Research and Development*, 16(5):470–481, September 1972.

[8] P. A. Brennan, N. Raver, and A. E. Ruehli, "Three-Dimensional Inductance Computations with Partial Element Equivalent Circuits", *IBM Journal of Research and Development*, 23(6):661–668, November 1979.

[9] A. E. Ruehli and P. K. Wolff, "Inductance Computations for Complex Three-Dimensional Geometries", in: *Proc. of the IEEE Int. Symp. on Circuits and Systems*, pages 16–19, New York, NY, 1981.

[10] C. Paul, *Analysis of Multiconductor Transmission Lines*, John Wiley & Sons, New York, 1992.

[11] R.-B. Wu, C.-N. Kuo, and K. K. Chang, "Inductance and resistance computations for three-dimensional multiconductor interconnection structures", *IEEE Transactions on Microwave Theory and Techniques*, 40(2):263–270, February 1992.

[12] M. Kamon, M. J. Tsuk, and J. White, "FastHenry: A Multipole-Accelerated 3-D Inductance Extraction Program", in: *Proc. of the IEEE Design Automation Conference*, pages 678–683, June 1993.

[13] A. E. Ruehli, "Circuit Models for Three-Dimensional Geometries Including Dielectrics", *IEEE Transactions on Microwave Theory and Techniques*, 40(7):1507–1516, July 1992.

[14] W. Pinello, A. C. Cangellaris, and A. E. Ruehli, "Hybrid electromagnetic modeling of noise interactions in packaged electronics based on the partial-element equivalent circuit formulation", *IEEE Transactions on Microwave Theory and Techniques*, 45(10):1889–1896, October 1997.

[15] G.Antonini, S. Cristina, and A. Orlandi, "PEEC modeling of high voltage tower under direct and nearby lightning strike", in: *Proc. of the Int. Symposium on High Voltage*, Montreal, Canada, 1997.

[16] H. Shi, J. Fan and J. Drewniak, "Modeling multilayered PCB power-bus designs using an MPIE based circuit extraction technique.", in: *Proc. of the IEEE Int, Symposium on EMC*, pages 647–651, Denver, CO, USA, August 1998.

[17] N. Marques *et al.*, "A mixed-nodal-mesh formulation for efficient extraction and passive reduced-order modeling of 3D interconnects", in: *Proc. of the IEEE Design Automation Conference*, pages 297–302, San Francisco, CA, USA, 1998.

[18] G. Antonini, S. Cristina, and A. Orlandi, "PEEC modeling of lightning protection system and coupling to coaxial cables", *IEEE Transactions on EMC*, 40(4):481–491, November 2001.

[19] A. M. Nikenejad and R. G. Meyer, "Analysis, design, and optimization of sprial inductors and transformers for SI RF ICs", *IEEE Journal of Solid-State Circuits*, 33(10):1470–1481, October 1998

[20] G. Wollenberg and A. Görisch, "Analysis of 3-D Interconnect Structures with PEEC Using SPICE", *IEEE Transactions on EMC*, 41(4):412–417, November 1999.

[21] M. Tröscher and H. Katzier, "Efficient PEEC modeling of multi-layer boards and multi-chipo modules", in: *Proc. of the Zurich Int. Symposium on EMC*, pages 269–273, Zürich, Switzerland, February 2001.

[22] J. F. Fan *et al.*, "Modeling DC power-bus structures with vertical discontinuities using a circuit extraction approach based on a mixed-potential intergral equation formulation", *IEEE Components, Packaging, and Manufacturing Technology Society*, 24(2):143–157, May 2001.

[23] R. F. Milsom *et al.*, "FACET – a CAE System for RF Analogue Simulation Including Layout", in: *Proc of the ACM/IEEE Design Automation Conference*. pages 622–625, Las Vegas, NE, USA, June 1989.

[24] Y. Wang, V. Jandjayla, and C.-J. R. Shi, "Coupled Electromagnetic-circuit simulation of arbitrary-shaped conducting structures using triangular meshes", in: *Proc. of the IEEE Int. Symposium on Quality Electronic Design*. San Jose, CA, USA, March 2002.

[25] A. Rong and A. C. Cangellaris, "Generalized PEEC models for three-dimensional interconnect structures and integrated passives of arbitrary shapes", in: *Proc. of the 10th Topical Meeting on Electrical Performance of Electronic Packaging*, pages 225–228, Boston, MA, USA, October 2001.

[26] A. E. Ruehli, G. Antonini, and A. Orlandi, "Extension of the partial element equivalent circuit method to non rectangular geometries", in: *Proc. of the IEEE Int, Symposium on EMC*, pages 728–733, Seattle, WA, USA, 1999.

[27] G. Antonini, A. Ruehli, and J. Esch, "Non orthogonal PEEC formulation for time and frequency domain modeling", in: *Proc. of the IEEE Int. Symposium on EMC*, pages 728–733, Minneapolis, MN, USA, August 2002.

[28] B. M. Kolundzija and B. D. Popovic, "Entire-domain Galerkin method for analysis of metallic antennas and scatterers", *IEE Proceedings - Microwaves, Antennas and Propagation*, 145(1):13–18, February 1993.

[29] H. Singer, H.-D. Brüns, and G. Bürger, "State of the art in the moment method", in: *Proc. of the IEEE Int. Symposium on EMC*, pages 122–127, Santa Clara, CA, USA, August 1996.

[30] A. W. Glisson and D. R. Wilson, "Simple and Efficient Numerical Methods for Problems of Electromagnetic Radiation and Scattering from Surfaces", *IEEE Transactions on Antennas and Propagation*, 28:593–603, 1980.

[31] A. E. Ruehli, J. Garrett, and C. R. Paul, "Circuit Models for 3D Structures with Incident Fields", in: *Proc. of the IEEE Int. Symposium on EMC*, pages 28–31, Dallas, TX, USA, August 1993.

[32] A. E. Ruehli *et al.*, "Transient analysis for printed circuit board problem using two different solvers", in: *Proc. of the Int. Symposium on EMC*, pages 1327–1332, Montreal, Canada, August 2001.

[33] B. Archambeault and A. E. Ruehli, "Analysis of power/ground-plane EMI decoupling performance using the partial-element equivalent circuit technique", *IEEE Transactions on EMC*, 43(4):437–445, November 2001.

[34] C.-T. Tai, *Generalized vector and dyadic analysis*. IEEE Press, 1992.

[35] C. A. Balanis, *Advanced Engineering Electromagnetics*, WILEY, 1989.

[36] A. E. Ruehli, "Equivalent Circuit Models for Three-Dimensional Multiconductor Systems", *IEEE Transactions on Microwave Theory and Techniques*, 22(3):216–221, March 1974.

[37] G. Antonini, A. Orlandi, and A. Ruehli, "Speed-up of PEEC Method by using wavelet transform", in: *Proc. of the Int. Symposium on EMC*, pages 95-100, Washington, DC, USA, August 2000.

[38] S. Ramo, J. R. Whinnery, and T. Van Duzer, *Fields and Waves in Communication Electronics*, WILEY, 1994.

[39] C. Ho, A. Ruehli, and P. Brennan, "The Modified Nodal Approach to Network Analysis", *IEEE Transactions on Circuits and Systems*, pages 504–509, June 1975.

[40] J. Garrett, A.E. Ruehli, and C.R. Paul, "Accuracy and Stability Improvements of Integral Equation Models using the partial element equivalent circuit PEEC approach", *IEEE Transactions on Antennas and Propagation*, 46(12):1824–1831, December 1998.

[41] F. W. Grover, *Inductance calculations: Working formulas and tables.* Dover Publications Inc., 1962.

[42] T.-H. Chen *et al.*, "INDUCTWISE: Inductance-Wise interconnect simulator and extractor", in: *Proc. of the Int. Conferece on Computer Aided Design*, pages 215–220, November 2002.

[43] J.-T. Kuo and K.-Y. Su, "Analytical evaluation of the MoM elements for the capacitance of a charged plate", *IEEE Transactions on Microwave Theory and Techniques*, 50(5):1435–1436, May 2002.

[44] G. Antonini, A. Orlandi, and A. E. Ruehli, "Analytical Integration of Quasistatic Potential Intergrals on Nonorghogonal Coplanar Quadrilaterals for the PEEC Method", *IEEE Transactions on EMC*, 44(2):399-403, May 2002.

[45] D. A. Lindholm, "Three-dimensional magnetostatic fields from point matching integral equations with linearly varying scalar sources, *IEEE Transactions on Magnetics*, 20(5):2025–2032, September 1984.

[46] A. E. Ruehli, Ed., *Circuit analysis, simulation and design, Part 2.* NHOLL, 1987.

[47] J. Vlach and K. Singhal, *Computer Methods for Circuit Simulation.* VANN, 1983.

[48] L. T. Pillage, R. A. Rohrer, and C. Visweswariah, *Electonic circuits and systems simulation methods.* McGraw-Hill Book Co. 1995.

[49] A. E. Ruehli, N. B. Rabbat, and H. Y. Hsieh, "Macromodular Latent Solutions of Digital Networks Including Interconnects", in : *Proc of the Int. Symposium on Circuits and Systems*, pages 515–512, New York, NY, USA, May 1978.

[50] H. Heeb, S. Ponnapalli, and A. E. Ruehli, "Frequency Domain Microwave Modeling Using Retarded Partial Element Equivalent Circuits", in: *Proc. of the IEEE Design Automation Conference*, pages 702–706, Dallas, TX, USA, June 1993.

[51] E. Chiprout and M.S. Nakhla, *Asymptotic waveform evaluation.* KLUWER, 1994.

[52] B.P. Rynne, "Comments on A Stable Procedure in Calculating the Transient Scattering by Conducting Surfaces of Arbitary Shape", *IEEE Transactions on Antennas and Propagation*, 41(4):517–520, April 1993.

[53] K. Aygün *et al.*, "A two-level plane wave time-domain algorithm for fast analysis of EMC/EMI problems", *IEEE Transactions on EMC*, 44(1):152–163, February 2002.

[54] S. M. Rao and T. K. Sarkar, "Transient analysis of electromagnetic scattering from wire structures using an implicit time-domain integral equation technique", *Microwave and Optical Technology Letters*, 17(1):66-69, January 1998

[55] M. J. Bluck and S. P, Walker, "Time-domain analysis of large three-dimensional electromagnetic scattering problems", *IEEE Transactions on Antennas and Propagation*, 45:894–901 May 1997.

[56] H.-M. Huang *et al.*, "A Comparative Study of Two Time-domain Simulation Algorithms for Lossy and Dispersive Transmission Lines", *IEEE Transactions on EMC*, 2002.

[57] P. Restle *et al.*, "Full-wave PEEC time-domain method for the modeling of on-chip interconnects", *IEEE Transactions on Computer Aided Design*, 20(7):877–887, July 2001.

# Paper E

# A comparative study of PEEC circuit elements computation

**Authors:**
G. Antonini[1], J. Ekman, A. Ciccomancini Scogna[1], A. E. Ruehli[2]

**Reformatted version of paper originally published in:**
Proceedings of the IEEE International Symposium on EMC, Istanbul, Turkey, May 2003.



[1]University of L'Aquila, Department of Electrical Engineering, Poggio di Roio, 67100 L'Aquila.
[2]IBM TJ Watson Research Center, Yorktown, New York, USA.

# A Comparative Study of PEEC Circuit Elements Computation

G. Antonini, J. Ekman, A. Ciccomancini Scogna, A. E. Ruehli

**Abstract**

A key use of the PEEC method is the solution of combined electromagnetic and circuit problems as they occur in many situations in todays very large scale integrated circuits (VLSI) and systems. An important aspect of this approach is the fast and accurate computation of PEEC circuit matrix elements, the partial inductances and coefficients of potential. Recently, Fast Multipole Methods (FMM) have been applied to the PEEC method in the frequency domain as a way to speed up the solution. In this paper, we consider the fast evaluation of the PEEC circuit matrix elements by two different methods, a matrix version of the (FMM)PEEC method and a method which we call the Fast Multi-Function (FMF)PEEC approach. In this technique, the matrix coefficients are evaluated using analytical functions approximation of the coefficients in combination with a proper choice of numerical quadrature formulas.

## 1 Introduction

Today, a multitude of mixed electromagnetic and circuit problems must be solved which are of an ever increasing size. Also, the problems which can be solved with quasi-static approaches are steadily decreasing as the frequencies increase and the rise times decrease. Simultaneously, computation times are becoming too large especially in the frequency domain where the entire problem is coupled at low frequencies, independent of the problem size. Further, twenty subdivisions are required in each spatial direction, at the shortest wavelength in the spectrum, for accurate impedance results. This leads to very large matrices especially for electrically large problem sizes. The Partial Element Equivalent Circuit (PEEC) method [1, 2] has become a very popular approach for the solution of mixed EM and circuits problems due to its flexibility and since it is possible to use Modified Nodal Analysis (MNA) [3] solution techniques used in most Spice type circuit solvers. In this paper, we consider the fast evaluation of the PEEC circuit matrix elements by two different methods, a matrix version of the (FMM)PEEC method [4] and a method which we call The Fast Multi-function (FMF)PEEC [5] approach. In this technique, the matrix coefficients are evaluated using analytical functions approximation of the coefficients in combination with a proper choice of numerical quadrature formulas.

We show that with a straightforward evaluation of the matrix elements, which are the PEEC circuit parameters, the partial inductances and potential coefficients evaluation can be very time consuming. Further, for the solution of dense problems with the PEEC method, we require very high accuracy for these circuit elements since it strongly impacts the accuracy of the results. Two factors are of key importance for the computation time. Using a straight forward numerical approach for the evaluation of each partial inductance for the general case can be very time consuming due to the six fold integral which needs to be evaluated. If, in a numerical evaluation, we subdivide each direction into $M$ sections, then this is an $O(M^6)$ process. It is clear that this evaluation must be done with upmost care to conserve computation time. This is where part of the time saving results from in the FMF approach. The second issue is the evaluation of close to $O(N^2)$ elements for a mostly dense circuit matrix where $N$ is the matrix size. Of course, this is the case where the problem involves predominantly PEEC elements and only a few conventional lumped circuit elements. The FMM has been developed to reduce the $O(N^2)$ evaluations. Here, we look at both approaches to come up with a comparison of the two. In all these methods, we want to keep both the matrix evaluation and matrix solution time small. However, we are concerned only with fast matrix element evaluation techniques and not the solution of the matrix system at hand.

The fast element evaluation techniques considered in this paper address the frequency domain only, but the approaches, with some modifications, apply to the time domain as well. Aspects of FMF have been practiced by a multitude of researchers [6, 7, 8] in different forms starting with the so called *subarea* method where all off diagonal matrix elements used collocation point approximations. Today, we know that the accuracy of this method is inadequate for PEEC. As is always the case, the FMF and the FMM approaches perform best for different problems. Hierarchy can play a considerable role in the speed up of both fundamental methods, provided that the geometry is suitable for a geometrical decomposition. However, the best range of applications have not been clearly identified since the methods are usually applied to a specific class of problem. Hence, much more work is required to classify the approaches. Here, we consider briefly the FMF methods and then in somewhat more detail the FMM type methods.

# 2 FMM Basic Theory

The Fast Multipole Method was introduced by Rokhlin for acoustic wave scattering in two dimensions [6], Lu and Chew [9] applied the FMM method in electromagnetics to compute the scattered field of two-dimensional dielectric coated conducting cylinders, and Coifman, Rokhlin and Wandzura [8] extended it to the three-dimensional wave equation.

The PEEC method is based on the electric field integral equation (EFIE) formulation using the free space Green's function.

$$G(\vec{r},\vec{r\prime}) = \frac{e^{jk|\vec{r}-\vec{r\prime}|}}{|\ \vec{r}-\vec{r\prime}\ |} \tag{1}$$

where $k$ denotes the wave number. This is the function to be approximated using the FMM. The FMM is based on two elementary identities which can be found in many texts and handbooks on mathematical methods such as [10] and [11], leading to the following representation of the Green's function in (1)

$$\frac{e^{jk|\vec{r}-\vec{r\prime}|}}{|\ \vec{r}-\vec{r\prime}\ |} = \frac{e^{jk|\vec{R}+\vec{d}|}}{|\ \vec{R}+\vec{d}\ |} \tag{2}$$

and

$$\frac{e^{jk|\vec{R}+\vec{d}|}}{|\,\vec{R}+\vec{d}\,|} = \frac{jk}{4\pi}\int_{S^2} d^2\,\hat{k}\; e^{j\vec{k}\cdot\vec{d}}\;\sum_{l=0}^{\infty} j^l\,(2l+1)\,h_l^{(1)}\,(kR)P_l\,(\hat{k}\cdot\hat{R}) \tag{3}$$

where $\vec{k} = k\hat{k}$ and the notation $\int_{S^2} d^2\hat{k}$ denotes the integration over a unit sphere $S^2$ according to

$$\int_{S^2} d^2\hat{k} = \int_0^{2\pi}\int_0^{\pi} sin\theta\; d\theta\, d\phi \tag{4}$$

where

$$\hat{k} = sin\theta\, cos\phi\,\hat{x} + sin\theta\, sin\phi\,\hat{y} + cos\theta\,\hat{z} \tag{5}$$

If we truncate the infinite sum in (3) to the first $L+1$ terms, then the scalar Green's function can be written as

$$\frac{e^{jk|\vec{r}-\vec{r\prime}|}}{|\,\vec{r}-\vec{r\prime}\,|} = \frac{e^{jk|\vec{R}+\vec{d}|}}{|\,\vec{R}+\vec{d}\,|} \simeq \frac{jk}{4\pi}\int_{S^2} e^{j\vec{k}\cdot\vec{d}}\alpha_L(kR,\hat{k}\cdot\hat{R})d^2\,\hat{k} \tag{6}$$

where

$$\alpha_L(kR,\hat{k}\cdot\hat{R}) \equiv \sum_{l=0}^{L} j^l\,(2l+1)\,h_l^{(1)}\,(kR)\,P_l\,(\hat{k}\cdot\hat{R}) \tag{7}$$

### 2.1 Elementwise expansion of FMM-based Green's function approximation

The basic idea of the FMM is to establish a matrix factorization from an analytic elementwise expansion. This means that the FMM allows to represent the Green's function in terms of matrix products. Let us consider two points $\vec{r}$ ad $\vec{r\prime}$ which are well separated in the sense that the conditions for applying the Gegenbauer's addition theorem are satisfied. Lets assume A fix order $L$ of the expansion in (6). As stated above the integration on the unit sphere is also performed by using Gaussian integration with $L+1$ points for the integral over $\theta$ and $2\,(L+1)$ points for the integral over $\phi$. Assuming as auxiliary variable $u = \cos\theta = \hat{k}\cdot\hat{R}$, let $w_u$ and $w_{phi}$ be the row vectors of the corresponding weights, $\Delta_u$ and $\Delta_\phi$ the stretching factors due to fact that the integration domain is not the unit square. Function $\alpha_L(kR,\hat{k}\cdot\hat{R})$ can be represented as a matrix of order $(L+1)\times(2L+2)$ when the vector $\vec{k}$ varies on the unit sphere. Furthermore also the function $\Psi \equiv e^{j\vec{k}\cdot\vec{d}}$ can be seen as a matrix of the same order. Therefore the evaluation of (6) can be done as

$$\frac{e^{jk|\vec{R}+\vec{d}|}}{|\,\vec{R}+\vec{d}\,|} \simeq \frac{jk}{4\pi}\int_{S^2} e^{j\vec{k}\cdot\vec{d}}\,\alpha_L(kR,\hat{k}\cdot\hat{R})d^2\,\hat{k} \;\simeq\; w_\phi\Delta_\phi(\Psi\odot\alpha_{L,ab})w_u^T\,\Delta_u \tag{8}$$

where $\odot$ denotes the Hadamard (elementwise) product of two matrices.

## 3 2-level FMM-based Computation of PEEC Parameters

An important part of the PEEC method is the evaluation of the circuit parameters, the partial inductances and the potential coefficients. The fast and accurate computation is a key aspect for the analysis of complex problems involving a large number of unknowns. Let us assume that the target inductive cell $m$ lies in a sphere, or group, $G_a$ with center $\vec{r_a}$ and the source inductive cell $n$ lies in a sphere, or group, $G_b$ with its center at $\vec{r_b}$. If the Green's function approximation in (6) is used a multipolar form for partial inductances and potential coefficients is obtained [4].

$$Lp_{mn} \simeq \frac{jk\mu\cos\theta_{mn}}{(4\pi)^2} \int_{S^2} \left[\frac{1}{s_m}\int_{v_m} e^{j\,\vec{k}\cdot(\vec{r_m}-\vec{r_a})} dv_m\right] \alpha_{L,ab}\left(\hat{r}_{ab}\cdot\hat{k}\right) \left[\frac{1}{s_n}\int_{v_n} e^{j\,\vec{k}\cdot(\vec{r_n}-\vec{r_b})} dv_n\right] d^2\hat{k} \tag{9}$$

Here, $s_{m,n}$ are the cross sections of volume cells $m$ and $n$. If two auxiliary functions are defined as the volume integrals

$$F_m(\vec{k}) = \frac{1}{s_m}\int_{v_m} e^{j\,\vec{k}\cdot(\vec{r_m}-\vec{r_a})} dv_m \tag{10}$$

$$\tilde{F}_n(\vec{k}) = \frac{1}{s_n}\int_{v_n} e^{-j\,\vec{k}\cdot(\vec{r_n}-\vec{r_b})} dv_n \tag{11}$$

equation (9) can be rewritten in a more compact form as

$$Lp_{mn} \simeq \frac{jk\mu\cos\theta_{mn}}{(4\pi)^2} \int_{S^2} F_m(\vec{k})\alpha_{L,ab}(\hat{r}_{ab}\cdot\hat{k})\tilde{F}_n(\vec{k})d^2\hat{k} \tag{12}$$

It is worth to note that functions $F_m(\vec{k})$ and $\tilde{F}_n(\vec{k})$ can be evaluated just once in the beginning and re-used for each computation involving inductive cells $m$ and $n$. The volume integrals in (10) and (11) are computed by means of Gauss-Legendre integration. The same procedure outlined above can be applied to the computation of mutual potential coefficients $P_{mn}$. It is straightforward obtain

$$P_{mn} \simeq \frac{jk}{(4\pi)^2\epsilon} \int_{S^2} \left[\frac{1}{A_m}\int_{A_m} e^{j\,\vec{k}\cdot(\vec{r_m}-\vec{r_a})} dA_m\right] \alpha_{L,ab}(\hat{r}_{ab}\cdot\hat{k}) \left[\frac{1}{A_n}\int_{A_n} e^{j\,\vec{k}\cdot(\vec{r_n}-\vec{r_b})} dA_n\right] d^2\hat{k} \tag{13}$$

where $A_{m,n}$ represents the surface area of the capacitive surface cells $m$ and $n$. Even in this case it is useful to define two auxiliary functions which correspond to the surface integrals in squared brackets as

$$S_m(\vec{k}) = \frac{1}{A_m}\int_{A_m} e^{j\,\vec{k}\cdot(\vec{r_m}-\vec{r_a})} dA_m \tag{14}$$

$$\tilde{S}_n(\vec{k}) = \frac{1}{A_n}\int_{A_n} e^{-j\,\vec{k}\cdot(\vec{r_n}-\vec{r_b})} dA_n \tag{15}$$

Therefore the final form for the partial mutual potential coefficients computation is

$$P_{mn} \simeq \frac{jk}{(4\pi)^2\epsilon} \int_{S^2} S_m(\vec{k})\;\alpha_{L,ab}(\hat{r}_{ab}\cdot\hat{k})\;\tilde{S}_n(\vec{k})\;d^2\hat{k} \tag{16}$$

## 3.1 Elementwise expansion of FMM-PEEC parameters

It is possible to find a matrix interpretation of FMM-based computation of PEEC parameters. The matrix interpretation of one-dimensional FMMs of complexity $O(n \log n)$ is well presented in [12]. A matrix version of FMM for the Laplace equation can be found in [13]. It is useful to give the same perspective also in the computation of PEEC parameters. The matrix version is more than a mere replacement for multiple summations and recursions by a clean matrix notation. The matrix viewpoint may help make the FMM more understandable to scientists and engineers who may want to use FMM for their computations.

In the following we assume that the (inductive or capacitive) target cell $m$ with center $\vec{r}_{cm}$ belongs to the target group $a$ and the cell $n$ with center $\vec{r}_{cn}$ belongs to the source group $b$. Let $\vec{r}_{cm} - \vec{r}_a = \vec{r}_{ma}$ the cell to group center distance for the target set and $\vec{r}_{cn} - \vec{r}_b = \vec{r}_{nb}$ that of the source set. The aim of the elementwise decomposition is to write the coupling matrix as

$$A = A_r + A \odot E, \tag{17}$$

where matrix $A_r$ is of the factored form

$$A_r = V_m^T \, \alpha_{ab} \, V_n, \qquad \alpha_{ab} \in \mathcal{C}^{r \times r} \tag{18}$$

and the elements of $E$ are bounded. By using the Addition Theorem in the hypothesis the following condition holds

$$\|\vec{r}_{ma} - \vec{r}_{nb}\|_2 < \|\vec{r}_a - \vec{r}_b\|_2 \tag{19}$$

then, for any $L \geq 0$, the matrix $A$, representing the electromagnetic coupling based on the Green's function, from (1), can be written as

$$A = A_{near} + A_{far} = A_{near} + A_r \tag{20}$$

where $A_{near}$ consists of coupling coefficients related to cells for which the condition in (19) is not valid, while $A_{far} = A_r$ takes into account the coupling between cells belonging to groups such that the condition in (19) is satisfied. As stated previously, the integration on the unit sphere is performed by using Gauss-Legendre integration with $L+1$ points for the integral over $\theta$ and uniform integration with $2(L+1)$ points for the integral over $\phi$. Let $w_u$ and $w_\phi$ be the row vectors of the quadrature weights and $\Delta_u$ and $\Delta_\phi$ the angular step for the integration over $u$ and $\phi$ respectively. Thus, for a fixed order $L$ of the multipole expansion, functions $F_m(\vec{k})$, $\tilde{F}_n(\vec{k})$, $S_m(\vec{k})$ and $\tilde{S}_n(\vec{k})$ can be treated as matrices of order $(L+1) \times (2L+2)$. For a fixed couple of inductive cells $m$ and $n$ belonging to two well separated groups $a$ and $b$ also the function $\alpha_{L,ab}$ is represented by a matrix of order $(L+1) \times (2L+2)$. It is clearly seen that computing the mutual partial inductance matrix $Lp_{mn}$ can be re-cast as

$$Lp_{mn} \simeq \cos\theta_{mn} \, w_\phi \, \Delta_\phi (F_m \odot \alpha_{L,ab} \odot \tilde{F}_n) w_u^T \, \Delta_u \tag{21}$$

where $\odot$ denotes the Hadamard (elementwise) product of two matrices. In the same way potential coefficient matrix $P_{mn}$ can be re-written as

$$P_{mn} \simeq w_\phi \, \Delta_\phi (S_m \odot \alpha_{L,ab} \odot \tilde{S}_n) w_u^T \, \Delta_u \tag{22}$$

The FMM-based computation of PEEC parameters provides a significant cpu-time saving because the number of interaction centers is strongly reduced. Near neighbors coupling can be evaluated just once at the beginning and stored in a sparse matrix. Non-near neighbors contribution, which involve the largest part of basis functions, can be efficiently computed by means of the FMM without storing the coefficients. This fact also allows a fast computation of matrix-vector products involving $\boldsymbol{Lp}$ and $\boldsymbol{P}$ matrices. The evaluation of PEEC circuit elements has been the topic of several papers over the last years e.g. [1, 14]. Closed form expressions of coefficients of potential are given in [2] in the static case for rectangular cells. The nonorthogonal case is analyzed in a more recent paper [15] where a combination of analytic integration and Gauss-Legendre quadrature is used for the evaluation of zero-thickness coefficients. Previous work in this field has shown that fast and high accurate results can be achieved also applying an appropriate choice of the procedure to evaluate the coefficients and the order of Gauss-Legendre quadrature as well. This issue is addressed in the next Section.

# 4 Multi-Function based Computation of PEEC Parameters

The basic idea of *The fast multi-function approach* is to use different routines with various Gauss-Legendre quadrature orders according to the desired accuracy. An adaptive choice of routines and orders may result in a significant reduction of cpu-time. First it is assumed that the space discretization is carried out such that the size of inductive and capacitive cell is less than $\lambda_{min}/20$ where $\lambda_{min}$ is the minimum wavelength in the frequency spectrum of excitation. Then the following geometric quantities are found:

- Find the maximum size, *maxSize*, of the cells.

- Find the center to center distance, $R_{c2c}$, between the two cells.

Then calculate:

- $farRatio = \frac{R_{c2c}}{maxSize}$.

Then a first decision has to be made according to:

- If ($farRatio > 30$): The center to center approximation is used.

- If ($farRatio \leq 30$): An accurate integration is needed.

If ($farRatio \leq 30$) a Gauss-Legendre quadrature is used with a properly chosen order. To this aim the gaps $EdgeDist_i$ between the edges of cells are evaluated in each direction $i = x, y, z$. Finally an a-dimensional parameter is evaluated for each dimension $i$ as $distRat_i = EdgeDist_i/Size_i$ for $i = x, y, z$. The following decision test is applied to choose the order:

$$\begin{aligned}
If(distRat_i < 1) &\quad\rightarrow\quad Order_i = 6\\
If(distRat_i < 3) &\quad\rightarrow\quad Order_i = 5\\
If(distRat_i < 10) &\quad\rightarrow\quad Order_i = 4\\
If(distRat_i < 20) &\quad\rightarrow\quad Order_i = 3\\
Else &\quad\rightarrow\quad Order_i = 2
\end{aligned}$$

for $i = x, y, z$, for each cell. This gives us an accurate computation for closely spaced cells from which the solution is highly effected. Further, the far cell couplings are approximated in a fast manner.

# 5 PEEC Parameters Approximation Results

In order to test the proposed FMM-based approach to PEEC parameters computation in the following mutual partial inductances and potential coefficients have been evaluated by means of the standard *9th* order Gauss-Legendre integration (GL), the FMM and the *multi-function approach*. More specifically this latter approach has been applied by using two different techniques. The first one uses a Gauss-Legendre volume integration with adaptive choice of the order (ad-VA). The second one subdivides the volume into filaments in the direction along which the current flows and evaluate the coefficient by means of Gauss-Legendre integration over the cross-section being the order adaptively chosen (ad-FA). The mutual partial inductance has been computed for various electrical distances between the cells. Two inductive cells $m$ and $n$ belonging to groups $a$ and $b$ have been considered. When using the FMM, by using the same notation as before $\vec{r}-\vec{r}' = \vec{R}+\vec{d}$, it is assumed that $d$ is small enough to make $\vec{R}$ be close at $\vec{r}-\vec{r}'$. The group center locations have been chosen such that $\vec{R} = R\hat{z}$ and $\vec{d} = 0.4\lambda\hat{z}$. An expansion order $L = 10$ has been adopted for the FMM. Figs. 1 and 2 show the magnitude and phase of the mutual partial inductance $Lp_{mn}$ as function of the electrical distance between the corresponding groups. The relative error (magnitude and phase) in the evaluation of $Lp_{mn}$ with order of expansion in the range $5-10$ assuming $\vec{R} = R\hat{z}$ are shown in figures 3 and 4.

As seen in Fig. 3 and 4 the adaptive volume integration approach (ad-VA) provides very good accuracy also for small electrical distances while the adaptive filament approach (ad-FA) provides almost constant accuracy for the magnitude while it is about equivalent to a *7-th* order FMM for the phase approximation. Of course ad-FA approach is much faster than the ad-VA one as a consequence of the reduced integration workload. Table 1 illustrates the speed up and the mean relative error (MRE) which the ad-FA and ad-VA approaches provide with respect to the *9-th* order Gauss-Legendre volume integration (GL-9).

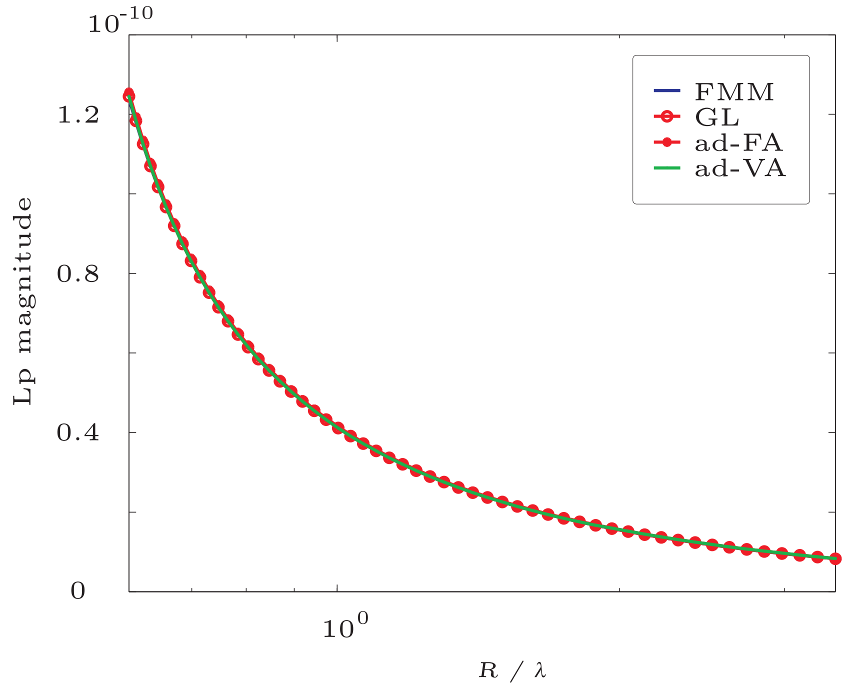


*Figure 1: Lp magnitude.*

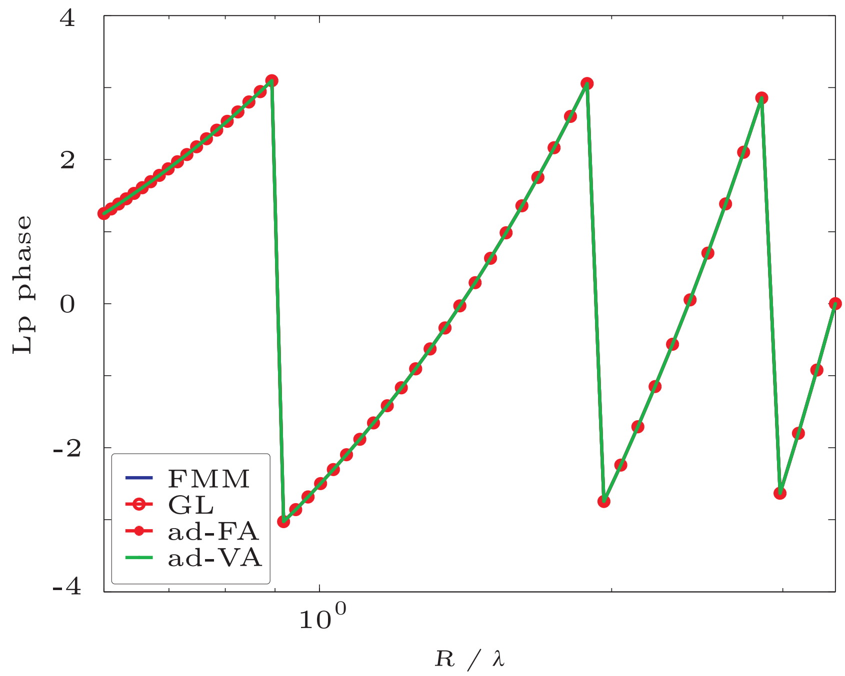


*Figure 2: Lp phase.*

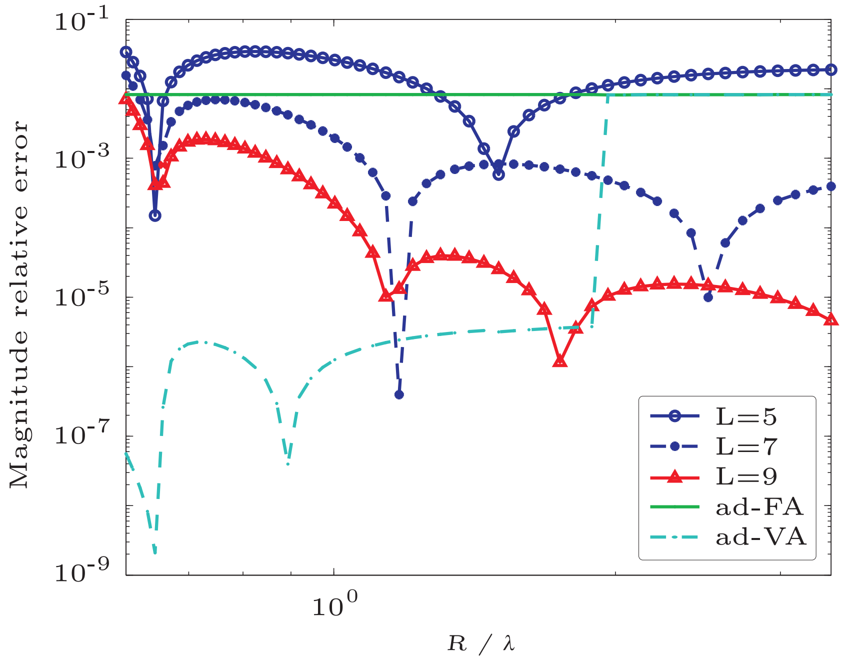


*Figure 3: Lp magnitude relative error.*

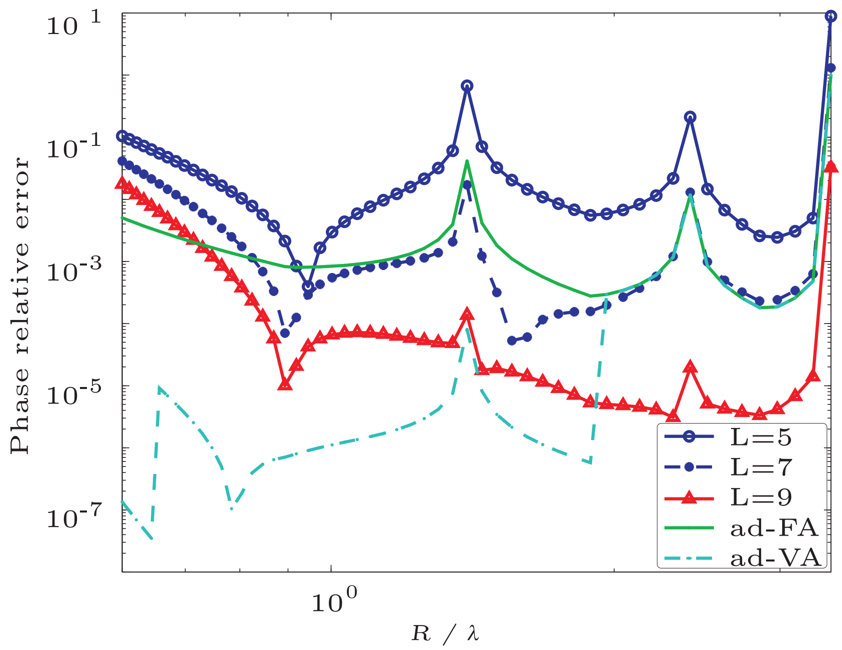


*Figure 4: Relative error on Lp phase.*

*Table 1: Speed up and mean relative error.*

| Method | speed up | MRE |
|---|---|---|
| GL-9 | 1 | 1 |
| ad-FA | 4402 | 8.7e-003 |
| ad-VA | 285 | 2.3e-003 |

*Table 2: FMM speed up and mean relative error*

| $L$ | $(T_{GL}/T_{FMM})$ | MRE |
|---|---|---|
| 5 | 7.050 | 1.16e-2 |
| 6 | 7.050 | 2.05e-3 |
| 7 | 7.050 | 2.64e-4 |
| 8 | 7.050 | 3.27e-5 |
| 9 | 7.047 | 2.60e-6 |
| 10 | 7.045 | 2.13e-7 |

The analysis of Table 1 reveals that the ad-FA approach provides an excellent speed up preserving a good accuracy. In order to better investigate the accuracy and the speed up that the FMM method provides a larger case study is analyzed. $N = 4000$ nonorthogonal inductive cells have been considered. They have been grouped into 64 groups. Their mutual partial inductances have been evaluated at the frequency $f = 3$ GHz by means of the standard Gauss-Legendre integration and the FMM based technique by using various expansion orders $L$. Cell dimensions are $\lambda/10 \times \lambda/10 \times \lambda/100$ and a fifth order Gauss-Legendre integration has been adopted. Let us also assume that the average number of nearby groups is 9. Table 2 shows the speed up which is evaluated as the ratio of the cpu-time required by the Gauss-Legendre integration to the cpu-time required by the FMM-based computation $(T_{GL}/T_{FMM})$. In the same table the mean relative error is shown. As seen in this case the speed up is not significantly affected by the order $L$ being the computation time dominated by the evaluation of nearby interactions. On the other hand relatively small values of $L$ provides very good accuracies.

# 6 Conclusions

Recent advances in the evaluation of PEEC circuit elements are presented. The FMM-based computation is compared with two *multi-function approaches* based on the adaptive choice of the Gauss-Legendre quadrature order. Several tests have pointed out that the adaptive filament approach (ad-FA) is able to provide a very good speed up without lost of accuracy.

# References


[1] A. E. Ruehli, "Inductance Calculations in a Complex Integrated Circuit Environment", *IBM Journal of Research and Development*, 16(5):470–481, September 1972.

[2] P. A. Brennan and A. E. Ruehli, "Efficient Capacitance Calculations for Three-Dimensional Multiconductor Systems", *IEEE Transactions on Microwave Theory and Techniques*, 21(2):76–82, February 1973.

[3] C. Ho, A. Ruehli and P. Brennan, "The Modified Nodal Approach to Network Analysis", *IEEE Transactions on Circuits and Systems*, pages 504–509, June 1975.

[4] G. Antonini, "The Fast Multipole Method for PEEC Circuits Analysis", in: *Proc. of the IEEE Int. Symposium on EMC*, Minneapolis, MN, USA, August 2002.

[5] G. Antonini, J. Ekman, and A. Orlandi, "Integration Order Selection Rules for a Full Wave PEEC Solver", in: *Proc. of the 15th Zurich Symposium on EMC*, pages 431–436, Zurich, Switzerland, February 2003.

[6] V. Rokhlin, "Rapid Solution of Integral Equations of Scattering Theory in Two Dimensions", *Journal of Computational Physics*, 86(2):414–439, 1990.

[7] J. M. Song and W. C. Chew, "Multilevel Fast-Multipole Algorithm for Solving Combined Field Integral Equations of Electromagnetic Scattering", *Microwave Opt. Tech. Lett.* 10(1):14–19, September 1995.

[8] R. Coifman, V. Rokhlin, and S. Wandzura, "The Fast Multipole Method for the Wave Equation: A pedestrian Prescription", *IEEE Transactions on Antennas and Propagation*, 35(3):7–12, June 1993.

[9] C. C. Lu, and W. C. Chew, "Fast Algorithm for Solving Hybrid Integral Equations", *IEE Proceedings. H, Microwaves, Antennas and Propagation*, 140(6):455–460, December 1993.

[10] G. Arfken, *Mathematical Methods for Physicists.* Academic Press, second edition, New York, NY, 1970.

[11] M. Abramowitz and I. A. Stegun, *Handbook of Mathematical Functions.* Dover Publications, New York, NY, 1972.

[12] L. Greengard and V. Rokhlin, "A Fast Algorithm for Particle Simulations", *Journal of Computational Physics*, 135:280–292, 1997.

[13] X. Sun and N. P. Pitsianis, "A Matrix Version of the Fast Multipole Method", *SIAM Review*, 43(2):289–299, September 2001.

[14] A. E. Ruehli and P. K. Wolff, "Inductance Computations for Complex Three-Dimensional Geometries", in: *Proc. of the IEEE Int. Symp. on Circuits and Systems*, vol. 1, pages 16–19, New York, NY, 1981.

[15] G. Antonini, A. Orlandi, and A. E. Ruehli, "Analytical Integration of Quasi-static Potential Intergrals on Nonorghogonal Coplanar Quadrilaterals for the PEEC Method", *IEEE Transactions on EMC*, 2002.

# Paper F

# 3D PEEC Capacitance Calculations

**Authors:**
Giulio Antonini[1], Jonas Ekman, Antonio Orlandi[1]

**Reformatted version of paper originally published in:**
Proceedings of the IEEE International Symposium on EMC, Boston, USA, August 2003.



[1]University of L'Aquila, Department of Electrical Engineering, Poggio di Roio, 67100 L'Aquila.

# 3D PEEC Capacitance Calculations

J. Ekman, G. Antonini, A. Orlandi

**Abstract**

The partial element equivalent circuit (PEEC) method has shown to be useful in mixed circuit and electromagnetic analysis. In PEECs, the extensions from two to three dimensional modeling are mainly in the calculation of the partial self and mutual capacitive couplings. The considerable increase in problem size for 3D PEEC models result in a large number of partial elements that has to be calculated. This results in excessive calculation times if the capacitive calculation routines are poorly constructed. In this paper it is shown that by using local reduction matrices for the capacitive calculations, the calculation time for PEEC model capacitance matrices can be decreased while keeping the accuracy.

## 1 Introduction

In the PEEC method [1, 2], conductors and dielectrics are represented by partial circuit elements. The partial elements for simple PEEC models are lumped inductances, capacitances and resistances that are calculated based on a discretization of a structure. For PEEC models including retardation the capacitive and inductive couplings must be delayed by the free space travel time between the source and field point disabling the use of most commercial circuit simulation software like SPICE [3]. Instead the circuit equations can be directly formulated and solved using a suitable method, for example, the modified nodal analysis (MNA) approach [4]. The notation $(L_p, P, R, \tau)$PEEC are used for PEEC models to emphasize the inclusion of each group of partial elements where $(L_p)$ is the partial inductances, $(P)$ the partial coefficients of potential, $(R)$ the losses in conductors and dielectrics and $(\tau)$ the retarded electric and magnetic field couplings.

Two discretizations are performed in the PEEC method, first the capacitive or surface cell discretization accounting for the charge distribution and electric field coupling and then the inductive or volume cell discretization representing the current flow in the structure and the magnetic field couplings. The discretization level and thus the number of partial elements are determined by conductors shapes and separations and most important the upper frequency limit of the PEEC model. A rule of thumb is to use a minimum of 10 cells per wavelength. When a geometry allows a discretization into orthogonal surface or volume cells the partial elements can be calculated using fast closed-form expressions. For nonorthogonal geometries [5], numerical integration routines must be used.

For PEEC models several surface cells can be connected to the same node or connection point, comparable to a SPICE circuit node. The routine to reduce and combine the

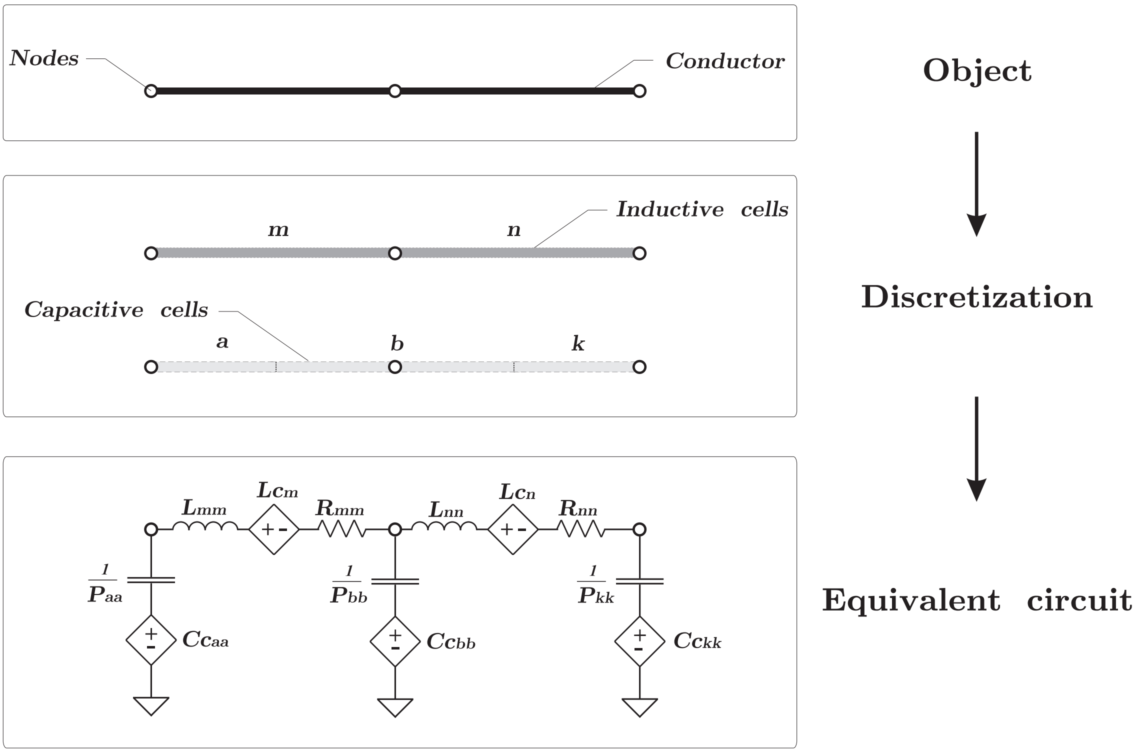


*Figure 1: PEEC discretization and equivalent circuit example.*

coefficients of potential of multiple surface cells to one single node coefficient of potential [6] is influencing the partial element calculating time and accuracy of the resulting PEEC model. This paper proposes three novel solutions for the reduction from surface- to node- coefficients of potential for the PEEC method. In the last section resulting node coefficients of potentials for the different methods are compared for basic PEEC model building blocks and a realistic PEEC model example is also given.

# 2 The PEEC Method

The theoretical derivation for the PEEC method starts from the expression of the electric field, at field point $\vec{r}$, by using the scalar and vector potentials $\phi$ and $\vec{A}$ respectively.

$$\vec{E}(\vec{r}) = -j\omega\mu\vec{A}(\vec{r}\prime) - \nabla\phi(\vec{r}\prime) \tag{1}$$

where $\vec{r}\prime$ denotes a source point. If the field point, $\vec{r}$, is on the surface of a conductor and the definitions of the potentials are used with the free space Green's function, $G(\vec{r}, \vec{r}\prime)$, (1) can be written as

$$
\begin{aligned}
\vec{E}^i(\vec{r}) &= \frac{\vec{J}(\vec{r})}{\sigma} + j\omega\mu \int_{v\prime} G(\vec{r},\vec{r}\prime)\vec{J}(\vec{r}\prime)dv\prime \\
&+ \frac{\nabla}{\varepsilon_0}\int_{v\prime} G(\vec{r},\vec{r}\prime)q(\vec{r}\prime)dv\prime
\end{aligned}
\tag{2}
$$

where $\vec{E}^i$ is an external applied electric field, $\vec{J}$ is the current density, and $\sigma$ is the conductivity at the field point, at the conductor. This integral equation and the concept of partial elements are the base of the PEEC method. For a more complete theoretical derivation see for example [7].

If the PEEC method is applied to a perfect conductor, *Object* in Fig. 1, and two inductive cells are used in the length direction, entitled $m$ and $n$ in the figure. Then the corresponding PEEC two cell model consists of two partial self inductances, entitled $L_{mm}$ and $L_{nn}$, and two volume cell DC resistances, $R_{mm}$ and $R_{nn}$ between the nodes. The capacitive coupling is realized by one partial self *pseudo-capacitance* [8] to each node, $C_a = \frac{1}{P_{aa}}$, $C_b = \frac{1}{P_{bb}}$ and $C_k = \frac{1}{P_{kk}}$. To account for the retarded electric and magnetic field couplings between the capacitive and inductive partitions, controlled voltage sources are used in the example in the figure, $C_c$ and $L_c$. As can be noted from Fig. 1, the capacitive cells (light grey) are shifted with regard to the inductive cells (dark grey) by half a cell length. This is due to a central difference approximation in the theoretical derivation [7].

The advantages with the PEEC method is noted in the simple example in Fig. 1. First, the method transforms the electromagnetic field problem to a circuit representation and offers a combined solution making it easy to include additional circuit elements such as transmission lines and power sources. Second, the same model can be used for time- and frequency-domain modeling. Third, the method offers a great deal of flexibility in the calculation of the partial elements (accuracy and speed) and macro-modeling techniques can be used to simplify large problems.

# 3 Reduction from Surface to PEEC Node Coefficients of Potential

For one and two dimensional PEEC models multiple surfaces can be associated to the same PEEC node if two discretized objects are put together. This is exemplified in the *1D PEEC* example in Fig. 2 where the two shaded capacitive cells share the same node. In three dimensional PEEC models, using a edge based formulation, up to three surfaces can share the same node in one object. This is also depicted in Fig. 2 where the three shaded surfaces of the 3D PEEC geometry share the same node, indicated with black circles. For each PEEC object a surface coefficients of potential matrix, $\mathbf{P}_S$, can be written. For the 1D PEEC example in Fig. 2 the $\mathbf{P}_S$ matrix is seen in (3) where $p_{sij}$, $(1 \leq i \leq 4)$ and $(1 \leq j \leq 4)$, are the coefficients of potential for the different surfaces.

Since the surfaces share the same PEEC node a combined self coefficient of potential need to be calculated from (3) to enable the derivation of the circuit equations. Also, combined mutual coefficients of potentials have to be calculated taking to account all surfaces in the PEECs.

$$\mathbf{P}_S = \begin{bmatrix} p_{s11} & p_{s12} & p_{s13} & p_{s14} \\ p_{s21} & p_{s22} & p_{s23} & p_{s24} \\ p_{s31} & p_{s32} & p_{s33} & p_{s34} \\ p_{s41} & p_{s42} & p_{s43} & p_{s44} \end{bmatrix} \tag{3}$$

The following sections displays three different techniques for the reduction from surface to PEEC node coefficients of potentials. The accuracy is enforced by theoretical conditions and node coefficients of potential are displayed and compared for basic PEEC building block geometries and for a simple application.

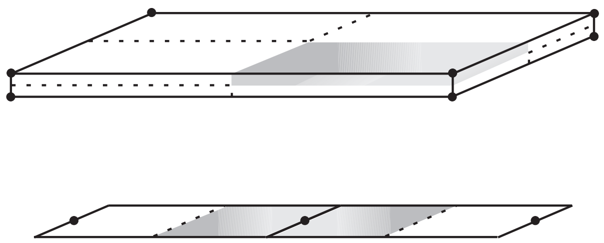


*Figure 2: Examples showing situations when multiple surfaces share the same node.*

## 3.1 Global reduction approach, $R_G$

The first technique is considered to be the most accurate since the theoretical conditions enforces:

1. An equi-potential condition to the node points in the complete PEEC model, meaning that the node potential before and after reduction is the same.

2. The charge conservation law to the complete PEEC model. This condition enforces the summation of charges for the surface connected to the same node.

This is done by introducing a reduction matrix, $\mathbf{R}_G$, that operates on the global surface coefficients of potential matrix, $\mathbf{P}_S$ to create the reduced node coefficients of potential matrix $\mathbf{P}_N$. In the global $\mathbf{P}_S$ the capacitive interactions between all the surfaces are displayed, consider (3) for the 1D structure in Fig. 2, while in the $\mathbf{P}_N$ all the capacitive interactions between the nodes are displayed.

The $\mathbf{R}_G$ matrix is constructed by writing out the node voltages and total charges before and after reduction as

$$\mathbf{V}_N = \mathbf{R}_G\, \mathbf{V}_S \tag{4}$$

$$\mathbf{Q}_S = \mathbf{R}_Q\, \mathbf{Q}_N \tag{5}$$

where subscript $S$ and $N$ represents PEEC model variables before (surface representation) and after reduction (node representation). In (5) $\mathbf{R}_Q$ is the charge reduction matrix created as $\mathbf{R}_G$. By writing the node voltages and total charges in this way the two equations, (4) and (5), can be linked by the relationship $\mathbf{V} = \mathbf{P}\,\mathbf{Q}$ to form (6).

$$\mathbf{Q}_N \; = \mathbf{R}_Q \, \mathbf{P}_S^{-1} \, \mathbf{R}_G \, \mathbf{V}_N \tag{6}$$

The conditions enforced by the global reduction approach results in $\mathbf{R}_Q = \mathbf{R}_G^T$ and the node coefficients of potential matrix can be written as (7)

$$\mathbf{P}_N = (\; \mathbf{R}_G^T \, \mathbf{P}_S^{-1} \, \mathbf{R}_G \;)^{-1} \tag{7}$$

Consider the 1D PEEC model in Fig. 2 where the second and third surfaces (shaded) share the same node. The reduction matrix is then written as (8)

$$\mathbf{R}_G = \begin{bmatrix} 1 & 0 & 0 \\ 0 & 1 & 0 \\ 0 & 1 & 0 \\ 0 & 0 & 1 \end{bmatrix} \tag{8}$$

And the surface coefficients of potential matrix is reduced from a $4 \times 4$ to the $3 \times 3$ node coefficients of potential matrix.

The drawback of this method are the matrix multiplications and inversions in (7) that has to be performed on large dense matrices, $\mathbf{P}_N[\mathrm{n}_n \times \mathrm{n}_n]$ and $\mathbf{P}_S[\mathrm{n}_s \times \mathrm{n}_s]$ where $\mathrm{n}_n$ and $\mathrm{n}_s$ are the number of nodes and surfaces respectively and $\mathrm{n}_n \leq \mathrm{n}_s$. The size of the $\mathbf{P}_S$ matrix can, in the worst case, be three times the size of the $\mathbf{P}_N$ matrix. For example, consider the 3D structure in Fig. 2 where the object is discretized into ($n_s =$) 24 surface cells (dashed lines) and ($n_n =$) 8 corresponding nodes (solid black circles).

The accuracy for this approach is guaranteed by the theoretical conditions enforced in the derivation of the reduction matrix, $\mathbf{R}_G$. Therefore, this method will be considered as the reference in the comparisons in Section 5.

## 3.2 Local reduction approach, $R_L$

The matrix operations on the large matrices in (7) are avoided in the second and third method where the node coefficients of potential matrix, $\mathbf{P}_N$, is built without creating the surface coefficients of potential matrix, $\mathbf{P}_S$, and the corresponding matrix operations.

In the second method the same conditions as for the *Global reduction approach* are enforced for the actual node/nodes involved in the reduction while the rest of the system is not considered. The advantage is that the size of the $\mathbf{P}_S$ matrix is equal to the number of surfaces involved in the reduction for each node. The reduction matrix, $\mathbf{R}_L$, is constructed in the same way as before but for the nodes involved in the actual computation. The $\mathbf{P}_N$ matrix for the 1D PEEC model in Fig. 2 is then calculated according to (9) - (12) where the $p_{sij}$ elements are the same as in (3).

$$\mathbf{P}_N = \begin{bmatrix} p_{s11} & \mathbf{A}(1,2) & p_{s14} \\ \mathbf{A}(2,1) & \mathbf{C}(1) & \mathbf{B}(1,2) \\ p_{s41} & \mathbf{B}(1,2) & p_{s44} \end{bmatrix} \tag{9}$$

$$\mathbf{A} = \begin{bmatrix} 1 & 0 & 0 \\ 0 & 1 & 1 \end{bmatrix} \begin{bmatrix} p_{s11} & p_{s12} & p_{s13} \\ p_{s21} & p_{s22} & p_{s23} \\ p_{s31} & p_{s32} & p_{s33} \end{bmatrix} \begin{bmatrix} 1 & 0 \\ 0 & 1 \\ 0 & 1 \end{bmatrix} \tag{10}$$

$$\mathbf{B} = \begin{bmatrix} 1 & 1 & 0 \\ 0 & 0 & 1 \end{bmatrix} \begin{bmatrix} p_{s22} & p_{s23} & p_{s24} \\ p_{s32} & p_{s33} & p_{s34} \\ p_{s42} & p_{s43} & p_{s44} \end{bmatrix} \begin{bmatrix} 1 & 0 \\ 1 & 0 \\ 0 & 1 \end{bmatrix} \tag{11}$$

$$\mathbf{C} = \begin{bmatrix} 1 & 1 \end{bmatrix} \begin{bmatrix} p_{s22} & p_{s23} \\ p_{s32} & p_{s33} \end{bmatrix} \begin{bmatrix} 1 \\ 1 \end{bmatrix} \tag{12}$$

Since the 1D PEEC object in Fig. 2 is a small system the speed up using this *Local reduction approach* is negligible. However, for larger systems the speed up is substantial, see Section 5.

The *Local reduction approach* enforces the equi-potential and conservation of charges to the local system. Therefore the method decouples the local system and performs the reduction from surface to node coefficients of potentials. The error introduced by the reduction is hard to quantify for a general PEEC model. But, the impact on single node coefficients of potential for basic PEEC geometries and a simple example is displayed in Section 5.

### 3.3 Local weighting approach, $R_W$

The third method uses a weighting mean value procedure to calculate the node coefficients of potential matrix, $\mathbf{P}_N$. The calculation is based on the areas, $A_i$, $0 < i \leq n_s$, and the surface coefficients of potentials , $p_{s_{ij}}$, for the capacitive surface patches, as shown in (13).

$$p_{n_{ij}} = \frac{\sum_i \sum_j p_{s_{ij}} \left(A_i \, + \, A_j\right)}{A_{TOT}} \tag{13}$$

For equal surface cell areas, $A_i = A_j$, this corresponds to the arithmetic mean value. In (13) the node coefficients of potential $\mathbf{P}_n$ is calculated without any matrix operations and is therefore the fastest method.

The equi-potential condition is fulfilled as for the other approaches. But the conservation of charges condition is transformed to depend on the charge distribution that in turn is considered in the surface coefficients of potential calculations, ie the orientation and position of the surface cells.

## 4 Circuit Equations for PEEC Problems

It is important to notice the use of the node coefficients of potential matrix, $\mathbf{P}_N$, when forming the circuit equations for the final PEEC model. When using the modified nodal approach the $\mathbf{P}_N$-matrix is used directly while for other formulations such as nodal (admittance matrix) formulations the inverse of the $\mathbf{P}_N$-matrix is used. This can result in the preferred use of the global reduction approach for the latter formulations since the accuracy is higher and one matrix inversion has to be done, the one in (7) or the one to transform the $\mathbf{P}_N$-matrix to the inverse $\mathbf{P}_N$-matrix. It is worth to notice the wide use of the modified nodal approach for automatic formulation of circuit equations in circuit analysis software and also for PEEC based EM solvers.

# 5 Numerical Experiments

The three methods have been implemented in a PEEC based full-wave solver. The numerical experiments presented in the following subsections involve computation of the self-and mutual-node coefficients of potential for basic PEEC geometries/PEEC model building blocks. A parallel plate capacitor is used to exemplify the impact of the different calculation techniques on PEEC model results.

## 5.1 Node coefficients of potential calculations

This section displays the impact of the different calculation routines on self- and mutual-node coefficients of potential calculations. The results are displayed in Fig. 3 to 7 with a *node coefficient of potential relative error*, $P_{rel.err.}$, defined as in (14).

$$P_{rel.err.} = \frac{P_{ij} - P_{ij_{R_G}}}{P_{ij_{R_G}}} \tag{14}$$

In (14) $P_{ij}$ is the calculated node coefficient of potential (node-cop), using the *local reduction-* or *weighting-approach*, and $P_{ij_{R_G}}$ is the same node-cop calculated using the *global reduction approach*.

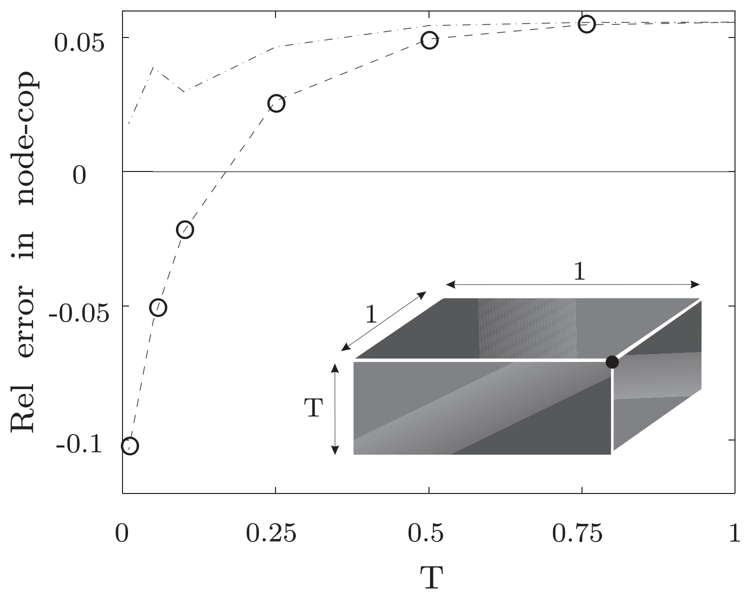


*Figure 3: Three surfaces to one node reduction. Relative error for the node-cop. $R_G$(solid), $R_L$(dash-dot), $R_W$(dash-circled).*

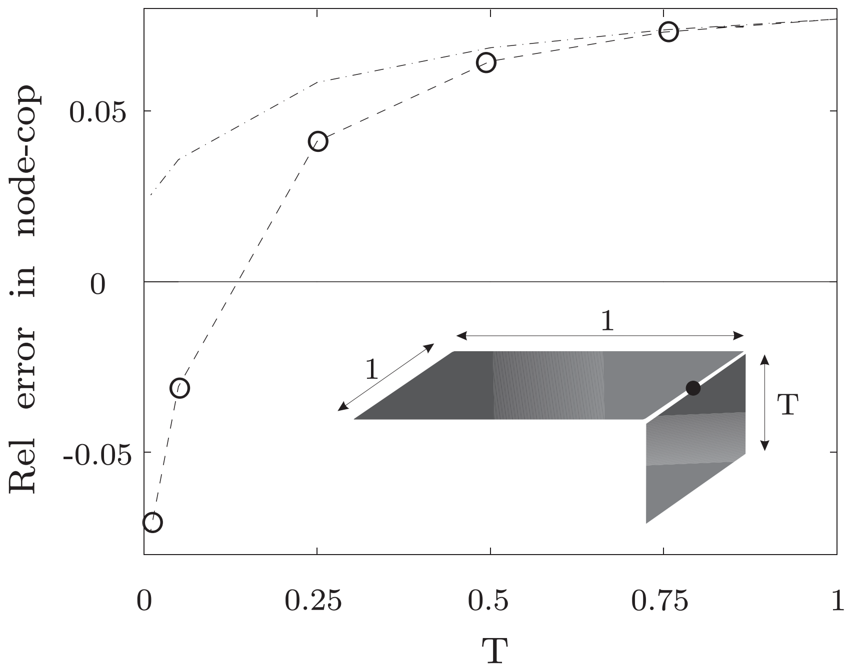


*Figure 4: Two surfaces to one node reduction. Relative error for the node-cop. $R_G$ (solid), $R_L$ (dash-dot), $R_W$ (dash-circled).*

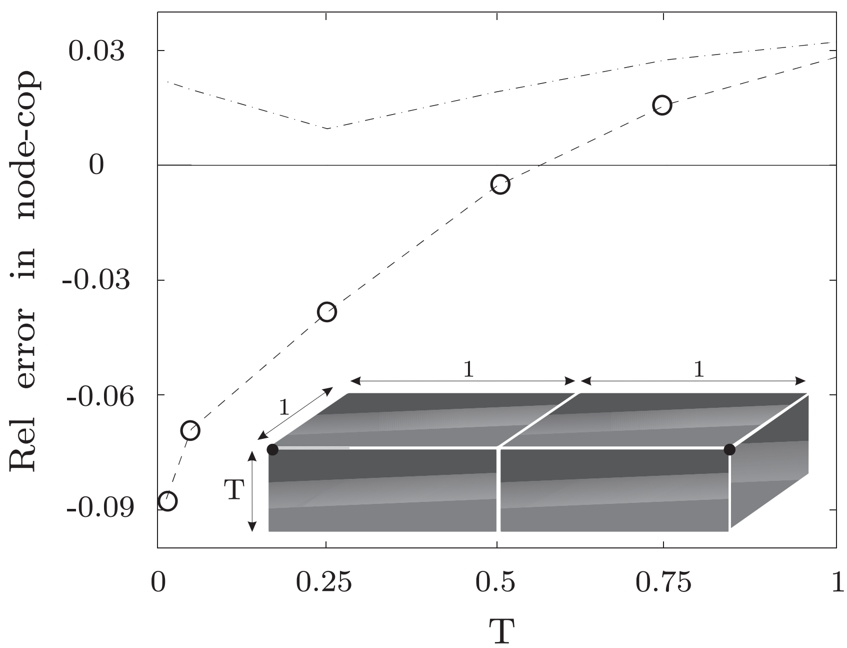


*Figure 5: Six surfaces to two nodes reduction. Relative error for the node-cop. $R_G$ (solid), $R_L$ (dash-dot), $R_W$ (dash-circled).*

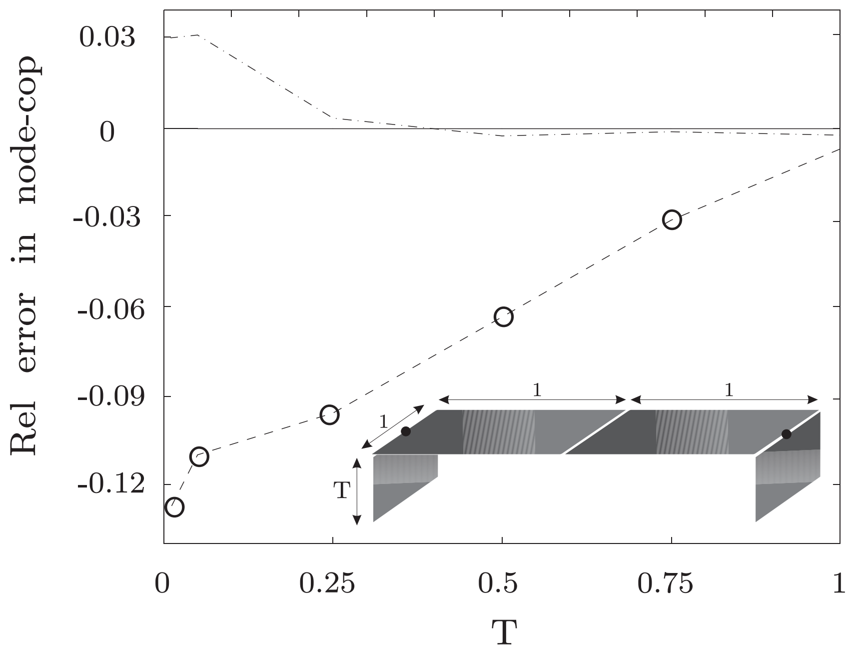


*Figure 6: Four surfaces to two nodes reduction. Relative error for the node-cop.* $R_G$ *(solid),* $R_L$ *(dash-dot),* $R_W$ *(dash-circled).*

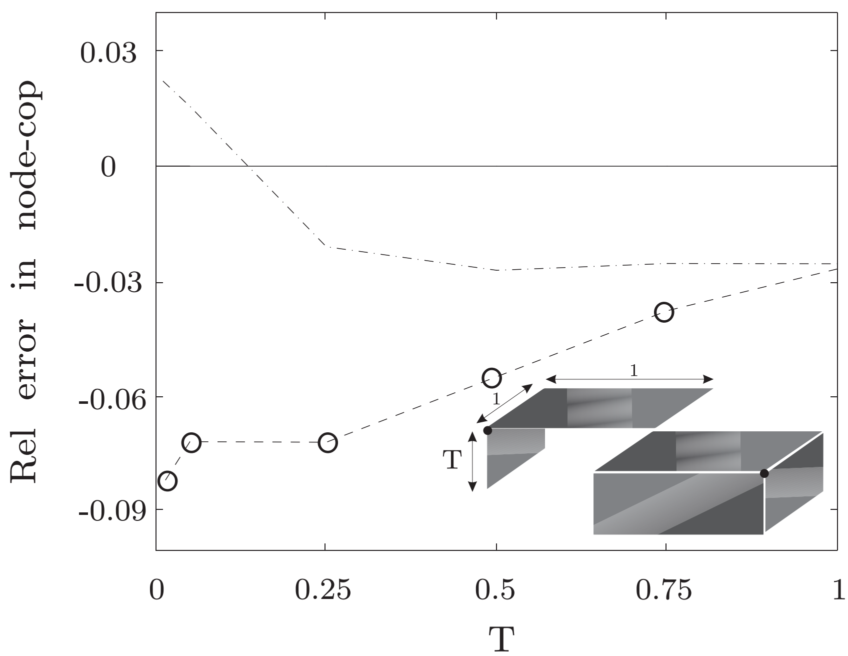


*Figure 7: Five surfaces to two nodes reduction. Relative error for the node-cop.* $R_G$ *(solid),* $R_L$ *(dash-dot),* $R_W$ *(dash-circled).*

In the results the *global reduction approach* is considered as the reference, thus the zero relative error indicated in the figures. All the figures show a reduced node-cop. relative error, (14), for nodes made up of homogenous patches when using the *local weighting approach*. The error is predominantly larger using the *local weighting approach* than for the *local reduction approach*. The maximum relative error using $R_L$ is 0.07, while the maximum error using $R_W$ is 0.13. It can be noted that the relative error is larger for the calculation of the self node-cop. compared to the mutual term when using the *local reduction approach*.

## 5.2 Parallel plate capacitor

To display the impact of the different node-cop calculation routines a $10 \times 10$ cm (L $\times$ W) parallel plate capacitor is modelled. The capacitor geometry is chosen since the capacitive effects are important in the resulting PEEC model and thus displays the impact of the different calculation routines effectively. The capacitor plates are 50 $\mu$m thick (T) and spaced 1 mm apart by a dielectric material with relative permittivity of 3.4 resulting in a theoretical capacitance value of 0.3011 nF. The capacitance value is then calculated or modelled based on $(L_p, P, R, \tau)$PEEC frequency domain simulations while varying.

- The 3D capacitance reduction methods:
  - $\mathbf{R}_G$.
  - $\mathbf{R}_L$.
  - $R_W$.
- The capacitor discretization:
  - 1 or 5 inductive cells for L and W directions for both conducting plates and dielectric material.
  - Zero thickness or 1 inductive cell for the conductor plate thicknesses (T).

The results from the test are shown in Table 1 where the *Speed up* is defined as $\frac{T_{R_G}}{T}$, where $T_{R_G}$ is the calculation time for the $\mathbf{P}_N$ matrix using the *Global reduction approach* and $T$ is the current $\mathbf{P}_N$ matrix calculation time. The $C_{error}$ is a relative error defined as

$$C_{error} = \frac{|C - C_A|}{C_A} \tag{15}$$

where $C_A$ is the analytical capacitance value, 0.3011 nF, and $C$ is the capacitance value from simulations. The impact on the modelled capacitance value for the different formulations is substantial, see Table 1, with a maximum relative error of 15%. The $(L_p, P, R, \tau)$PEEC simulations based on the *Global reduction approach* is predicting the capacitance value best with a maximum relative error of 2.8%. The other formulations displays a variation in relative error but also a considerable speed up, in the order of 22 times, for this small problem.

*Table 1: Capacitance relative error and $\boldsymbol{P}_N$ calculation speed up using different reduction approaches.*

| **Ind. disc.** | | **Cap. cells** | | **Cap. reduction method & results** | | | | |
|---|---|---|---|---|---|---|---|---|
| L & W | T | $n_s$ | $n_n$ | $\mathbf{R}_G$ | $\mathbf{R}_L$ | | $R_W$ | |
| | | | | $C_{error}$ | $C_{error}$ | *Speed up* | $C_{error}$ | *Speed up* |
| 1 | 0 | 32 | 16 | 0.025 | 0.150 | 1 | 0.150 | 1 |
| 5 | 1 | 360 | 210 | 0.026 | 0.123 | 22 | 0.022 | 29 |
| 1 | 1 | 72 | 24 | 0.025 | 0.012 | 1 | 0.092 | 1 |
| 5 | 0 | 192 | 144 | 0.028 | 0.153 | 16 | 0.151 | 19 |

# 6 Conclusions

Three different formulations for the calculation of the PEEC model node coefficients of potential is presented and evaluated. The *global reduction approach* offer theoretically very good accuracy but suffers from the matrix operations involved resulting in large computation times. The *local reduction approach* performs the same matrix operations on maximum two nodes at a time thus reducing the computational effort and a considerable speed up is obtained. The third method calculates the node-cop by using a *local weighting procedure* for the individual surfaces but suffers from poor accuracy for certain cell aspect ratios. To be noted is that the speed up is strongly dependent on the speed and efficiency of the matrix routines used in the PEEC implementation. However the speed up is increasing proportional to problem size, ie number of nodes and surfaces in the PEEC model, when using the *local reduction approach* or the *local weighting approach* instead of the *global reduction approach*. For the parallel plate capacitor example, consisting of maximum 210 nodes, the speed up is in the order of 22 times with a maximum relative error of 15%. For one test, in Table 1, the *local weighting approach* showed a reduced relative error and a speed up of 29 times compared to the *global reduction approach*.

# References


[1] A. E. Ruehli, "Inductance Calculations in a Complex Integrated Circuit Environment", *IBM Journal of Research and Development*, 16(5):470–481, September 1972.

[2] A. E. Ruehli and P. A. Brennan, "Efficient Capacitance Calculations for Three-Dimensional Multiconductor Systems", *IEEE Transactions on microwave Theory and Techniques*, 21(2):76–82, February 1973.

[3] L. W. Nagel, *SPICE: A computer program to simulate semiconductor circuits.* Elecrt. Res. Lab. Report ERL M520, University of California, Berkeley, May 1975.

[4] C. Ho, A. Ruehli, and P. Brennan, "The Modified Nodal Approach to Network Analysis", *IEEE Transactions on Circuits and Systems*, pages 504–509, June 1975.

[5] A. E. Ruehli *et al.*, "Nonorthogonal PEEC Formulation for Time- and Frequency-Domain EM and Circuit Modeling", *IEEE Transactions on EMC*, 45(2):167–176, May 2003.

[6] A. E. Ruehli, P. A. Brennan and H. W. Young, "Recent Progress in Capacitance Computation Methods", in: *Proc. of the IEEE Int. Symp. on Circuits and Systems*, Phoenix, Az, USA, 1975.

[7] J. E. Garrett, *Advancements of the Partial Element Equivalent Circuit Formulation.* Ph.D. Dissertation, The University of Kentucky, 1997.

[8] H. Heeb and A. E. Ruehli, "Approximate Time-Domain Models of Three-Dimensional Interconnects", in: *Proc. of the IEEE Int. Conference on Computer Design*, pages 201–205, 1990.